Active Target Localization and Tracking with Application to Robotic Environmental Monitoring

A DISSERTATION
SUBMITTED TO THE FACULTY OF THE GRADUATE SCHOOL
OF THE UNIVERSITY OF MINNESOTA
BY

Joshua David Vander Hook

IN PARTIAL FULFILLMENT OF THE REQUIREMENTS
FOR THE DEGREE OF
Doctor of Philosophy

Prof. İbrahim Volkan İşler

September, 2015

© Joshua David Vander Hook 2015
ALL RIGHTS RESERVED

Acknowledgements

I thought when I finished this dissertation I would feel great. As in *large or capable significantly above the average amount.* Completing a large project like this over five years is not something to attribute to my own abilities. Any milestone is the sum of the individual decisions that led to it and when I look at the amount of guidance, encouragement, patience, and downright goading that it took to make the decisions that led to this point, I feel only gratitude.

Understanding that this list is incomplete, I first thank the person most influential to this work: my advisor, Dr. Volkan Isler. You reminded me to be calm under stress, to do good work first and find a place for it second, to treat those around me with the utmost respect, and to never use a colon to break a sentence. Thanks for taking a chance on a terrified first-year that walked into your office. I owe you much.

Thanks to my committee, Professors Roumeliotis, Banerjee, Frew, and Jovanovic, for your feedback before (and possibly after) my submissions for publication, your patience with my answers, challenges to my assumptions, and guidance and assistance in finding a place to grow now that my time here is over.

Thanks to my lab mates for dinners after experiments, sympathy when the equations would not work, feedback when my ideas were ridiculous, and help pulling the robot out of the muck or snow when it got lost. Thanks especially to Pratap, Patrick, Narges, and Haluk, with whom I lived and worked the closest. We publish singly but we suffer and celebrate in aggregate. I wish you the best. Remember, everyone wears the waders.

Thanks to my family and those I've added to it. Friends you make during the hard times are friends you make for life. For your patience, encouragement, much-needed distractions, perspective, and love, I'm grateful. Thanks, Jared, for brewing and inspiration. Chase, you got me through a tough year and I'm glad we could adventure.

Thanks to Lisa, Andy, Pete and my boxing buddies at Uppercut for the bruises, blood, and confidence. Thanks to Hanna for hannalysis, Marie, Robert, Emery, and Ben for commiseration in the dungeon of Keller Hall, and the rest of the outstanding grad student population for all the happy hours. Thanks to Worms, Bergo, Andy, and Matt for teaching me to pile in and cleave. To Geoff, Bryce, Willard and the rest: skol. To Chrissy, a picture is worth a thousand words. I can't say it any better: "*Vamos*"

And finally, thank you to the National Science Foundation, ARCS Foundation, University of Minnesota, Sigma Xi, and patient parents for providing financial support.

Dedication

For mom, dad, and my family.

Abstract

Thanks to advances in miniaturization, computing power, reliable sensors, and battery life, mobile robots are increasingly being used for a wide variety of environmental monitoring tasks. No longer confined to factory floors or controlled environments, robots for remote sensing in dangerous or hard-to-reach environments could provide the same scalability, precision, and reliability to environmental monitoring as they did to industrial applications. To enable this kind of long-term, reliable, autonomous mobile sensor deployment, algorithms which can ensure that the robots achieve their sensing tasks are required.

In this dissertation, we present fundamental results in using mobile sensors to locate targets of interest. This *Active Localization* problem forms the core study of the thesis. The dissertation is roughly separated into three main parts.

In the first part of the thesis, we study the problem of using one or more mobile robots equipped with bearing sensors to locate a stationary target in minimum time. The problem requires optimizing the measurement locations of the robots to gather the required information about the target's location. In addition, when multiple robots collaborate, we include communication constraints in the path planning objective. Two formulations for this problem are studied. First, we study the *offline* problem of finding measurement trajectories when the true target location is known. Second, we study the *online* version and show how to adapt the offline solution to the situation when the target location is not known, while preserving the quality guarantees of the offline solution.

In the second part of the thesis, we study the problem of locating multiple stationary targets using a single mobile robot. We formulate a novel coverage problem and provide two main results. We first study the problem of initializing consistent estimate of the targets' locations. These initial estimates are used to seed an active localization algorithm which is shown to localize the targets quickly. In a second formulation, we assume that the targets are within a set of polygonal regions, but have no further information about the distribution or number of targets in the environment. An algorithm

is provided which can choose measurement locations to localize all the targets to within desired precision in near optimal time.

In the third part of the thesis, we study the problem of using bearing information to track and capture a moving target. We present two formulations based on pursuit-evasion games. In the open plane, the objective is for a mobile robot to minimize the distance to a maneuvering target when only uncertain bearing information is available to the robot. Then, we study the problem of *capturing* the maneuvering target in a closed environment by moving close to it. We show that the size of the environment relative to the sensing noise determines if this is possible.

In addition to theoretical results, we present field studies of using one or more mobile robots to detect radio transmitters using these results. We show that the algorithms presented are suitable for use in monitoring invasive fish.

This dissertation provides both fundamental theoretical studies of active localization using bearing sensors and extensive field studies which verify the usefulness of the results in environmental monitoring tasks.

Contents

Acknowledgements **i**

Dedication **iii**

Abstract **iv**

List of Tables **x**

List of Figures **xi**

1 Introduction **1**

1.1 Contributions 5

1.1.1 Target Localization with a Single Bearing Sensor 5

1.1.2 Time Bounds For Cooperative Localization 5

1.1.3 Multi-Target Initialization and Localization for Closely Clustered Targets 6

1.1.4 Geometric Sensing Model and Pursuit Evasion Games 7

2 System Description **9**

3 Technical Background and Problem Definitions **13**

3.1 Filtering Methods 17

3.2 Quality of Estimator Output 19

3.3 Active Localization Problem Formulation 21

4 Related Works **24**
4.1 Sensing and Estimation 24
4.2 Active Localization using Bearing Measurements 25
4.3 Communication Constrained Active Localization 28
4.4 Coverage Algorithms 28
4.5 Locating Multiple Stationary Targets Adaptively 29
4.6 Pursuit Evasion Games 30

5 Near-Optimal Localization of a Stationary Target with One Robot **32**
5.1 Addressing Ambiguity 33
5.2 The β-Cautious Algorithm 38
5.2.1 Algorithm Description 39
5.3 Bounding the Cost of the β-Cautious Algorithm 39
5.4 Bounds on the Optimal Cost 45
5.4.1 Lower Bound for an Offline Algorithm 46
5.4.2 Comparison with the β-Cautious Strategy 49
5.4.3 Worst Case Online Cost 51
5.4.4 Comparison of Worst Case Online Performance 52
5.5 Simulations 53
5.6 Field Experiments 58
5.7 Discussion 59

6 Optimal Offline Localization of a Stationary Target with Many Robots **65**
6.1 The Optimal Offline Algorithm 66
6.2 Optimal Active Localization Using a Single Robot 68
6.3 Optimal Active Localization with Two Robots 73
6.4 Near-Optimal Active Localization with Distance-Constrained Communications 78
6.5 Discussion 81

7 Offline to Online Algorithms and Near-Optimal Localization of a Single Target **83**
7.1 The Online Algorithm 84

7.2 Implementations and Experiments 89
7.2.1 Simulations 89
7.2.2 Field Experiments 91
7.3 Discussion 92

8 Initialization and Localization for Clusters of Targets 94
8.1 Motivation 95
8.1.1 The Initialization Problem 96
8.2 Local Search 98
8.2.1 Single-Target Local Search 98
8.2.2 Multi-Target Local Search 100
8.2.3 Discussion 102
8.3 Simulations 103
8.4 Experiments 105
8.5 Discussion 106

9 Guaranteed Localization for Many Targets 108
9.1 Preliminaries 109
9.1.1 Uncertainty Model 109
9.1.2 Problem Statement 110
9.2 Gathering Bearing Data 112
9.3 Simulations 113
9.4 Field Experiments 116
9.4.1 Sensing Model Validation 116
9.4.2 Lake Experiments 117
9.5 Discussion 122

10 Tracking Adversarial Targets in the Open Plane 123
10.1 Open Plane Pursuit 124
10.1.1 Evader Strategy 125
10.2 Discussion 132

11 Tracking and Capturing Adversarial Targets in Bounded Environments **133**
11.1 The Lion and Man Game 134
11.1.1 Evader's Winning Strategy 135
11.1.2 Pursuer Strategy for Small Uncertainty 143
11.2 Discussion 153

12 Conclusions and Future Work **154**
12.1 Contributions and Open Problems 154
12.2 Future Research Directions 158
12.2.1 Kinematic Models 158
12.2.2 Long-Term, Collaborative Autonomy 159
12.2.3 Self and Collaborative Localization 160
12.3 Concluding Remarks 160

References **162**

List of Tables

5.1 Simulation Parameters 55

List of Figures

1.1 Our robotic system consists of radio tags, a radio antenna and receiver mounted on autonomous boat in summer and wheeled rover in winter (to operate on frozen lakes). 4

2.1 The robotic systems used in field experiments. The 2-meter boats were designed to track invasive fish autonomously. Each is equipped with wireless communications, directional antenna used as bearing sensors, a navigation suite, and computing hardware. Our algorithm was implemented on this system and was shown to localize targets to within small uncertainty. 10

2.2 The two ground rovers used in field trials over frozen lakes. 11

3.1 Example of the bearing-only localization task. A robot takes two measurements of a stationary target at the red dot. If there is no noise in the measurements, the target is perfectly localized as long as the measurement locations are not collinear with the target (3.1a). If there is some noise on the measurements, the target could be anywhere within the dark shaded region with high probability (3.1b). If the measurement locations are closer together, two measurements produces a much larger area that the target could be in. The *active localization* problem is to choose measurement locations which are not spread too far, but produce low uncertainty. 14

3.2 The notation and problem formulation. The robots take their i^{th} measurement from location $s_{u,i}$. Each location is described in polar coordinates $(r_{u,i}, \alpha_{u,i})$. For much of the thesis, the coordinate frame is fixed to the target location and oriented with respect to the current covariance. Thus, $r_{u,i}$ is the range from the sensor to the current hypothesis, $\hat{x}_i$, and $\alpha_{u,i}$ denotes the orientation with respect to the line formed by the major axis of the covariance ellipse, Σ_i, with eigenvalues $\sigma_{x,i}$ and $\sigma_{y,i}$ and orientation θ_i with respect to a global frame. 15

3.3 By repeatededly taking bearing measurements of tags deployed in known locations, we can accumulate the error profile for the bearing measurements, a process known as calibration. Shown here is one such trial. The error is verified to be zero-mean and roughly Gaussian. 16

5.1 **(a)**. Problem setup. A robot, without knowledge of the true target location $x^\star$ but with an initial hypothesis of the target location, $\hat{x}_0$, must find measurement locations to shrink the uncertainty about $x^\star$. Measurements taken far from $x^\star$, for example, near $\hat{x}_0$ will ultimately provide small information about $x^\star$ and are thus wasteful. Shown is an example of a "double wedge" or ambiguous measurement cone: From just one measurement, it is not clear if the target is near $\hat{x}_0$ or $x^\star$. **(b)**. The notation and problem formulation. A sensor location at time i, denoted s_i, is described by (r_i, α_i). Here r_i is the range from the sensor to the current hypothesis, $\hat{x}_i$, and α_i denotes the orientation with respect to the line formed by the major axis of the covariance ellipse, Σ_i, with eigenvalues $\sigma_{x,i}$ and $\sigma_{y,i}$ and orientation θ_i with respect to a global frame. 34

5.2 **(a)** Ambiguous measurements produce two possible bearings (z and z'). **(b)** The EKF approximates the measurement probability as a Gaussian with mean zero and variance S_i. **(c)** The PDF of the target hypothesis after updating the Gaussian prior shown in (a) with measurements z' and z. 35

5.3 One measurement step of the cautious strategy presented in Algorithm 5.1. Shown is a covariance ellipse and target hypothesis (circle) along with the true target location (star). **(a)** The robot moves to a location perpendicular to the direction of highest uncertainty. **(b)** A bearing measurement is collected, and the hypothesis is updated. The "backward facing" cone (dashed lines) is discarded. **(c)** The now-reshaped covariance ellipse has a new direction of highest uncertainty, and the process repeats. 38

5.4 A simulated execution of the cautious strategy. This figure is best viewed in color. **(a)** the full run. **(b)** Detail of the boxed region in the first figure. A red ellipse denotes the final target covariance, the black circle is the desired uncertainty, blue is prior estimate, and green is the robot path and measurement locations. The robot travels in a roughly zig-zag path toward the target, while the target hypothesis shifts rectilinearly toward the true target. 40

5.5 The measurement sequence $S = \{s_0 \dots s_4\}$. **(a)** the target hypothesis shifts vertically because of the measurement received at s_1. **(b)** The next measurement location (s_2) must be shifted by the same amount to satisfy the range constraint. 41

5.6 An illustration of the sequence S'. An arbitrary trajectory (left) is lower-bounded by a well-structured trajectory S' (right), according to Lemmas 5.6 through 5.7. 47

5.7 **(a)** The observed probability that the MH-EKF tracks a different hypothesis than the β-Cautious Strategy. Note that for small β, the β-Cautious strategy causes the EKF to track the correct hypothesis more often. **(b)** The normalized error of the final estimate ($||\hat{x}_n - x^\star||/||\hat{x}_0 - x^\star||$) as a function of the β parameter. The median error is shown for the Gaussian Sum Filter, MH-EKF, and β-Cautious Strategy using an EKF. Note that increasing β results in more error, but at less cost as shown in Figure 5.9. 54

5.8 Two examples of the effect of the parameter β, comparing the difference in final estimates using an EKF, MH-EKF, and Gaussian Sum Filter. Shown is the median error over 1000 trials, after each measurement, for all three filters, as well as an "omniscient" EKF which was given the correct, unambiguous measurements. **(a)** With $\beta = .01$, we notice agreement and small final error. **(b)** With $\beta > .2$, we notice reduced performance in all filters. These observations suggest that the measurement locations corresponding to low values of β are useful for mitigating the effect of ambiguous measurements, as suggested by Lemma 5.1. 55

5.9 Simulations studies of the possible configurations and the resulting upper bound. We vary the final required uncertainty (γ), and evaluate the costs as shown in Theorem 5.1. **(a)** the distance traveled as γ decreases (corresponding to a more precise final estimate). **(b)** the number of measurements taken. **(c)** the total execution time as γ decreases. In **(d)**, is the tradeoff between increasing the parameter β and the resulting time required to localize the target. Note that the target can be localized more quickly by increasing risk. The discrete drops in time correspond to removing a measurement from the sequence and the remaining reduction in time is from placing the measurements closer together. Both will cause more error in the final estimate, as shown in Figure 5.7b. 61

5.10 The theoretical performance ratio (Eq (5.15)) and observed performance ratio ($\mathbb{E}[T(S_\beta)]/\mathbb{E}[T(S')]$) as a function of: **(a)** the starting range to the hypothesis, $\hat{r}_0$, **(b)** the desired risk (increasing β), and **(c)** the measurement time (increasing t_m). Note that in some cases the theoretical bounds are quite loose. This results from our analysis: we provide an upper-bound on the worst case. In practice, the worst-case is rarely if ever encountered. 62

5.11 **(a)** The robotic platform employed in field tests. Notice the octagonal antenna used to detect nearby radio transmitters, and the servo-motor used to rotate the antenna. The robot has been tested on multiple lakes in Minnesota, USA, including Lakes Gervais, Staring, Keller, and Phalen. **(b)** The antenna used to gather bearing measurements. The antenna is radially symmetric, producing *ambiguous* bearing measurements. The antenna is approximately 56cm (22 in) in diameter and is mounted on a servo-motor attached to the robotic chassis. **(c)** A radio transmitter which is surgically implanted in invasive fish. Each transmitter (or "tag") has a unique frequency and transmits an uncoded pulse at approximately 1.1 Hz. The tags are nearly 7.5cm (3 in) long. 63

5.12 Two single-target field trials. Parameters were $\sigma_\beta^2 = 1$ and $\sigma_s^2 = \left(\frac{\pi}{8}\right)^2$. In both cases, the time for the system to localize the target adhered to the theoretical bounds. **(a)**: The 2 σ uncertainty ellipses are shown for the prior and final estimates. The final error was less than 5 meters after only 4 measurements. The total experiment area was approximately 70 meters by 64 meters. **(b)**: At Lake Gervais, MN. USA. With no prior information, the initial estimate was constructed using the routine described in Chapter 8, producing the large red circle shown. The measurement locations narrowed the uncertainty to the final circle given as a dashed line. The true target location is labelled as a black 'x'. 64

6.1 The *target-local* coordinate frame. By expressing the measurement locations (black dots) with respect to the frame rotated by θ, $\mathbb{F}$ is a diagonal matrix. The covariance ellipse's eigenvectors are aligned with the frame in which we express sensor locations. 67

6.2 An illustration of Lemma 6.2. Three or more measurement locations are sub-optimal in the case of a single robot. Two measurement locations s_1 and s_2 can be moved closer together to produce a lesser-cost trajectory with the same information. This process can be repeated until the pair of measurement locations is collapsed to the same point. 69

6.3 Examples of the contours described by Equation (6.10) and (6.11) for a target at $(0,0)$ (shown as a star), $r_1 \in \{1, 1.5, 2\}$ and λ_d set to .01 (black lines of lesser curvature) or .05 (blue). σ_s was 1 and N_1 was 1. For example, if the robot first travels to the position $s_1 = (2,0)$ and takes one measurement then it can take all remaining measurements from anywhere on the dashed curve (e.g., s_2 as labelled) to ensure both eigenvalues of $\mathbb{F}$are greater than λ_d. 72

6.4 These optimal one-robot offline trajectories corresponding to values of $\lambda_d \in \{1, 2, 4, 6, 12\}$. Note the robot begins at location $(5,0)$ and moves along the x-axis to the first marked location. 73

6.5 The steps of the proof of Lemma 6.4. First, the optimal two-robot strategy, $S^\star = \{S_u + S_v\}$, is "mirrored" about the line $\overline{x^\star s_0}$. Since the information from the two pairs of symmetric strategies, $S'_u + S_u$ or $S'_v + S_v$, is twice the required information, it is clear that one of the two pairs produces the required information. 75

6.6 An illustration of the constraints on the measurement sequences. (a) by Equation 6.2, (b) by Equation 6.3, and (c), the intersection. Note the radius in (b) is never greater than the radius in (a). Assuming the other measurements are placed, the last measurement U, must fall in the regions specified, while traveling the least. The dotted line adjoining U and the starting location illustrates the shortest path. 76

6.7 Optimal two-robot trajectories for various system parameters. In all figures the robots started at location $(3,0)$ and the true target was at $(0,0)$. Communication constraints were only considered in the top right figure and all other parameters were held fixed. Top-left: $\lambda_d \in \{.1, 1, 3, 8\}$. Top-right: $r_c \in \{2.1, 1.1, .1\}$. When $r_c = .1$, the robots rendezvous after measuring. When $r_c = 2.1$ the output is the same as the result from unbounded r_c. Bottom-right: $t_m \in \{.01, .1, 1\}$ Note that as t_m increases, the optimal algorithm travels to more informative locations so that fewer measurements are required. Bottom-left: $\sigma \in \{.1, 1, 4, 8\}$. Note that changing the sensor noise produces the same effect as requiring more information (compare left two figures). 79

6.8 An illustration of two different choices for communication-constrained measurement locations. s_u and s_v represent the output of Algorithm 6.2. From these locations, the robots can move directly toward each other to communicate. Alternatively, they can move to s'_u and s'_v, and remain in communication during measurement. Algorithm 6.3 finds the optimal placement of symmetric measurements to minimize the cost while including the rendezvous cost. 82

7.1 An illustration of the two-robot `MULTI-STEP` algorithm (solid paths) and the optimal $\mathcal{A}$ algorithm (dashed paths). The robots begin at s_0. The optimal choice is to move directly to $x^\star$, but we are unsure of the location of $x^\star$. Thus, we form a convex region R such that the probability $x^\star$ is in R is high. At each step of the `MULTI-STEP` algorithm, we do less work than $\mathcal{A}(s_0, x^\star)$ by Lemma 7.1. Since the number of $\mathcal{A}$ executions is bounded by Lemma 7.2, we do not do significantly more work than optimal by Theorem 7.1. 86

7.2 Experiment results from Lake Staring, Minnesota, USA. **(a)**: The experiment area. The true target (and camera in [1]) were placed on the docks near the bottom right corner (labelled with a star). The robots began near the top-middle (circle). **(b)**: The two calls to Algorithm 6.3 produced the dark paths shown, and reduced the uncertainty (the blue circles). The final actual uncertainty was the solid ellipse. **(c)**: More execution details. The solid red circles are the points where the robots exchanged information. The figure covers an area approximately 200m vertically by 150m horizontally. 90

7.3 The aggregate results of numerical studies as a function of the starting and final information. Left: the number of calls to $\mathcal{A}$. Right: the ratio of costs of online algorithm to optimal offline algorithm. Shown is the maximum value encountered during simulations. 91

8.1 Failed triangulation due to incorrect initialization for trials conducted on Lake Staring, MN. The initial estimate for the first trial was inconsistent and resulted in the localization to diverge and move the robot out of the tag's sensing range. During a second trial, with a consistent initial estimate, the target was successfully localized. 96
8.2 Examples of search patterns (Figure 8.2a) and ambiguous bearing measurements (Figure 8.2b). High sensor noise, ambiguity and unknown sensing range makes it difficult to transition from search to localization. 97
8.3 (a) While on its coverage path (curved arrow), the robot, at O, detects a non-zero signal for some frequency X. (b) The initialization strategy determines the sensing circle for X by moving along search paths as shown until X is not detectable again. Shown is a case where three search paths fail to uniquely identify the sensing circle. (c) An example of a Four-path search. 99
8.4 The robot continues along an arbitrary but fixed direction until it cannot detect the signal from X (at position A). The robot then returns to O and repeats the same strategy along a perpendicular line (B). In general, the O can lie in the interior of the sensing circle, hence the robot also searches along C and D 100
8.5 (a) The single target search fails to intersect all the sensing circles in the case of an aggregation. (b) An example of searching for an aggregation using two separate search steps. The robot first finds the boundary of C_X (dashed), centered at O'. Then, after moving to O', searches along four paths to identify the boundaries of each sensing circle. 101
8.6 In general, the starting location of local search can lie anywhere on the boundary or interior of the sensing circle. In each case, we obtain a different number of points as shown. For all cases, we can determine the sensing circle uniquely. 102
8.7 To extend the single target local search strategy, we need at least twelve search paths (separated by less than $\frac{\pi}{6}$) to intersect each sensing circle at least thrice. 103

8.8 Simulation comparing the time taken to initialize all 10 fish in the lake, as the number of aggregations varies. The Four-Path strategy performs better than the Twelve-Path. The bars indicate the minimum and maximum times, and the trend line plots the mean time of 50 instances. 105
8.9 Mean, minimum and maximum time taken as the number of fish increases in one aggregation for the Four-Path strategy. For lower sampling time, the time to travel dominates and thus scales well for larger aggregations. 106
8.10 A successful experiment demonstrating the local search strategy and localization steps. 107
9.1 Gathering Bearing Data: Shaded areas are the input regions which need to be searched. The goal is to compute measurement locations (squares) and a tour (dashed line) along them so that no matter where the targets are, the uncertainty in localizing them is small. 109
9.2 A simulated example tour generated by the algorithm. The four areas are known to contain targets, and a sensing tour is computed to localize all the targets. Theorem 9.1 shows that the tour of the measurement locations is near optimal, and Lemma 9.1 shows that any target in the area will be localized to desired uncertainty. The green crosses are computed measurement locations, the yellow path is the tour, and the red crosses are the target locations. 114
9.3 (a) A sample scenario with $U^\star = 32$ and $\sigma = \pi/12$. Each measurement location is shown by blue solid circle. Black squares denote true target positions. Red crosses are the positions of the estimates. Uncertainty areas is shown as red ellipses. (b) Number of occurrences of areas of the uncertainty ellipses for 1000 random target locations with $U^\star = 32$ and $\sigma = \pi/12$. 115
9.4 (a) Average uncertainty area and (b) average estimation error for varying the uncertainty threshold $U^\star$ and the measurement noise σ. 115

9.5 (a) A tag sends an uncoded transmission on a specific frequency once per second. (b) The antenna is shown in the foreground, and radio transmitters were placed in the field nearby. A direction-sensitive antenna is rotated to estimate the bearing to the transmitting radio tag. The signal strength is strongest when the plane of the antenna loop is roughly aligned with the tag. 116
9.6 Number of occurrences of areas of the uncertainty ellipses for the experiment results with $U^\star = 2.5$ and $\sigma = \pi/18$. 117
9.7 Actual and estimated positions for the field experiment results. Each measurement location is shown by a blue solid circle. Red squares show true target positions and black crosses show estimate positions. 118
9.8 Lake experiment: gathering bearing data on a windy day. 119
9.9 Actual and estimated positions for a lake experiment result. The measurement locations are denoted by square. While the diamond denotes true target position, the cross estimate position. 120
9.10 Two measurement regions. Green and red squares denote the desired and actual measurement locations, respectively. While green stars denote true target positions, red stars estimate position. The boat began from the location labeled with the yellow diamond and followed the yellow trajectory. The boundary of the measurement regions is denoted by dashed line. 121
10.1 The evader's simulation, which is used to find the final pursuer's location after time T, given measurement sequence B. The evader path is shown along with one possible pursuer path. The true bearing ($b^\star(t)$) and offset bearing ($b(t)$) are solid lines. 125

10.2 The pursuer starts location $p(0)$ and the evader at $e(0)$ separated by distance $d(0)$. After time T, the pursuer is in a closed disc C of radius T centered at $p(0)$. The key component of the evader strategy is to generate two motions which produce the same set of bearing measurements. Since the pursuer's strategy is deterministic (as a function of the bearing measurement), the evader knows which half of C the pursuer ends in (above or below the line $\overline{p(0)e(0)}$). If the pursuer is anywhere in the lower half of C, (shaded portion), the evader will be at location $e(T)$ (the other case is symmetric). The closest position the pursuer can take is at $p^\star(T)$, and the ending distance between the players is given by $d(T)$. 126

10.3 An illustration of Lemma 10.1: The angle $\widehat{axb}$, labelled $\beta(x)$, is maximized at the distance d along the perpendicular bisector of a and b. 128

10.4 An illustration of Lemma 10.2: An evader at position e or e' can generate the measurement $b(t)$ because the angle $\widehat{ep^\star e'}$ is less than 2α. 129

11.1 11.1a: The lion-and-man starting configuration (Note the boundary of the playing area is not shown. At the start of the game, the evader chooses his location diametrically opposite the pursuer's location inside a home region H. 11.1b: The three-phase strategy starts when the pursuer enters (or starts within) the *home region* H, a circle of radius R_α, or moves to within distance $2r$ of the evader. The boundary of the arena is assumed to be much larger than R_α, but is upper-bounded in Theorem 11.1. 11.1c After sufficiently increasing the distance between players (Phase 1), and inducing an angular offset (Phase 2) the evader dashes back to the home region, re-entering without being captured (Phase 3). 135

11.2 At the end of Phase 1 the pursuer p and evader e are separated by a distance d given in Corollary 1. At the start of Phase 2, the evader examines the angle θ. If $\theta > \frac{\alpha}{3}$ the evader can move on to Phase 3. Otherwise, he chooses his next move based on the next pursuer location, in region I, II, or III, as stated in Lemma 11.1. 136

11.3 11.3a and 11.3b By Lemma 11.1, the evader can choose to move to location e_1 or e_2, based on the pursuer's chosen location in region I or II, producing θ_1 or θ_2 greater than $\frac{\alpha}{3}$, respectively. If the pursuer moves to region III, the evader will remain at position e. 138
11.4 During Phase 2, the evader will move at an angle $\phi + \frac{\pi}{2}$, where ϕ is measured with respect to the line from the center of the circle to the point p. After Phase 2, the evader is at position e_2. Lemma 11.1 shows $\theta \geq \frac{\alpha}{3}$ and bounds $|p|$ and Lemma 11.2 bounds the distance from the center to e'. Note $\phi = \theta - \sin^{-1}\frac{r}{d}$ and d is chosen such to ensure $\phi > 0$. 140
11.5 The shaded region is $\Omega(p)$, the area covered by the pursuer at position p as defined in Definition 3. 144
11.6 Placing the pursuer on the lower dashed curve (defined by β and one step from p), will place the point $u(p')$ on the upper dashed curve. Two configurations are shown: $\beta = 0$ (blue) and $\beta = \frac{\pi}{2}$ (black). 145
11.7 Illustration of the "Feasible Region", defined in Definition 5. Before the evader's turn, it is known to be inside the covered region, $\Omega(p)$. After the evader's move the region is dilated by one step, forming E. At the start of the pursuer's turn, a bearing measurement, b is obtained. Since the bearing measurement may be adjusted by up to α by the evader, the evader may be within $\pm\alpha$ of the bearing measurement. Thus, the feasible region for the evader is the intersection of E and a cone of angular width 2α. 146
11.8 Separation of the cases in Lemma 11.3. The region I is a subset of $\Omega(p)$, such that all points in I are covered and have angle θ of less than $\tan^{-1}\left(\frac{r}{|p|+1}\right)$. If $F \subseteq I$ then the pursuer can make a single step outward to cover it. If, however, some point in F has a larger angle, then the pursuer must move with $\beta > 0$ to cover it, but no larger than $\frac{\pi}{2}$. 147
11.9 Case I: When the feasible region F is a subset of I (the set of covered points with "small" angle relative to $\overline{cp}$), the pursuer steps outward by one step to location p'. Now, $\Omega(p') = I$, and therefore all points in F are covered. 148

11.10Case IIa: When the feasible region F is above the line $\overline{cp}$. The pursuer moves vertically one step. A pursuer at p' covers all possible evader locations above the line $\overline{cp}$. It is proven that the line $\overline{cv(p)}$ passes below b, meaning all points in F are in $\Omega(p')$. 148
11.11Illustration of Case IIa. 11.11a: The definition of the point $e^\star$, and the regions E_1 and E_2. Note $E_1 \bigcup E_2 \bigcup \Omega(p)$ represents all possible evader locations after its move. 11.11b: With a move of $\beta = \frac{\pi}{2}$, the upper boundary of $\Omega(p')$, defined by the line $\overline{cu(p')}$ would pass above $e^\star$. In the proof, it is shown that $u(p')$ is on the arc between a and b, the points where the line $\overline{ce^\star}$ intersects the capture radius of the pursuer after the move to p'. 149
11.12Case IIb: When F straddles the line $\overline{cp}$. The point p' covers the point which lies outside of $\Omega(p)$ (shaded region) by moving to p' which places the upper anchor point, $u(p')$ on the line $\overline{ca}$. A pursuer making this move also covers all other points in F because the angle between a and b is less than the angle between $u(p')$ and $v(p')$. 151
11.13The pursuer can reach a radial distance of $\frac{r}{\tan\alpha}$ from the center while keeping the evader in the covered region. If the arena is no larger than this, the covered region falls entirely outside the arena, implying the pursuer must move into the capture region. 152

Chapter 1

Introduction

Modern industry owes a great deal of its success to robotics. From the first mechanized industrial processes—a programmable mechanical loom was controlled by punch cards as early as 1801— to the modern semiconductor industry, the precision, speed, and strength of robotic manipulators have enabled modern manufacturing processes to achieve an unparalleled efficiency. Because of the strong connection to industrial automation, the majority of robotic systems were, in the past, confined to static manipulation tasks, such as welding car parts or fabricating circuit boards.

Thanks to advances in miniaturization, computing power, reliable sensors, battery life, and decades of research on the algorithms necessary to use these technologies, we are now in the midst of a fast-paced transition from the controlled factory floor to the less-predictable world of outdoor applications. Mining and agriculture are poised to be the next "outdoor factories" which are revolutionized by the availability of inexpensive and reliable robotic systems. In these settings, robots must act side-by-side with human operators, making decisions in a semi-autonomous way while acting with the same predictability, speed, and precision that is important in traditional production environments.

We see the early successes of this transition in autonomous vehicles that are already being used for point-to-point delivery in mining operations [2]. Similarly, Kiva Systems automates the fetching of goods in warehouse environments to enable greater efficiency for Amazon's human workforce [3]. A wide range of companies are developing autonomous vehicles for use on roadways. Even the robotic systems on the surface of

Mars are capable of making occasional path planning decisions without human input [4].

These applications are classified as semi-autonomous because the robots can make small adjustments to their paths e.g., to avoid collisions or save energy. However, in every example we see today, the robot is led and supervised by a human operator, which stands ready to interrupt in case of error or provide new objectives. The autonomy of today is mostly dedicated to lessening the responsibilities of humans, instead of removing them.

Greater autonomy can open up the next set of great problems in domains where human intervention and supervision is not possible or desirable. In radioactive disaster areas, the deeper reaches of the solar system, or the bottom of the oceans, it is often extremely challenging, if not impossible, to send a human. Because we cannot send humans deep underwater, we know more about the surface of the moon than we do of the terrestrial ocean floor. Robots for remote sensing in these environments could provide the same scalability, precision, and reliability to environmental monitoring as they did to industrial manufacturing.

In the broad reaches of environmental monitoring, the conditions are not only unstructured, but also uncontrolled and unpredictable. For example, remote controlled boats are used to monitor bodies of water for algae blooms, which form quickly and unpredictably and are toxic to animal and plant life. Aircraft are used to monitor forests for new fires which can break out spontaneously and spread quickly. In another example, scientists spend hours in boats tracking the low-powered radio transmission from radio-tagged invasive fish and waiting for them to aggregate.

The constant human vigilance required to continuously monitor the environment for these fast-acting occurrences limits the scalability of human-controlled remote sensing. What is needed is a new class of autonomous systems: those capable of searching for and detecting the phenomena of interest, adapting their actions accordingly, and intervening to collect the information necessary quickly, and all without human intervention.

In these settings the machine must be able to not only alter its behavior to suit the environment (obstacle avoidance, energy optimization, etc), but must *decide* on the next best action by taking into account battery life, mission statements, or sensing and actuation capabilities. These *active* robots are not just helping a human, they can truly do the job on their own in an adaptive form.

In this thesis we study how to enable this level of autonomy in a fundamental problem setting: target localization. In target localization, the goal is to estimate the position of a target in the environment. The target could take any form, e.g., a hostile robot, lost human, flight recorder, algae bloom, or protected wildlife. Specifically, we study how a robot can decide how to act so as to gain the required information about the target as quickly as possible. This problem remains challenging because the sensing capabilities of the robot are heavily dependent on the position of the sensor with respect to the target. To quickly locate a target, the robot must seek informative measurement locations relative to the *actual location* of the target. This is not simple when only a rough estimate of the target's location is known, if any estimate is available at all. This chicken-and-egg problem of planning informative paths to locate a target in the face of uncertainty about its location is what we call the *Active Localization Problem*, and forms the core study of this thesis.

From a technical standpoint, we focus on *competitiveness*. In many cases, we are able to show that through careful design of a sensor's trajectory, the resulting estimate of the target (or the time required to reach such an estimate) is always close to the best possible. Our work is thus considered competitive with respect to any algorithm. We accomplish this by establishing bounds on the optimal solution. When the absolute best solution is not available, a bound on its cost can still be derived, allowing direct comparison to our algorithms.

We do not settle with theoretical analysis; it is important to test the validity of the assumptions and models in real-world deployments. Thus, a second major contribution of this thesis is extensive field tests of our results. While the applications of target localization are widespread, we ground our study in a particular environmental monitoring application. We develop both hardware and software for an autonomous robot to search lakes for aggregations of invasive fish, in particular the common carp.

The common carp is an ecologically damaging freshwater fish found in many regions around the world [5]. Biologists are interested in developing efficient methods for controlling carp populations. To this end, they catch a small sample of the population and implant each fish with radio transmitters (tags). These tagged fish are reintroduced to the lakes and periodically tracked using radio receivers over the course of a year. When multiple tagged fish seem to aggregate, it is assumed a larger population is nearby.

Figure 1.1: Our robotic system consists of radio tags, a radio antenna and receiver mounted on autonomous boat in summer and wheeled rover in winter (to operate on frozen lakes).

When these large aggregations of carp are found, typically during the winter, they can be removed by netting. This provides a safe and environmentally-friendly method for controlling the population of carp.

The radio tags (Figure 1.1) are small, low duty-cycle transmitters which are implanted into the skin of the fish. Each tag emits a pulsed signal on a dedicated frequency approximately once per second. A human operator carries a loop antenna and a receiver which converts the signal to a Received Signal Strength Indicator (RSSI). By monitoring the RSSI and rotating a directionally sensitive antenna, the operator can discern a bearing to the radio tag. Typically a human operator will take 2-3 bearing measurements to estimate the location of one tag. However, this manual tracking approach is tedious, time consuming and possibly inaccurate at times. By deploying robots to locate the fish, we hope to enable greater precision in the fish estimates, more quickly, and by keeping robots deployed long term, more often.

Thus, the thesis contains two major contributions: First, detailed algorithmic studies of what is possible using bearing sensors, and second, a verification that the models, assumptions, and methods developed are useful for real world environments.

We organize the rest of the text as follows. We first discuss the detailed contributions and provide an outline for subsequent chapters. In the next chapter, we review the details of the robotic system used in field trials. Chapter 3 is dedicated to defining the problems studied precisely, and reviewing necessary background material. In Chapter 4 we review the prior literature and position this thesis with respect to existing work.

Chapters 5 to 8 are dedicated to localizing stationary targets using one or more mobile, robotic bearing sensors like those shown in Figure 1.1. In Chapter 9 we formulate the localization of many targets as a coverage problem, and provide a near-optimal solution. In Chapters 10 and 11 we discuss the more difficult problem of localizing and capturing a target which is trying to evade the robot.

1.1 Contributions

In this section, we briefly present an overview of Chapters 5 through 11.

1.1.1 Target Localization with a Single Bearing Sensor

In Chapter 5, we study the problem of optimally choosing bearing measurement locations for localizing a stationary target in minimum time. The targets are transmitting radio tags, the same kind used to locate invasive fish, and bearing measurements are acquired from radio signal strength by a robot carrying a direction-sensitive radio antenna.

An active localization algorithm is provided in order to locate a target up to desired uncertainty. The time required to locate the target includes time spent in traveling as well as taking measurements. Since bearing measurements inferred from radio signals have an inherent ambiguity associated with them, the proposed algorithm chooses measurements to minimize the effect of ambiguous measurements on the target estimate.

We present a closed-form bound on the time required to locate a target using the presented active localization strategy. We also present the first known lower bound on the time required by any active localization algorithm (including the unknown optimal). Finally, we bound the ratio of the upper and lower bounds, showing the expected cost of our algorithm is within a constant factor of the expected cost of the optimal solution. Our algorithm is shown to reliably locate radio tags to a desired uncertainty in simulations and multiple field experiments.

1.1.2 Time Bounds For Cooperative Localization

In Chapter 6 and 7, we study the problem of actively locating a static target using mobile robots equipped with bearing sensors. As in Chapter 5, the goal is to reduce

the uncertainty in the target's location to a value below a given threshold in minimum time. Because of the possibility of using many robots in collaboration, we also consider distance-based communication constraints between the robots.

We provide the following theoretical results. First, we study the properties of an optimal offline strategy for one or more robots with access to the target's true location. We derive the optimal offline algorithm and bound its cost when considering a single robot or an even number of robots. In other cases, we provide a close approximation. Our algorithm is shown to be adaptive to any distance-based communication constraint. Surprisingly, we show that the optimal algorithm will occasionally break communication to establish more informative measurements before bringing the robots back together to synchronize their estimates.

Chapter 7, provides a general method of converting the offline algorithm into an online, adaptive algorithm (that does not have access to the target's true location) while preserving near optimality. Combined with the previous offline algorithm, we present an online strategy proven to locate the target up to a desired uncertainty level at near-optimal cost. In addition to theoretical analysis, we validate the algorithm in simulations and multiple field experiments performed using autonomous surface vehicles carrying radio antennas to localize radio tags.

1.1.3 Multi-Target Initialization and Localization for Closely Clustered Targets

The problem studied in Chapter 8 lies at the intersection of search-based methods whose objective is to detect a target, and active target localization methods whose objective is to precisely localize a target given its initial estimate. Real-world sensing constraints such as limited and unknown range, large measurement time, and ambiguity in bearing measurements make it imperative to have an intermediate initialization phase to transition from search to localization. We present a local search strategy aimed at reliably initializing an estimate for a single target based on observations from field experiments. We then extend this strategy to initialize multiple targets, exploiting the proximity of nearby aggregated tagged fish to decrease the cost of initialization per target. Finally, the single-target algorithm from Chapter 5 is used to adaptively select measurement locations to localize each target precisely. We evaluate the performance of

our algorithm through simulations and demonstrate its utility through a field experiment where the robot successfully detects, initializes and then localizes nearby targets in real-world conditions on a frozen lake.

The results of Chapter 8 are extended in Chapter 9. We present a novel coverage problem wherein a robot must take measurements from a set of positions such that if a target is within a bounded region it is guaranteed to be localized to within desired precision. This is accomplished by formulating a novel coverage problem, which we call the data gathering problem. It is shown that without any prior knowledge of target locations, it is possible to design a measurement set and trajectory so that any target is localized and the travel time is near optimal. These results are also validated in simulation and field experiments.

1.1.4 Geometric Sensing Model and Pursuit Evasion Games

Chapters 10 and 11 are dedicated to the study localizing a moving target. In particular, we study the effect of adversarial motion and sensing on the objective. The target is modelled as an evader which moves to avoid the robot. The robot tries to move to within a specified distance of the target. By modelling the target as an evader, if the robot is able to succeed, then the strategy used by the robot is guaranteed to work against any other motion employed by the target. Such formulations are often called pursuit-evasion games.

In this context, we investigate how the sensing capability of the pursuer affects the game outcome. In particular, we consider a pursuer which can sense only the bearing to an evader. Furthermore, the measurements are uncertain in that the evader may adjust each bearing measured by an angle up to α away from the true value.

We consider two classical pursuit evasion games under this bearing uncertainty model. The first game is played on the open plane (Chapter 10). The pursuer tries to maintain the distance to an evader with equal speed. If the pursuer has full knowledge of the evader's location the pursuer can maintain the separation between the players by moving toward the evader. However, when an adversarial sensing model is introduced, we show that for any pursuer strategy, the evader can increase the distance to the pursuer indefinitely. The rate at which the distance increases is linear in time.

In the second game (Chapter 11), both players are inside a bounded circular area.

This version is known as the Lion-and-Man game, and has been well studied when no sensing limitations are imposed. In particular, the pursuer (lion) is known to have an $O(\frac{R}{r}\log\frac{R}{r})$ strategy to capture the evader (man), where R is the radius of the circle and r is the capture radius of the pursuer. In contrast, when sensing uncertainty is introduced, we show that large sensing uncertainty and large environments enable the evader to win the game, while reducing either the sensor uncertainty or the size of the environment tips the game back into the pursuer's favor.

The rest of the paper is organized as follows. The next chapter introduces the robotic system used in our field experiments. Chapter 3 covers the necessary background material and builds up a formal problem definition. In Chapter 4, we review the existing literature. Chapters 5–11 are dedicated to the technical contributions listed above. We conclude with Chapter 12 which identifies open problems and discusses future research directions.

The work presented in this thesis appears in [6–11] and was funded by NSF#1111638, #0917676, #1317788.

Chapter 2

System Description

In Chapter 1 we have discussed the field application which grounds our theoretical studies in a real-world setting. A major component of this field work is the development of a working robotic system for localizing radio-tagged fish. As such, we have been developing a robotic system (Figure 1.1) to enable a mobile sensor network to monitor the common carp (Cyprinus carpio), an invasive fish. In this chapter, we discuss the details of our system.

Our platform, shown in Figure 5.11, is composed of an autonomous vehicle and directional antenna mounted on a servo motor. During the summer, we use autonomous boats, and in the winter an autonomous rover drives over the ice (Figure 2.2). During winter, the chassis is a Clearpath Robotics Husky A100 [12]. The Husky has a maximum velocity of less than 2m/s. Typically, we operate at 1m/s. The summer-time aquatic robots used were OceanScience QBoats, pictured in Figure 2.1. Although designed for remote operation, the boats were augmented with on-board laptops and motor control boards for autonomous navigation, and pan-tilt servos, antennas, and real-time spectral analyzers to produce bearing measurements. They are 2 meters in length and have an average speed of 1 meter per second.

The antenna and an example tag are shown in Figure 5.11 and were developed by Advanced Telemetry Systems [13]. The radio tags operate in the 48-50 MHz range and emit an uncoded pulse at approximately 1.1 Hz. These transmissions are detectable from approximately 100 meters, but the sensing range can be very low if the tag is far underwater. It is possible to determine if a target is nearby simply by sampling a

Figure 2.1: The robotic systems used in field experiments. The 2-meter boats were designed to track invasive fish autonomously. Each is equipped with wireless communications, directional antenna used as bearing sensors, a navigation suite, and computing hardware. Our algorithm was implemented on this system and was shown to localize targets to within small uncertainty.

non-zero signal strength indicator. The radio tags are detected by attaching a real-time spectrum analyzer to the antenna. We use the SignalHound BB60A [14].

We operate on lakes which have 10-20 tagged fish and the list of frequencies present in each lake is known a priori. Signals from the tags attenuate as a function of the humidity, salinity of the water, ice or snow thickness, and the depth of the fish it is attached to. These factors cause variations in the range at which tags can be detected. Therefore we do not use the absolute signal strength to estimate range, and instead use the directional nature of the antenna to estimate bearing. In practice this is accomplished by rotating the antenna to find the orientation which corresponds to the maximum Received Signal Strength Indicator (RSSI). We typically sample every 15°. To find a bearing with maximum signal strength which does not lie directly on a sampled orientation, we fit a polynomial to the samples and solve for the bearing of maximum signal strength as shown in [15]. We have established from field trials that the process of taking a reliable bearing measurement requires approximately 1-2 minutes.

By placing radio transmitters in known locations and repeating the bearing measurement process we can estimate the accuracy of the received bearings. Using the data set gathered in [7, 15] we have established that the measurements have approximately a

Gaussian error of $\sigma_s \approx 15°$. Of particular importance in RSSI-based bearing measurements is the symmetry of the antenna. Since the antenna is symmetric, the true bearing is unknown. Instead, the inferred bearing could point toward or away from the target. For any estimated bearing z, $z + \pi$ is also a valid bearing measurement. We show how to address this issue in Chapter 5.

The robots estimate their own pose and navigate using an Extended Kalman Filter (EKF) combining information from a Global Positioning System unit and a digital compass (on the boat) or encoders (on the wheeled rover). The robots have approximately a six hour battery life and have been deployed on autonomous coverage patters of up to 6km while searching for invasive fish [16].

An on-board laptop computer controls the majority of the high-level planning. Our software architecture is based on the Robot Operating System [17]. We have developed waypoint navigation, closed-loop control for the two chassis types, and the high-level path planning algorithms described in this dissertation.

Figure 2.2: The two ground rovers used in field trials over frozen lakes.

In Chapter 7 we use multiple robots to locate stationary targets. To allow the robots to communicate their target estimates, we have added two primary inter-robot communication channels. First, A ZigBee radio can provide low-bandwidth communication for up to one kilometer. Second, a wifi network connects the robots and a base station.

In the rest of the thesis, this system is used to verify the algorithms developed for localizing radio-tagged fish. Experiments were performed in the winter and summer

months on lakes near the University of Minnesota. The lakes were shallow, fresh-water parks with radio-tagged carp present. Our goal is to localize radio-tagged invasive fish. As such, we develop algorithms which can move the robots described in this section to measurement locations which provide the necessary information about a radio transmitter's position in the lake. A key component of this process is the method used to estimate the target's location given the measurements. In the next section, we review common methods for *filtering* the measurements to produce an accurate estimate of the location of the radio tag.

Chapter 3

Technical Background and Problem Definitions

In Chapter 1 it was mentioned that fish biologists use direction-sensitive antennas to estimate the bearing to a radio-tagged fish. In the previous chapter we discussed the system we have been building which can replicate and automate this process. However, the accuracy of the fish location's estimate is dependent on the method used to combine the bearing measurements.

Therefore, in this chapter we introduce the notation and provide a review of the material on which the thesis is built. We first cover the notation and measurement model. Then, we discuss the filtering methods used to estimate the target location. Following this, we show how we use the Fisher Information Matrix to quantify the quality of the target estimate. Finally, we formalize the active-localization problem in Section 3.3.

Our problem concerns locating targets in the two dimensional plane. For a given point p, its coordinates in the plane are given by $p(1)$ and $p(2)$. A target is located in the two dimensional environment at position $x^\star$. A robotic bearing sensor can take a bearing measurement. The point at which the sensor takes the i^{th} measurement is denoted s_i. The measurement value obtained will be labelled z_i. If there is more than one sensor operating in the environment, we label the i^{th} measurement location for robot u as $s_{u,i}$ (similarly $z_{u,i}$ for measurement values). When the time index is clear from context, we

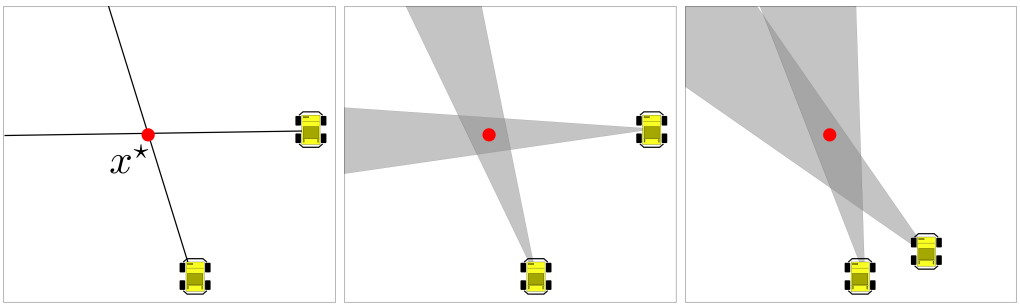

(a) (b) (c)

Figure 3.1: Example of the bearing-only localization task. A robot takes two measurements of a stationary target at the red dot. If there is no noise in the measurements, the target is perfectly localized as long as the measurement locations are not collinear with the target (3.1a). If there is some noise on the measurements, the target could be anywhere within the dark shaded region with high probability (3.1b). If the measurement locations are closer together, two measurements produces a much larger area that the target could be in. The *active localization* problem is to choose measurement locations which are not spread too far, but produce low uncertainty.

will simply specify s_u and z_u for a particular robot u. For convenience and to simplify many equations, the robot positions $s_{u,i}$ will be specified in a coordinate frame centered on the true target location, and in polar coordinates. Thus, $s_{u,i} = (r_{u,i}, \alpha_{u,i})$, where $r_{u,i}$ is the range to the target and $\alpha_{u,i}$ is the angle of the line passing between the sensor and target.

When the sensor takes a bearing measurement, it measures the direction to the target. As illustrated in Figure 3.1a, two such measurements are enough to localize any target, as long as the two measurement locations are not collinear with the target. However, in practical applications, the bearing measured is not the true bearing, but is instead an estimate of the bearing. In all but Chapters 10 and 11, we will assume that the robot receives a bearing of the form

$$z = h(s_i, x^\star) + \eta \tag{3.1}$$

where, η is a Gaussian random variable with known variance σ^2 and,

$$h(s_i, x^\star) = \tan^{-1}\left(\frac{x^\star(2) - s(2)}{x^\star(1) - s(1)}\right) \tag{3.2}$$

is called the *measurement function*. The full sequence of N_u measurement locations for robot u is $S_u = \{s_{u,1}, \cdots, s_{u,N_u}\}$. S is the union of all measurement locations taken by all robots, and $N = |S|$ is the total number of measurements taken among all robots. The values are similarly $\mathcal{Z}_u = \{z_{u,1}, \cdots, z_{u,N_u}\}$ for a particular robot u and $\mathcal{Z}$ for the set of all measurement values. We use the notation $d(a, b)$ for the Euclidean distance between points a and b. Without loss of generality, we assume that traveling between locations a and b takes $d(a, b)$ units of time.

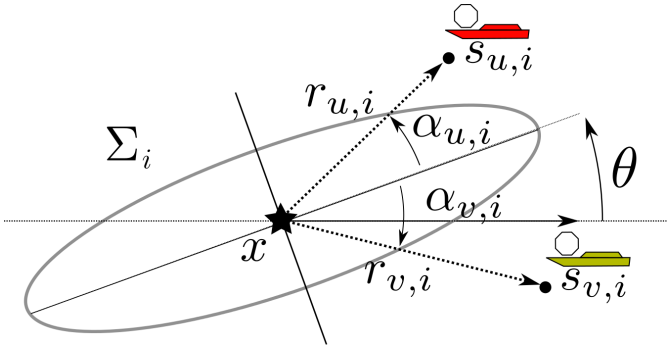

Figure 3.2: The notation and problem formulation. The robots take their i^{th} measurement from location $s_{u,i}$. Each location is described in polar coordinates $(r_{u,i}, \alpha_{u,i})$. For much of the thesis, the coordinate frame is fixed to the target location and oriented with respect to the current covariance. Thus, $r_{u,i}$ is the range from the sensor to the current hypothesis, $\hat{x}_i$, and $\alpha_{u,i}$ denotes the orientation with respect to the line formed by the major axis of the covariance ellipse, Σ_i, with eigenvalues $\sigma_{x,i}$ and $\sigma_{y,i}$ and orientation θ_i with respect to a global frame.

In practice, the process of estimating the distribution of the measurements around the true value is known as calibration. We have calibrated our bearing sensor and determined that Gaussian noise is a good fit, and $\sigma = \frac{\pi}{12}$. See, for example, Figure 3.3.

When the bearing measurements are not exact, some method must be used to estimate the target's position from the noisy bearing measurements. For any point x we can estimate the probability that $x = x^\star$ by evaluating the probability that the measurements are centered around x. This is the *filtering* task. A filter returns a Probability Density Function which estimates the likelihood of the target being at a given location.

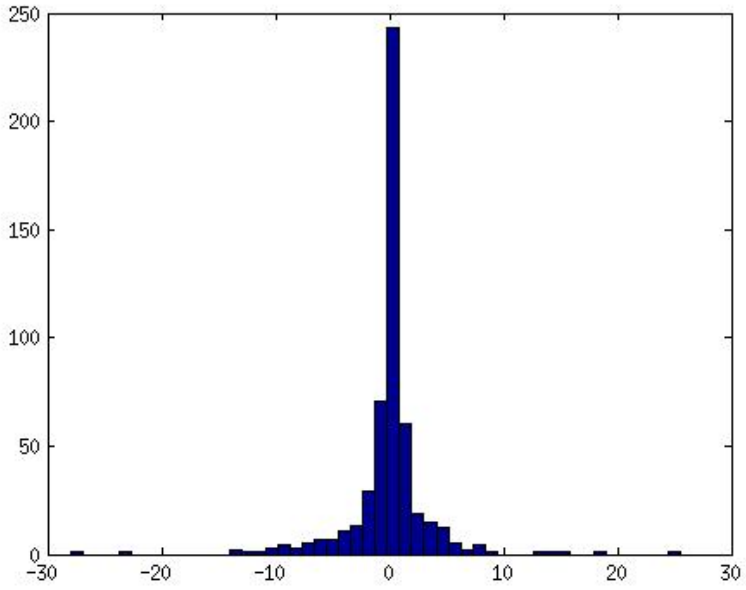

Figure 3.3: By repeatededly taking bearing measurements of tags deployed in known locations, we can accumulate the error profile for the bearing measurements, a process known as calibration. Shown here is one such trial. The error is verified to be zero-mean and roughly Gaussian.

3.1 Filtering Methods

The most common way to estimate the target's location is to find the point $\hat{x}$ which best agrees with the measurements, given knowledge of the measurement noise. That is, $\hat{x}$ is the *maximum likelihood* estimate, given by,

$$\hat{x} = \arg\max_{x} \mathcal{L}(x, \mathcal{Z}, S) \tag{3.3}$$

where $\mathcal{L}$ is the *likelihood* function, S is the set of measurement locations, and $\mathcal{Z}$ is the set of measurements obtained. The function $\mathcal{L}$ determines the probability of a given measurement set Z, given a candidate target location x and sensor locations S.

The uncertainty of the estimate depends on the filter used, sensor configuration, and true target position and is measured by the covariance matrix of its Probability Density Function, Σ. The covariance, or expected error, is given by the following.

$$\Sigma = \mathbb{E}_x ||x - \hat{x}||^2 \tag{3.4}$$

where $\mathbb{E}_x$ is the expectation taken over the PDF returned by the filter. Since we deal with a two dimensional state vector x, the covariance is a 2×2 matrix. The matrix Σ is Positive Semi-Definite and has the following diagonalization [18].

$$\Sigma = R(\theta) \begin{bmatrix} \sigma_x^2 & 0 \\ 0 & \sigma_y^2 \end{bmatrix} R(\theta)^T \tag{3.5}$$

Note, $R(\theta)$ is a two dimensional rotation matrix of angle θ, and without loss of generality, $\sigma_x^2 \geq \sigma_y^2 \geq 0$.

The covariance matrix will depend on the type of estimation filter used, since some use more restrictive approximations of the likelihood function.

An often used estimator (and one we employ in Chapter 5) is the Extended Kalman Filter (EKF). Given a prior target estimate, $\hat{x}_i$, a covariance of the estimate, Σ_i, a bearing measurement z_i, and a known sensor noise σ, we can form the posterior estimate, $\hat{x}_{i+1}$ and covariance Σ_{i+1} using the EKF update equations. The equations that describe the steps of the EKF updates are [19],

$$\hat{x}_{i+1} = \hat{x}_i + K_i y(i) \tag{3.6}$$

$$\Sigma_{i+1} = \Sigma_i - \Sigma_i \left(H_i^T R_i^{-1} H_i \right) \Sigma_i \tag{3.7}$$

with:

$$R_i = H_i \Sigma_i H_i^T + \sigma^2 \tag{3.8}$$
$$K_i = \Sigma_{i-1} H_i^T R_i^{-1}$$
$$y_i = z_i - h(\hat{x}_i, s_i)$$

The H matrix is the Jacobian of the measurement function. Given the form of the measurements from Eq (3.2), the Jacobian satisfies,

$$H_i = \left[\frac{\partial}{\partial x(1)} h(s_i, x^\star) \quad \frac{\partial}{\partial x(2)} h(s_i, x^\star) \right] \tag{3.9}$$
$$= \left[\frac{s(2)-x(2)}{r_i^2} \quad \frac{x(1)-s(1)}{r_i^2} \right] \tag{3.10}$$

Since the target's location, $x^\star$ is not known, in practice, h is linearized with respect to the current best estimate.

By setting the target estimate (or true, if known) at the origin of the coordinate frame and specifying the sensor locations in polar coordinates as shown in Figure 3.2, H becomes,

$$H_i = \nabla_{\hat{x}_i} h(\hat{x}_i, s_i) = \frac{1}{r_i} \left[-\sin \alpha_i \quad \cos \alpha_i \right] \tag{3.11}$$

As noted by [20], the covariance update step (Eq (3.7)) can be rearranged to a more convenient form by applying the matrix inversion lemma to Eq (3.7). The alternative update is used in a filter known as the Extended Information Filter.

$$\Sigma_{i+1}^{-1} = \Sigma_i^{-1} + \frac{1}{r_i^2 \sigma^2} \begin{bmatrix} \sin^2 \alpha_i & -\sin \alpha_i \cdot \cos \alpha_i \\ -\sin \alpha_i \cdot \cos \alpha_i & \cos^2 \alpha_i \end{bmatrix} \tag{3.12}$$

The EKF is attractive in part because only one vector and covariance matrix need to be maintained, since it is assumed $\hat{x}$ incorporates all prior measurements. Thus, it is known as a recursive filter. However, it can suffer from *consistency* issues for a number of reasons. One key reason is the H matrices are not necessarily linearized at the correct points, and without keeping the measurement values and sensor locations the matrices cannot be re-linearized when the target state is updated. In addition, the EKF has a measurement-ordering dependency, meaning if the state is updated with two measurements but in different orders, the target estimate and covariance may be very different.

A more expensive, but in practice more robust filtering method can be obtained by keeping the entire measurement sequence and maximizing the full likelihood. Methods which operate on the entire measurement sequence are known as *batch* filters.

If the entire measurement sequence is saved and an initial guess is available as $\hat{x}_0$, then an estimate of $x^\star$ can be obtained by iterating the following equation.

$$\hat{x}_{i+1} = \hat{x}_i + \left(\sum_{i=1}^{N} \frac{1}{\sigma^2} H_i^T H_i \right)^{-1} \left(\sum_{i=1}^{N} \frac{1}{\sigma^2} H_i^T (z_i - h(\hat{x}_i, s_i)) \right) \tag{3.13}$$

At each iteration the H_i matrices are re-evaluated using the current best guess of the target's location. The iteration is continued until the difference, $||\hat{x}_{i+1} - \hat{x}_i||$ is sufficiently small. This method can be computationally difficult if a very large number of measurements are used, or if the state size of $\hat{x}$ (and thus the size of H_i is large). The covariance of the resulting estimate is given by,

$$\Sigma^{-1} = \sum_{i=1}^{N} \frac{1}{\sigma^2} H_i^T H_i. \tag{3.14}$$

In practice, when several robots collaborate to estimate a target's location, the robots store their individual measurements sequences. When the robots meet, they form the union of their measurements, and use the previous method to estimate the target location.

Given an estimation framework, it is important to measure the quality of the target estimate. Since we seek to localize a target, the uncertainty of the target's location is a natural metric to consider.

3.2 Quality of Estimator Output

In literature, several metrics of this type have been proposed. For a given probability density function which describes the target's possible locations, the covariance is almost ubiquitous as the metric of choice. A fundamental result in estimation literature is given by the Cramer-Rao Lower Bound ($\mathbb{C}$) [21]. The CRLB is the *minimum possible covariance* of any unbiased estimator (c.f. Chapter 2.7 in [19]). The CRLB is defined as the inverse of the Fisher Information Matrix (FIM) which is defined with respect to the true target location ($x^\star$), and measurement locations (S) as $\mathbb{F}(S, x^\star)$ or simply

$\mathbb{F}(S)$. The FIM for a single measurement of the vector x has each (i,j) element given with respect to the i^{th} element of x as follows.

$$\mathbb{F}(i,j) = \mathbb{E}\left[\frac{\partial}{\partial x(i)} \ln\left(\mathcal{L}(s,x)\right) \frac{\partial}{\partial x(j)} \ln\left(\mathcal{L}(s,x)\right)\right] \tag{3.15}$$

Because $\mathcal{L}(s_i, x^\star)$ is distributed according to a Gaussian PDF with mean $\tan^{-1}\frac{x^\star(2)-s(2)}{x^\star(1)-s(1)}$ and variance σ^2, the FIM for a single measurement location becomes,

$$\mathbb{F}(s, x^\star) = H_i^T H_i \tag{3.16}$$

where H_i is the Jacobian of the measurement equation with respect to $x^\star$ from Eq (3.11) [22].

Given a true target location $x^\star$, and measurement locations S, it is possible using the CRLB to derive the expected distance between the true target and the output of an estimator used to process the bearing measurements, Z received at the locations S. This is known as the *true* covariance. It is defined as follows.

$$\mathbb{C}^{-1} = \mathbb{F}(S) \tag{3.17}$$

$$= \sum_{i=1}^{N} \mathbb{F}(s_i, x^\star) \tag{3.18}$$

$$= \sum_{i=1}^{N} \frac{1}{\sigma^2} H_i^T H_i \tag{3.19}$$

If we again adjust the coordinate frame so that $x^\star$ is at the origin, then $\mathbb{F}$ reduces to the following.

$$\mathbb{C}^{-1} = \mathbb{F}(S) = \sum_{i=1}^{N} \frac{1}{r_i^2 \sigma^2} \begin{bmatrix} \sin^2\alpha_i & -\sin\alpha_i \cdot \cos\alpha_i \\ -\sin\alpha_i \cdot \cos\alpha_i & \cos^2\alpha_i \end{bmatrix} \tag{3.20}$$

If $\mathbb{F}$ is rank-deficient, then no efficient estimator exists with finite variance for the given observation sequence and target x.

The only difference between the covariance of the EKF output (Eq (3.12)), the batch filter (Eq (3.14)), and the CRLB (Eq (3.19)) is the choice of H_i, i.e., the target estimate. Thus, if all the Jacobians, H_i, are evaluated at the true target location, then the covariances from the EKF and batch filter will match the CRLB. A filter outputting a covariance matching the CRLB is known as *efficient*.

3.3 Active Localization Problem Formulation

Our goal in all localization tasks is to constrain the maximum diameter of the true covariance of the target estimate, i.e., the maximum eigenvalue of $\mathbb{F}^{-1}$, denoted by $\bar{\lambda}\mathbb{F}^{-1}$. Other commonly used measures are the determinant and trace. Note that by bounding $\bar{\lambda}$ we also bound the determinant as $\bar{\lambda}^2$ and the trace as $2 \cdot \bar{\lambda}$.

The total time spent by robot u for localization is the time required to travel to each point where the robot takes a measurement plus the measurement cost (for example, in seconds):

$$C(S_u) = t_m \cdot N_u + \frac{1}{v}\text{len}(S_u) \tag{3.21}$$

where $\text{len}(S_u)$=$\sum_{i=1}^{N_u} d(s_{u,i}, s_{u,i-1})$, and v is the velocity of the robot. We assume unit velocity where v is not given.

Each measurement a robot takes requires a fixed amount of time t_m, and is corrupted by zero-mean Gaussian noise with variance σ^2.

Since $\mathbb{F}$ is the inverse of the uncertainty, and the eigenvalues of a matrix inverse are the inverse of the matrix eigenvalues, our information constraint is given by the minimum eigenvalue,

$$\underline{\lambda}\mathbb{F}(S, x^\star) \geq \lambda_d \tag{3.22}$$

For brevity, $\underline{\lambda}\mathbb{F}(S)$ is used whenever the position, $x^\star$, does not change.

Here λ_d defines the requested precision (information) in the final estimate. For example, in our application, it is desirable to obtain estimates accurate to 5 meter resolution ($\sqrt{\bar{\lambda}\Sigma} = 5m$), so λ_d is equal to $1/25$ during field experiments.

We formally state the problem solved in Chapters 5 through 9 as follows.

Problem 1 (Active Target Localization for Stationary Targets)**.** *Given n mobile robots, find a sequence (S_u) of measurement locations ($s_{u,i}$ for $i = 1$ to N_u) for each robot u, such that the maximum cost,*

$$\max_u C_u = N_u t_m + \sum_{i=1}^{N_u} \frac{1}{v} d(s_{i,u}, s_{i-1,u}) \tag{3.23}$$

is minimized. Furthermore, the measurement locations must satisfy,

$$\underline{\lambda}\mathbb{F}(S, x^\star) \geq \lambda_d \tag{3.24}$$

where $\mathbb{F}(S, x^\star)$ is the Fisher Information Matrix resulting from all measurement locations S, evaluated with respect to the true target location $x^\star$, and $\underline{\lambda}A$ is the minimum eigenvalue of the matrix A.

In Chapter 5, we will address a special case of Problem 1 for the case of one robot and using an EKF to estimate the target location. Beginning in Chapter 6, an arbitrary number of collaborating robots are considered, and a distance-based communication constraint (which states that the robots may not communicate unless they are within a given distance r_c) will be introduced. If the robots do not communicate the results of their measurements, they cannot form a joint estimate of the target's position. Thus, the uncertainty in target estimate is a function of the measurements gathered up to the last time the robots met.

Note, the Active Localization problems described here are quite difficult to pose as general optimization problems for the following reasons.

1. N is unknown. The objective function requires minimizing the size of the measurement sequence, as well as the displacement between measurements. This is especially crucial when the measurement time t_m is non-negligible. As we will see in the next section, previous literature often assumes a fixed N, corresponding to a fixed time horizon.

2. We wish to find or approximate the *global* optimal solution. A gradient-based search may find a local minimum which satisfies the constraints but cannot make any statements about convergence relative to global optimality. A *search* for the global optimal strategy is exponential in N, and therefore infeasible.

3. We cannot assume a constant time interval between measurements. In the next chapter we show this assumption is commonly used but is not valid for the problem of choosing discrete measurement locations.

4. In Chapter 5, each bearing measurement is ambiguous. The bi-modal nature of the radio bearing measurements complicates the filtering process. In the worst case, an exponential number of hypotheses must be maintained.

With the problems clearly stated, we are ready to position this thesis with respect to the existing literature.

Chapter 4

Related Works

In this chapter we position the thesis with respect to relevant literature. We break the literature roughly into six categories, each of which influenced this work in different ways. The first section provides references for the bearing-only estimation problem. Next, in Section 4.2, the relevant results in Active Localization are discussed, including communication constraints in Section 4.3. Results in planning coverage algorithms to detect radio transmitters are relevant to Chapter 9 and are presented in Section 4.4. Finally, pursuit-evasion games are surveyed in Section 4.6.

4.1 Sensing and Estimation

In *active localization*, the objective is to decide where to take measurements to maximize the performance of a given estimator. Tracking and estimation literature takes a passive approach: the task is to design an estimator which is robust when given arbitrary measurements. In particular, the problem of estimating a track for a maneuvering target using bearing-only measurements has been well studied (e.g., [23–33]). However, designing an estimator does not address the problem of choosing good measurement locations. Thus, work on improved filter design would be orthogonal, but easily incorporated into this work. Much of the technical background for tracking and estimation literature is covered in [19–21].

In Chapter 5, we discuss how to structure a measurement sequence to deal with ambiguous bearing measurements. Previously, [34] considered ambiguous, radio-based

measurements in the context of cooperative localization for teams of mobile robots. A Multi-Hypothesis Extended Kalman Filter was used and it was shown that the robots' motion could disambiguate the hypotheses. However, no *active* motion strategy was provided. Similarly, [35] designed a particle filter-based estimator for disambiguating the *sign* of the bearing measurement toward a transmitting tag embedded on leopard sharks, but active localization was not considered.

4.2 Active Localization using Bearing Measurements

Most active-tracking algorithms can be classified as locally optimal, gradient-ascent (e.g., work by Grocholsky et al. [22] or Zhou and Roumeliotis [36]). Another approach is track enumeration (e.g., Frew et al. [37,38]). The work in [38] searches over the action space for a feasible sensor trajectory. Passerieux [39] and Oshman [40] numerically optimized sensor trajectories given a maneuvering target with known location. These works do not bound the cost of the resulting trajectories and did not take into account measurement time or information constraints.

Hoffmann [41] explored such an objective, though their main contribution was a distributed approximation for the mutual information between the sensors and target, which is not applicable to this work, since a single robot will visit all measurement locations. Frew [42] provided a fixed-horizon optimization for the so-called Fixed Information, Minimum Time problem. In these works no global optimality conditions were explored and no time bounds were given for the algorithms. Additionally, we relax the constraint of fixed travel time (or constant distance) between measurements.

A novel aspect of our formulation is that we optimize the trajectory of the robots with respect to the measurement cost *and* the distance traveled. Incorporating measurement time is relevant in a variety of real-world problem settings. In the fish-tracking application, we previously used sensors to sample radio signal strength over one to two minutes to discern the bearing toward the target [6, 15, 16]. Another possible measurement cost is local maneuvers during a measurement. For example, Derenick et al. [34] used rotations in the robot chassis to construct bearing measurements to targets. Similarly, Forney et al. [35] use an S-shaped maneuver to resolve the direction to a target when using a hydrophone array. These maneuvers do not significantly change

the robot-target configuration, but cost time and energy, a cost ignored by traditional active-localization literature.

A possible approach to the active-tracking problem is to formulate it as finding the optimal policy of a Markov Decision Process [43]. When the true target location is unknown and measurements are imprecise, a Partially Observable Markov Decision Process (POMDP) is appropriate [43,44]. In our case, the state space would be given by the locations of the robots and their individual belief of the target space. The optimal strategy would choose measurement locations and a way for robots to exchange beliefs. Solving POMDPs in general is intractable, and we are not aware of dedicated methods to solve for the POMDPs which would arise from our setup.

However, in [16] and [15] we investigated three algorithms to find measurement locations, each based on a search over the discretized space around the robot. Discretization and search over state space was computationally demanding, and the results were limited to a fixed-sized displacement between measurements because of the discretization size. Furthermore, there was no systematic approach for dealing with the ambiguity of measurements.

Other results exist which use simplified noise models but cannot be directly applied to real-world deployments. Regarding the ambiguous sensing model, the infinite-line sensor was considered by [45], in the context of pursuit-evasion games. A finite-time capture strategy was provided by using pairs of measurements to resolve the ambiguity. Sensor noise was not considered, making localization of a static target trivial under the assumptions and sensing model proposed. More recently, [46] considered the problem of locating a stationary target using a fixed, small number of stationary *half-plane* sensors deployed. The goal, similar to ours, was to minimize the number of sensor queries and the length of the tour between them. However, the target was restricted to a discrete set of locations, and sensor positions were known a priori, resulting in a divide-and-search strategy which does not generalize to our setting. In this work we use noise models calibrated from real-world data and confirm our findings with field deployments. We also require no discrete constraints on the environment or target location to solve a more general version of the problem.

Similar to ambiguous bearing measurements, range-only measurements can lead to multiple hypotheses about the target location. Merino et al. [47] studied the problem of

active localization using range-only measurements from radio sensors. They represent multiple hypotheses with a Gaussian Mixture Model (GMM). The robot's direction is greedily chosen from a discretized set which maximizes the change in the entropy of the GMM.

Morbidi and Mariottini [48] studied the single and multi-target active tracking problem with a team of robots with 3D range sensors. The authors present a gradient-based controller for controlling the team of robots to (locally) minimize the uncertainty in estimating the target's location. [49] used radio signal strength to estimate the range to radio sources and a grid-based Bayesian filter to estimate the location of each radio source. A path-search algorithm based on Rapidly Exploring Random Trees was proposed but lacked any theoretical guarantees. Due to the differences in sensing model, these results for range-only sensors cannot be directly applied for bearing sensors. Furthermore, unlike these works, we consider the case where each measurement takes non-zero time and the objective is to minimize the travel and measurement time to localize the target to a desired uncertainty bound.

In chapters 5 and 6 we present a lower bound on time required by the optimal bearings-only localization algorithm. The study of optimal, offline, active-localization algorithms using the Fisher Information Matrix dates to Hammel et al., [50], and has seen more recent results by Logothetis et al. [51], Bishop et al. [52, 53], and Martinez and Bullo [54]. Of these, only [50] considered time-constrained trajectories. However, the results were for a single robot with a continuous sensor, and are not directly applicable to the setup considered in the present work. Results in this direction include [50], who numerically calculated an optimal trajectory using the determinant of the Fischer Information Matrix (FIM) evaluated at the true target location. No closed-form solution was provided, and the bounds presented in this paper generalize the result by optimizing the number and spacing of the measurements. Our work is limited to bearing measurements. However, Bishop [52] proved that a solution to an optimal bearing sequence also applies (with minor modification) to range sensors that have modeled to have range-dependent sensor noise.

4.3 Communication Constrained Active Localization

The active localization problem is significantly more complicated when considering communication constraints. The problem of estimating the target state despite loss of connectivity has recently gained attention. Hollinger and Singh [55] considered the problem of re-establishing estimation task after losing connectivity. Makarenko, Durrant-Whyte [56], and Nerurkar et al. [57,58] studied estimation when connectivity was either enforced, or intermittent. This was similar to Leung et al. [59] who showed how to maintain a consistent estimate of a multi-robot system while relying on future reconnection. Spletzer and Taylor [60] studied the problem of assigning robots to targets while also enforcing network connectivity. In these works, the optimality of maintaining connectivity was assumed, but we provide an algorithm which may break connectivity between robots so they can reach better measurement locations, leading to quicker estimate convergence.

4.4 Coverage Algorithms

Chapter 9 is dedicated to formulating the bearing-only localization task as a *coverage* problem. In this formulation, bearing measurements are placed at regular intervals to ensure localization of any nearby target. In [16], we defined a *search* algorithm which guaranteed that the robot would find a position from which it can detect a tagged fish in pre-defined regions of the lake. Similarly, [61] and [62] considered a similar problem of searching for and localizing multiple radio sources. The objective was to find a location which corresponds to the maximum signal strength of the transmitting source. A "Ridge Walking Algorithm" was proposed to repeatedly traverse the area around each radio source, making the final uncertainty a function of the signal strength. The main results apply to radio sources which are infrequently transmitting, and so the time-to-locate a source is an unbounded random variable. These works are complementary, since we assume the robot begins in detection range and use bearing measurements to reduce the uncertainty. Furthermore, we allow the final required precision to be specified and provide explicit, absolute bounds on localization time.

For the case when we cannot guarantee that the target is nearby, chapter 8 is dedicated to a coverage-based formulation for bearings-only localization. Robot coverage is

a fundamental robotics problem which has been studied extensively [63]. In the traditional coverage problem, in order to cover a point, it suffices to "sense" it by visiting a point within the sensing range. However, if the robot can take only bearing measurements, at least two measurements must be taken. The uncertainty in localizing a target at location x is a function of not only distance but also the angle $\measuredangle s_1 x s_2$ where s_1 and s_2 are the two measurement locations [64].

There are very few coverage results under the bearing-only sensing model. Borri et. al [46] consider a mobile robot collecting measurements from a *fixed set* of possible locations in a bounded environment. We relax these restrictions to optimize the tour directly and consider localization of multiple targets.

4.5 Locating Multiple Stationary Targets Adaptively

Recently, there has been significant interest in developing algorithms for locating transmitting radio sources using mobile robots. Song et al. [62] considered the problem of localizing an unknown number of transient radio sources using a mobile robot. They used an occupancy grid in a Bayesian framework to update the probability of a radio source being located in a given grid cell. They further proposed a path-planning algorithm for the robot to improve the convergence time for locating all sources. In [61], Kim et al. presented a centralized multi-robot search algorithm for the same problem setting, where the robots are controlled in pairs to allow detection of unknown transmission powers from the radio sources.

In [65], Tekdas et al. consider the problem of finding a point of high signal strength inside the sensing disc of transmitting sources. They assume a prior estimate of the source's location is given but sensing range is unknown. Here, we consider the problem of finding a good point to begin triangulation, while estimating sensing range and target location simultaneously.

Fink and Kumar [66] presented methods to build a radio signal strength map in an unknown indoor environment and presented control laws for mobile robots to seek the transmitting radio source. Recently, Twigg et al. [67] addressed the problem of exploration while seeking a radio source. The algorithm builds a gradient of the RSSI by collecting samples locally. Their work involves indoor environments and areas with

significant multi-path effects, and so is not directly applicable to our work. In addition, the directional sensitivity of our antenna makes it difficult to determine and follow a gradient.

The problem of simultaneously localizing a robot and multiple transmitting sources was considered in [68]. It was assumed that range could be explicitly recovered from the transmissions, and an arbitrary robot path was reconstructed while simultaneously estimating the position of each radio. An iterative, offline algorithm was proposed and evaluated. This problem is fundamentally different because we cannot recover range directly, and must solve the problem online, i.e., as measurements become available. Furthermore, we have direct control over the robot's path. In fact, defining the robot's path to aid the estimation problem is the what we address in the following sections.

4.6 Pursuit Evasion Games

A pursuit-evasion game is a mathematical abstraction in which two (or more) players maneuver to gain advantage. Typically, the goal is for one player (the pursuer) to "capture" another (the evader), often by moving onto the evader's position. A survey of robotics-related pursuit evasion games can be found in [69]. However, very few game models consider sensing uncertainty.

A notable exception is the result by Rote who studied the problem of chasing the target in the open plane [70]. In the game proposed, the pursuer must maintain a finite distance to the evader as the players maneuver in the unbounded plane. In his model, the evader can hide its true location and present any location within distance d from his true location as the measurement. It was shown that the evader can increase his distance from the pursuer at a rate of $\Theta(\sqrt[3]{t})$, where t is the time spent playing. In case of bearing measurements, we show that the evader can do much better and ensure that the increase in the distance is linear in t. Independent from this work, Klein showed a linear rate for a different, distance-dependent position error with and without obstacles in the open plane [71].

Starting in chapter 11, we consider the classical Lion and Man game. In this game, the pursuer seeks to move to within a specified distance of the evader as they maneuver in a closed disc. The Lion and Man game has been a mathematical curiosity for some

time [72]. Alonso et al. present a near optimal strategy for capture [73]. Their strategy however requires measuring the exact location of the man. Sgall et al. studied the game in the first quadrant, showing that a pursuer can capture an evader if he starts in a favorable position [74]. Karnad et al. extended this game to include bearing measurements and showed that the pursuer can close to within a small distance (one step) [75]. However, the exact position of the evader was required after every pursuer move, and it was only during the evader's move that the bearing uncertainty model was used. Finally, Bopardikar showed that it was possible to capture an evader on the open plane using exact bearing measurements if the pursuer was much faster than the evader [45].

We have presented our formal problem definition in Chapter 3 and surveyed existing approaches in this chapter. We now move on to the main results of our thesis. The next chapter is dedicated to the study of using a single mobile bearing sensor to locate a single stationary target.

Chapter 5

Near-Optimal Localization of a Stationary Target with One Robot

This chapter is dedicated to the design of an algorithm which can localize a stationary radio transmitter to desired precision. This problem is challenging because the measurement locations must be computed without knowledge of the true location of the source. As discussed in Section 2 radio-source localization is particularly challenging because instead of returning the bearing toward the source (or "target"), the returned result is a line which passes through the target and sensor. These "ambiguous" measurements further complicate the source-estimation problem. In Section 5.1, we show why radio signal strength measurements often require complicated filters to estimate the source. The first contribution of this chapter is a discussion on how to move the sensor after each measurement to deal with these problems, removing the need for complicated filtering algorithms.

The chapter provides both an online algorithm to locate a radio source, and a cost analysis of the algorithm which applies to any measurement sequence. In particular, we are able to bound the cost of executing the algorithm even in the worst case, as well as provide an expected-case analysis. To preserve generality, we include system parameters such as the cost per measurement, cost to relocate the robot, and sensor noise, making

the closed-form solution useful for many different systems or application domains. We present the details of the algorithm in Section 5.2.1. The cost of our algorithm is derived in Section 5.4.3.

To show the robustness of our algorithm to various starting conditions, we provide a direct comparison of the performance of our algorithm to that of the (unknown) optimal algorithm. We find that the gap between the two is small and bounded by a constant. We provide an analytical proof of this bound in Section 5.4. A novel result of our analysis is a general lower bound on the cost of any active localization algorithm which uses bearing sensors, presented in Section 5.4.1.

Finally, the algorithm is experimentally validated in simulation (Section 5.5) and using a mobile robot deployed on frozen lakes in Minnesota, USA, as shown in Section 5.6. We present a series of field deployments in which a mobile rover can initialize a consistent hypothesis, and choose a small, bounded number of measurement locations to locate multiple radio tags with good accuracy, all with close adherence to the theoretical results.

We have had success in field experiments using the Extended Kalman Filter (EKF) for this application, and hence base our algorithm with respect to this common filtering technique. The closed-form representation of the EKF equations allow us to make guarantees about algorithm execution time and completeness as elaborated in the next sections. Refer to Chapter 3 for a review of the EKF equations. We leave the generalization to other filtering techniques to future work, but provide a direct comparison in Section 5.5.

5.1 Addressing Ambiguity

The first problem is to structure a measurement sequence to minimize the impact of ambiguous bearing measurements. To see the effect of ambiguous measurements, consider the situation shown in Figure 5.2. In Figure 5.2a, a mobile robot arrives at position s_i and takes a measurement, as shown by the line z–s_i–z'. Notice that the line can be separated into two rays, which we define s_i–z and s_i–z' with the angles $0 \leq |z| < |z'| \leq \pi$. Note that $z' = z + \pi$, and z is the "forward-facing" part of the measurement, or the part of the line segment which passes closer to the point $\hat{x}_i$. Both rays represent a deviation

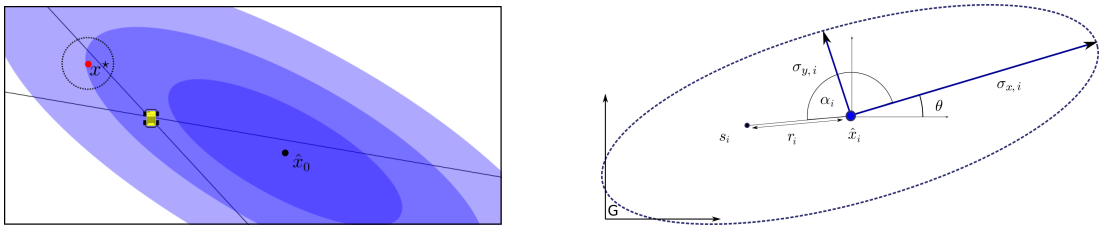

(a) (b)

Figure 5.1: **(a)**. Problem setup. A robot, without knowledge of the true target location $x^\star$ but with an initial hypothesis of the target location, $\hat{x}_0$, must find measurement locations to shrink the uncertainty about $x^\star$. Measurements taken far from $x^\star$, for example, near $\hat{x}_0$ will ultimately provide small information about $x^\star$ and are thus wasteful. Shown is an example of a "double wedge" or ambiguous measurement cone: From just one measurement, it is not clear if the target is near $\hat{x}_0$ or $x^\star$. **(b)**. The notation and problem formulation. A sensor location at time i, denoted s_i, is described by (r_i, α_i). Here r_i is the range from the sensor to the current hypothesis, $\hat{x}_i$, and α_i denotes the orientation with respect to the line formed by the major axis of the covariance ellipse, Σ_i, with eigenvalues $\sigma_{x,i}$ and $\sigma_{y,i}$ and orientation θ_i with respect to a global frame.

from the expected measurement (the line between s_i and $\hat{x}_i$, corresponding to angle 0). After performing a Bayesian update of the target hypothesis using the ambiguous measurement, the target PDF will also be bi-modal, as shown in Figure 5.2c.

Analytically, we can see this as follows. Let $p(\hat{x}_{i+1})$ represent the posterior PDF of the target, $Z = \{z\} \cup \{z'\}$ be an ambiguous measurement which we decompose as described into two rays, s_i be the sensor location, and x_i the prior hypothesis.

$$\begin{aligned} p(x_{i+1}|x_i, s_i, Z) \;\propto\; & p(x_{i+1}|x_i, s_i, z) \cdot p(z|x_i, s_i) \\ & + p(x(i+1)|x_i, s_i, z') \cdot p(z'|x_i, s_i) \end{aligned} \tag{5.1}$$

This PDF is well approximated by a mixture of two Gaussians, one for each peak in the PDF given the new measurement (see Figure 5.2c). A reasonable practice is to use two Gaussian hypotheses, weighted as shown. However, splitting the PDF with each measurement will lead to an exponential number of hypotheses over multiple measurements. To address this problem, it is common to discard or combine hypotheses with low relative weights (see [32, 76, 77]). However, if the robot takes a measurement from a location very close to the peak of the prior hypothesis, the weights $p(z|x_i, s_i)$ and $p(z'|x_i, s_i)$ may be equal and no hypothesis can be discarded.

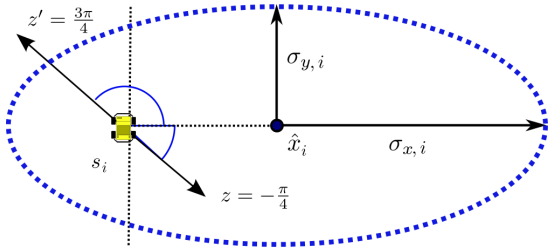

(a)

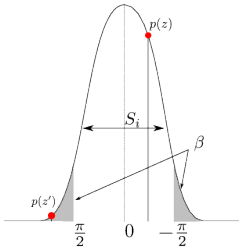

(b) $p(z|\hat{x}_i, s_i)$

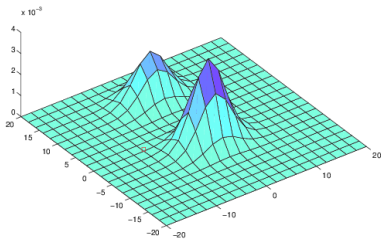

(c) The posterior PDF given an ambiguous measurement.

Figure 5.2: **(a)** Ambiguous measurements produce two possible bearings (z and z'). **(b)** The EKF approximates the measurement probability as a Gaussian with mean zero and variance S_i. **(c)** The PDF of the target hypothesis after updating the Gaussian prior shown in (a) with measurements z' and z.

The key observation which motivates our choice of measurement locations is the following: The likelihood $p(z'|x_i, s_i)$ is highly dependent on the sensor location relative to the target hypothesis. As we will show below, one can always choose measurement locations such that $p(z|x_i, s_i)$ is much higher than $p(z'|x_i, s_i)$. In this way *only one* Gaussian hypothesis will have a high weight after each measurement.

Specifically, we choose measurement locations such that $p(z'|x_i) \ll p(z|x_i)$ *for any* value of z. This is challenging because the measurement value (z) is only given as the approximate distribution $p(z|x_i)$. To proceed, let β be a parameter describing the maximum acceptable probability that the target is in fact "behind" the sensor (corresponding to z' being the correct bearing). We can choose locations such that $p(z'|x_i)$ is always less than β using the following lemma (a proof of which is delayed until Section onerobot:pf:sigbeta).

Lemma 5.1. *Let $\Phi(a)$ be the Gaussian CDF such that $\Phi(a) = p(x \leq a)$ when $x \sim \mathcal{N}(0, 1)$. Define a threshold parameter β and true measurement $z^\star$. Define sensing locations in radial coordinates (α_i, r_i) centered around the current target hypothesis. Then any sensing location satisfying,*

$$r_i \geq \sqrt{\frac{\sigma_{x,i}^2 \sin^2 \alpha_i + \sigma_{y,i}^2 \cos^2 \alpha_i}{\sigma_\beta^2 - \sigma_s^2}} \qquad \textit{with constant: } \sigma_\beta = \frac{\pi}{2 \cdot \Phi^{-1}\left(1 - \frac{\beta}{2}\right)} \tag{5.2}$$

will also satisfy $p(z'|x_i, s_i) \leq \beta$.

Proof. Essentially, we want the probability mass of the target distribution outside the $\pm\frac{\pi}{2}$ window to be less than β, as shown in Figure 5.2b. Recall that the innovation, $(z - \hat{z})$ is assumed to be normally distributed with variance given by S from Eq (3.8). This implies $\frac{z-\hat{z}}{\sqrt{S}} \sim \mathcal{N}(0, 1)$. Thus,

$$\begin{aligned} p(z - \hat{z} \geq \frac{\pi}{2}) &= p(\frac{z - \hat{z}}{\sqrt{S}} \geq \frac{\pi}{2\sqrt{S}}) \\ &= 1 - \Phi\left(\frac{\pi}{2\sqrt{S}}\right) \end{aligned} \tag{5.3}$$

with the function Φ representing the standard Gaussian CDF. We want this probability to be less than $\frac{\beta}{2}$.

$$1 - \Phi\left(\frac{\pi}{2\sqrt{S}}\right) \leq \frac{\beta}{2} \leftrightarrow \sqrt{S} \leq \frac{\pi}{2 \cdot \Phi^{-1}\left(1 - \frac{\beta}{2}\right)} \tag{5.4}$$

We call the right hand side σ_β in the remainder of the paper, which makes the variance constraint in (5.4) $S \leq \sigma_\beta^2$. From this relationship we can derive a constraint on the measurement locations as follows. We begin by substituting the value of S from the EKF formulation.

$$\begin{aligned} S &= H\Sigma H^T + R \\ S &= \begin{bmatrix} \frac{-\sin\alpha}{r} & \frac{\cos\alpha}{r} \end{bmatrix} \begin{bmatrix} \sigma_x^2 & 0 \\ 0 & \sigma_y^2 \end{bmatrix} \begin{bmatrix} \frac{-\sin\alpha}{r} \\ \frac{\cos\alpha}{r} \end{bmatrix} + \sigma_s^2 \\ S &= \frac{1}{r^2}\left(\sigma_x^2 \sin^2\alpha + \sigma_y^2 \cos^2\alpha\right) + \sigma_s^2 \end{aligned}$$

Notice that all values of the previous equation are known, except for the position of the sensor (r_i and α_i). Applying the maximum variance constraint $S \leq \sigma_\beta^2$ allows us to find a range constraint for measurement locations.

$$r \geq \sqrt{\frac{\sigma_x^2 \sin^2\alpha + \sigma_y^2 \cos^2\alpha}{\sigma_\beta^2 - \sigma_s^2}} \tag{5.5}$$

Consider the information form of the covariance update given in Eq (3.12). Substituting the value of H and R gives a one-step closed form recursion as follows.

$$\Sigma_{i+1}^{-1} = \Sigma_i^{-1} + \frac{1}{\sigma_s^2}\begin{bmatrix} \frac{-\sin\alpha_i}{r_i} \\ \frac{\cos\alpha_i}{r_i} \end{bmatrix}\begin{bmatrix} \frac{-\sin\alpha_i}{r_i} & \frac{\cos\alpha_i}{r_i} \end{bmatrix}$$

Note that α alternates between $\frac{\pi}{2}$ and 0 to find the following recursion for each pair of measurements.

$$\Sigma_{i+2}^{-1} = \Sigma_i^{-1} + \begin{bmatrix} \frac{1}{\sigma_s^2 r_i^2} & 0 \\ 0 & 0 \end{bmatrix} + \begin{bmatrix} 0 & 0 \\ 0 & \frac{1}{\sigma_s^2 r_{i+1}^2} \end{bmatrix}$$

Substitute the value for r_i from (5.7) and expand Σ to find:

$$\Sigma_{i+2}^{-1} = \begin{bmatrix} \frac{1}{\sigma_{x,i}^2} & 0 \\ 0 & \frac{1}{\sigma_{y,i}^2} \end{bmatrix} + \begin{bmatrix} \frac{\sigma_\beta^2 - \sigma_s^2}{\sigma_s^2\sigma_{x,i}^2} & 0 \\ 0 & \frac{\sigma_\beta^2 - \sigma_s^2}{\sigma_s^2\sigma_{y,i}^2} \end{bmatrix} = \begin{bmatrix} \frac{1}{\sigma_{x,i}^2}\left(1 + \frac{\sigma_\beta^2 - \sigma_s^2}{\sigma_s^2}\right) & 0 \\ 0 & \frac{1}{\sigma_{y,i}^2}\left(1 + \frac{\sigma_\beta^2 - \sigma_s^2}{\sigma_s^2}\right) \end{bmatrix}$$

Since $1 + \dfrac{\sigma_\beta^2 - \sigma_s^2}{\sigma_s^2} = \left(\dfrac{\sigma_\beta^2}{\sigma_s^2}\right)$ the above factors to

$$\Sigma_{i+2}^{-1} = \left(\frac{\sigma_\beta^2}{\sigma_s^2}\right) \cdot \Sigma_i^{-1} \tag{5.6}$$

Thus each pair of measurements is a constant-factor increase in information, or a decrease in prior uncertainty. Suppose the measurement sequence takes N measurements. The covariance at the end of the measurement sequence is required to be

$$\Sigma_N = \begin{bmatrix} \gamma^2 \cdot \sigma_{x,0}^2 & 0 \\ 0 & \gamma^2 \cdot \sigma_{y,0}^2 \end{bmatrix} = \gamma^2 \cdot \Sigma_0$$

Since each pair of measurements reduces the uncertainty in both x and y direction by a constant factor, we have from Eq (5.8),

$$\Sigma_{i+2}^{-1} = \left(\frac{\sigma_\beta^2}{\sigma_s^2}\right) \cdot \Sigma_i^{-1}$$

The above shows,

$$\frac{1}{\gamma^2}\Sigma_0^{-1} = \left(\frac{\sigma_\beta^2}{\sigma_s^2}\right)^{\frac{N}{2}} \cdot \Sigma_0^{-1} \leftrightarrow N = 4\log_{\left(\frac{\sigma_\beta^2}{\sigma_s^2}\right)}\left(\frac{1}{\gamma}\right)$$

□

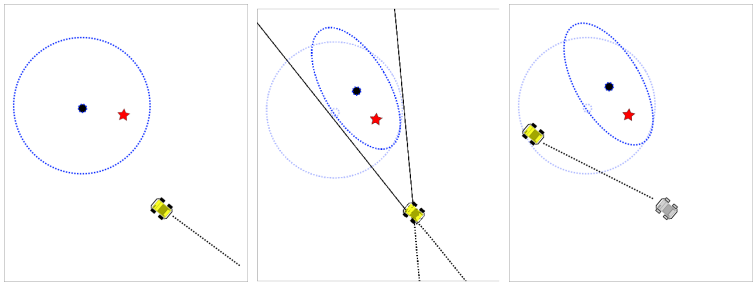

(a) (b) (c)

Figure 5.3: One measurement step of the cautious strategy presented in Algorithm 5.1. Shown is a covariance ellipse and target hypothesis (circle) along with the true target location (star). **(a)** The robot moves to a location perpendicular to the direction of highest uncertainty. **(b)** A bearing measurement is collected, and the hypothesis is updated. The "backward facing" cone (dashed lines) is discarded. **(c)** The now-reshaped covariance ellipse has a new direction of highest uncertainty, and the process repeats.

Eq (5.1) defines an "ellipse of closest approach" around the target hypothesis, with principal axes defined as a function of the uncertainty in the estimate. Effectively, we have defined a strategy which truncates part of the PDF by discarding the possibility that the target is behind the sensor. The amount of discarded probability mass is approximated by the β parameter. As $\beta \to 0$, none of the PDF is truncated, but the measurement locations become infinitely far away. Perhaps intuitively, in the following sections we show that the parameter β captures the trade-off between time spent localizing a target and the accuracy of the final estimate. In particular, the time required to locate a target will follow directly in closed form in Section 5.4.3 as a function of β. In the rest of the paper we formalize this intuition. First, we specify our algorithm.

5.2 The β-Cautious Algorithm

We now introduce our main algorithm. In essence, we present a greedy algorithm which outputs a measurement location based on the current hypothesis. At each time step, it will output a measurement location which can minimize the maximum eigenvalue of the covariance matrix. Such an algorithm is often called E-Optimal in literature [78].

5.2.1 Algorithm Description

Each measurement location is subject to the constraint given in Lemma 5.1. Specifically, fix $\alpha = \frac{\pi}{2}$ with respect to the larger eigenvalue / eigenvector pair at every time step (σ_x in this notation). Thus, Eq (5.2) simplifies to,

$$r \geq \frac{\sigma_x}{\sqrt{\sigma_\beta^2 - \sigma_s^2}} \tag{5.7}$$

As $\sigma_x \to 0$, r strictly decreases, and thus the range (relative to the hypothesis) between measurements decreases as well. Since the algorithm produces measurement locations which begin far away from the hypothesis (as a function of β) and only approach when the variance decreases, we call the algorithm β-Cautious.

Algorithm 5.1 presents the detailed implementation of our algorithm. At each time step, the robot moves to a position perpendicular to the eigenvector with the largest eigenvalue. The robot chooses the smallest range satisfying Eq (5.7). Figure 5.3 shows a pair of measurements and the path of the robot. In general, there are two such locations, so it is easiest to choose the closer of the two. This process repeats until both eigenvalues are below the desired threshold. Figure 5.4 shows a full simulated execution of the algorithm. As the uncertainty (σ_x) decreases the measurement locations are chosen closer to the hypothesis (see Eq (5.7)).

Since the algorithm reduces the largest eigenvalue at every measurement step, it is guaranteed to satisfy the constraint $\Sigma_N \leq \gamma \cdot \Sigma_0$ in finite time. We use the EKF update routine (Eq (3.6) and Eq (3.7)) as a subroutine. Since all operations are available in closed form, and the size of the covariance is small and fixed, Algorithm 5.1 has a constant computational complexity. While a greedy, multi-target extension is possible, we focus on the analysis of the single-target algorithm in this work.

5.3 Bounding the Cost of the β-Cautious Algorithm

To bound the time required to execute the algorithm on a real system, we first consider the number of measurements required to achieve the requested covariance reduction. We begin by showing that a β-Cautious measurement sequence decreases covariance (increases information) by a constant factor at each time step. From this follows a

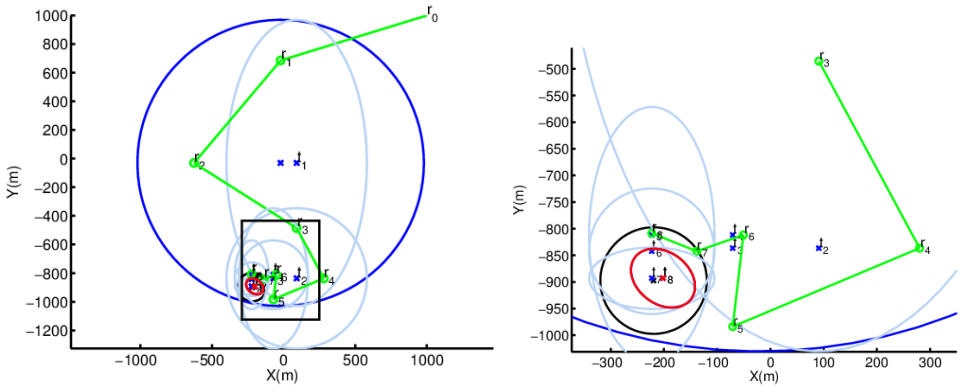

(a) Full run (b) Zoomed in boxed area

Figure 5.4: A simulated execution of the cautious strategy. This figure is best viewed in color. **(a)** the full run. **(b)** Detail of the boxed region in the first figure. A red ellipse denotes the final target covariance, the black circle is the desired uncertainty, blue is prior estimate, and green is the robot path and measurement locations. The robot travels in a roughly zig-zag path toward the target, while the target hypothesis shifts rectilinearly toward the true target.

bound on the number of measurements required to reach the desired covariance in Lemma 5.3. Because the measurement values are unknown (random) variables, the state of the target is unknown for each time step. Therefore it is necessary to find a worst-case change in hypothesis location for each measurement, and bound the time required to shift the measurement location to compensate. The results derived here are confirmed in simulations (see Section 5.5) and field experiments (Section 5.6).

We begin by deriving the exact covariance reduction from a β-Cautious measurement strategy.

Lemma 5.2. *If a pair of measurements is taken from $\alpha_i = \frac{\pi}{2}$ with range constraint (from Lemma 5.1) $r_i = \frac{\sigma_{x,i}}{\sqrt{\sigma_\beta^2 - \sigma_s^2}}$, the variance both x and y directions is decreased by a constant factor,*

$$\sigma_{x,i+2}^2 = \frac{\sigma_\beta^2}{\sigma_s^2}\sigma_{x,i}^2 \text{ with } \sigma_\beta > \sigma_s \text{ (see Lemma 5.1)} \tag{5.8}$$

In addition, the alignment of the major and minor axes of the posterior covariance does not rotate from the prior.

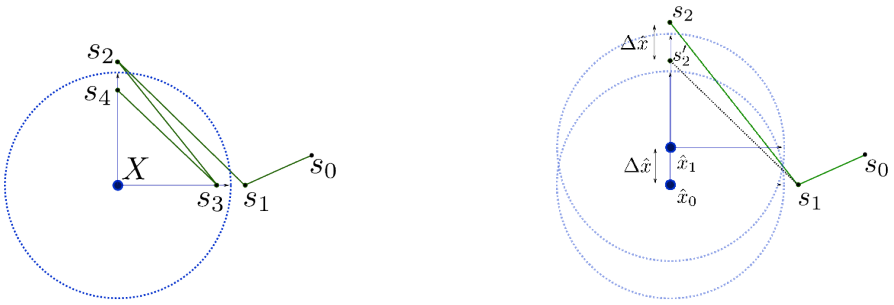

(a) Local frame (b) World frame

Figure 5.5: The measurement sequence $S = \{s_0 \dots s_4\}$. **(a)** the target hypothesis shifts vertically because of the measurement received at s_1. **(b)** The next measurement location (s_2) must be shifted by the same amount to satisfy the range constraint.

The above lemma guarantees that after each pair of measurements the covariance decreases by a factor of $\frac{\sigma_\beta^2}{\sigma_s^2}$. A straightforward derivation shows an upper bound on the number of measurements required to reduce the eigenvalues of the covariance by a factor of γ, to achieve the desired bounds.

Lemma 5.3. *Let the time-stamped range for each measurement be r_i, and the corresponding maximum variance be $\sigma_{x,i}^2$ (covariance Σ_i), at time-step i. While constraining the range as defined in Lemma 5.1, such that $r \geq \frac{\sigma_x}{\sqrt{\sigma_\beta^2 - \sigma_s^2}}$, the number of measurements required to satisfy the uncertainty objective, $\sigma_{x,N} \leq \gamma \cdot \sigma_{x,0}$ with $0 < \gamma \leq 1$ is*

$$N = 4 \log_{\left(\frac{\sigma_\beta^2}{\sigma_s^2}\right)} \left(\frac{1}{\gamma}\right)$$

Using the number of measurements for a problem instance, it is possible to estimate the distance traveled over a tour of the measurement locations. Note that the measurement locations are specified as (r_i, α_i) pairs with respect to $\hat{x}_i$, the hypothesis at each time-step. An example of a measurement sequence with $N = 4$ is shown in Figure 5.9. Because the hypothesis may move after new measurements, it is not trivial to solve for the distance traveled. The general form of the distance traveled is,

$$D(S_{alg}) \leq \sum_{i=1}^{N-1} ||s_{i+1} - s_i|| + ||\hat{x}_{i+1} - \hat{x}_i||$$

The first quantity is the total distance traveled by the robot *in the target's frame* fixed at each step (Figure 5.5a). The second quantity is the shift between the hypothesis, i.e., the shift in the target's local frame after each measurement (Figure 5.5b). Both quantities admit upper bound, as follows.

Since the covariance does not rotate, in the local frame of the target hypothesis, the measurement sequence simply alternates between both principal axes (as shown in Figure 5.5a). Each measurement takes place at fixed range, $r_i = \frac{\sigma_i}{\sqrt{\sigma_\beta^2 - \sigma_s^2}}$ in the corresponding local frame. Intuitively, this allows an upper-bound on the worst case travel distance of the robot in the local frame in terms of the covariance at each step.

Lemma 5.4. *The total displacement between sensor locations in the local frame of the hypothesis (i.e., disregarding hypothesis displacement) satisfies*

$$\sum_{i=1}^{N-1} ||s_{i+1} - s_i|| \leq \sum_{i=1}^{N-1} \frac{\sqrt{2}}{\sqrt{\sigma_\beta^2 - \sigma_s^2}} \sigma_{x,i}$$

Proof. In the local frame of the target hypothesis, measurements are taken along the x and y axis at fixed, decreasing ranges. To derive an upper bound, we can solve a circular case with both starting variances equal to the maximum, i.e. $\sigma_{x,0} = \sigma_{y,0} = \max(\sigma_x, \sigma_y)$.

First, note that each sensor location is along a principal axis of the local coordinate frame, with $\hat{x}$ at the origin. Note also that there are $\frac{N}{2}$ movements from the x axis to the y axis and $\frac{N}{2} - 1$ movements from y to x axes. Each measurement takes place at fixed range, $r_i = \frac{\sigma_i}{\sqrt{\sigma_\beta^2 - \sigma_s^2}}$ and $r_{i+1} \leq r_i$. Thus, we have the following relationship.

$$\begin{aligned}
\sum_{i=1}^{N-1} ||s_{i+1} - s_i|| &= \sum_{i=1}^{\frac{N}{2}} ||s_{2i-1} - s_{2i}|| + \sum_{i=1}^{\frac{N}{2}-1} ||s_{2i} - s_{2i+1}|| \\
&\leq \sum_{i=1}^{\frac{N}{2}} \sqrt{2} \cdot r_{2i-1} + \sum_{i=1}^{\frac{N}{2}-1} \sqrt{2} \cdot r_{2i} \\
&\leq \sum_{i=1}^{\frac{N}{2}} \frac{\sqrt{2}}{\sqrt{\sigma_\beta^2 - \sigma_s^2}} \sigma_{x,2i-1} + \sum_{i=1}^{\frac{N}{2}-1} \frac{\sqrt{2}}{\sqrt{\sigma_\beta^2 - \sigma_s^2}} \sigma_{y,2i}
\end{aligned}$$

Note that $\sigma_{x,0} = \sigma_{y,0}$ and after a pair of measurements, the variances are again equal (i.e., $\sigma_{x,i} = \sigma_{y,i+1}$). The desired result follows. □

Using the EKF update equations we can compute the maximum displacement between the target hypothesis for any measurement that can be obtained in terms of the covariance at that step (Figure 5.5b). This allows us to bound the total shift in the local frame centered at the hypothesis at each measurement step.

Lemma 5.5. *The total shift in the target hypothesis from a measurement sequence of size N is bounded above as,*

$$\sum_{i=1}^{N-1} ||\hat{x}_{i+1} - \hat{x}_i|| \leq \sum_{i=1}^{N-1} \sigma_{x,i} \frac{\pi\sqrt{\sigma_\beta^2 - \sigma_s^2}}{\sigma_\beta^2}$$

Proof. To examine $||\hat{x}_{i+1} - \hat{x}_i||$ (the shift from a single measurement), observe that the difference between two hypothesis locations is given in closed form by the EKF as $\hat{x}_{i+1} = \hat{x}_i + K_{i+1}[z_i - \hat{z}_i]$. We can find the maximum shift as follows (we drop the current time indices i for clarity).

$$\begin{aligned}
\hat{x}_{i+1} - \hat{x} &= K[z - \hat{z}] \\
&= \Sigma H^T \left[H\Sigma H^T + \sigma_s^2\right]^{-1} [z - \hat{z}] \\
&= \begin{bmatrix} \sigma_x^2 & 0 \\ 0 & \sigma_y^2 \end{bmatrix} \begin{bmatrix} -\frac{1}{r}\sin\alpha \\ \frac{1}{r}\cos\alpha \end{bmatrix} \left[\frac{1}{r^2}\left(\sigma_x^2 \sin^2\alpha + \sigma_y^2 \cos^2\alpha\right) + \sigma_s^2\right]^{-1} [z - \hat{z}]
\end{aligned}$$

Observe that α, takes the value $\frac{\pi}{2}$ and 0 over a pair of measurements. The two possible values of $\hat{x}_{i+1} - \hat{x}$ are,

$$\hat{x}_{i+1} - \hat{x} = \begin{bmatrix} \frac{-\sigma_x^2}{\frac{1}{r}\sigma_x^2 + r \cdot \sigma_s^2} \\ 0 \end{bmatrix} |z - \hat{z}| \qquad \text{if } \alpha = \frac{\pi}{2}$$

$$\hat{x}_{i+1} - \hat{x} = \begin{bmatrix} 0 \\ \frac{\sigma_y^2}{\frac{1}{r}\sigma_y^2 + r \cdot \sigma_s^2} \end{bmatrix} |z - \hat{z}| \qquad \text{if } \alpha = 0$$

From which we can see that when the sensor is at a location perpendicular to the direction of σ_x (resp. σ_y), the target hypothesis will shift only in the $\pm x$ (resp. $\pm y$) direction. We can proceed with measurements corresponding to $\alpha = \frac{\pi}{2}$, as the other

direction is similar. By including the constraint on range, $r = \frac{\sigma_x}{\sqrt{\sigma_\beta^2 - \sigma_s^2}}$

$$||\hat{x}_{i+1} - \hat{x}|| = |z - \hat{z}| \cdot \left(\frac{\sigma_x \sqrt{\sigma_\beta^2 - \sigma_s^2}}{\sigma_\beta^2} \right)$$

Finally, notice that the innovation, $z - \hat{z}$, cannot be more than π in a bearing-only setting. This gives a final upper bound on the displacement of the hypothesis along the perpendicular axis as,

$$||\hat{x}_{i+1} - \hat{x}|| \leq \sigma_x \cdot \frac{\pi \sqrt{\sigma_\beta^2 - \sigma_s^2}}{\sigma_\beta^2}$$

□

We add the target displacement at each step to the distance traveled between each measurement, which preserves the upper bound by the triangle inequality (cf. Figure 5.5b). The above three lemmas together give a bound on the number of measurements and distance traveled by the robot. We can now fully bound the time required to localize a target.

Theorem 5.1. *The total time taken by the β-Cautious strategy is given as,*

$$T(S_\beta) \leq \sigma_{x,0} \cdot \left(\frac{\sqrt{2}}{\sqrt{\sigma_\beta^2 - \sigma_s^2}} + \frac{\pi \sqrt{\sigma_\beta^2 - \sigma_s^2}}{\sigma_\beta^2} \right) \cdot \left[\frac{1 - \sqrt{\gamma}}{1 - \frac{\sigma_s}{\sigma_\beta}} \right] + 4 \log_{\left(\frac{\sigma_\beta^2}{\sigma_s^2}\right)} \left(\frac{1}{\gamma} \right) + D(s_0, s_1) \tag{5.9}$$

Proof. The time spent localizing a target consists of travel time and measurement time. The time spent measuring is simply $N \cdot t_m$, where N follows from Lemma 5.3. To bound the time spent traveling, we use the distance bounds from Lemmas 5.4 and 5.5. Note that we have assumed unit velocity, otherwise, the following must be scaled by the velocity of the robot.

$$D(S_{alg}) \leq \sum_{i=1}^{N-1} \sigma_{x,i} \frac{\sqrt{2}}{\sqrt{\sigma_\beta^2 - \sigma_s^2}} + \sum_{i=1}^{N-1} \sigma_{x,i} \frac{\pi \sqrt{\sigma_\beta^2 - \sigma_s^2}}{\sigma_\beta^2}$$

Note the two series can be combined. Factoring out and grouping all constants yields,

$$D(S_{alg}) \leq \left(\frac{\sqrt{2}}{\sqrt{\sigma_\beta^2 - \sigma_s^2}} + \frac{\pi\sqrt{\sigma_\beta^2 - \sigma_s^2}}{\sigma_\beta^2} \right) \cdot \sum_{i=1}^{N-1} \sigma_{x,i}$$

To proceed, note that $\sigma_{x,i} = \left(\frac{\sigma_s}{\sigma_\beta}\right)^i \sigma_{x,0}$ (See Eq (5.8)). Then the summation on the right is a geometric series, with solution as follows.

$$\sigma_{x,0} \cdot \left[\sum_{i=1}^{N-1} \left(\frac{\sigma_s}{\sigma_\beta}\right)^i \right] \leq \sigma_{x,0} \cdot \left[\sum_{i=1}^{N} \left(\frac{\sigma_s}{\sigma_\beta}\right)^i \right] = \sigma_{x,0} \cdot \left[\frac{1-\sqrt{\gamma}}{1-\frac{\sigma_s}{\sigma_\beta}} \right]$$

The desired result follows. Note we have added $D(s_0, s_1)$, the time to travel between the initial sensor location and the first measurement location. □

From here we would like to point out some intuitive results of this upper bound. First, as $\gamma \to 1$, the algorithm requires no time to execute. This is because the difference between the final (requested) covariance and the initial covariance becomes small. Essentially, this shows the adaptivity of the algorithm: A good initial estimate or less restrictive desired uncertainty will lower execution time.

Notice also that as $\frac{\sigma_s}{\sigma_\beta} \to 1$, the work required approaches infinity. Intuitively, constraining the variance, with caution, to a value comparable to the noise in the sensor results in measurements taken from very distant locations (see Eq (5.7)), which provide small information gains (see Eq (3.12)). The effect of σ_β as a function of β is further explored using simulations studies in Section 5.5.

5.4 Bounds on the Optimal Cost

The previous section established an upper-bound on the worst-case cost of using the β-Cautious strategy to locate a stationary target. In this section we establish lower-bounds on the cost of the *optimal* measurement sequence. Using these bounds, we then show that no other algorithm can localize a stationary target significantly faster, as a function of the system parameters and desired final uncertainty.

In the following section, we present a general lower bound on the cost of any bearing-only active localization sequence, even one which does not suffer from ambiguous measurements. We compare this to the cost of the proposed algorithm in Section 5.4.2.

Beginning in Section 5.4.3, we consider the worst-case execution time for the proposed algorithm, compared to that of any other online algorithm. We specify both costs as a function of the same true target location and hypothesis. This allows a direct comparison of both algorithms against a common, uncontrollable adversary (e.g., Nature) in Section 5.4.4.

5.4.1 Lower Bound for an Offline Algorithm

We begin by deriving a lower bound on the time required to execute the optimal measurement sequence which is planned *offline*—in other words, with respect to the true target location. This lower bound is a function of the system parameters, and therefore is general and applies to any mobile bearing sensor and any reasonable method of fusing the measurements. This result is presented in Theorem 5.2.

Our proof makes use of the Cramer-Rao Lower Bound (CRLB or $\mathbb{C}$) [21] as follows. We can now explore the structure of the CRLB for an optimal measurement sequence. Let an optimal trajectory be denoted $S = \{s_0, s_1, \cdots s_k\}$ with cost $T(S)$ as follows.

$$\begin{aligned} T(S) &= k \cdot t_m + D(S) \\ &= k \cdot t_m + \sum_{i=1}^{k} ||s_i - s_{i-1}||_2 \end{aligned}$$

We make no assumptions about the algorithm used to localize the target, other than a non-zero time requirement for each measurement. Notice in this case the number of measurements k, and the corresponding measurement locations are both unknown. Also, note that the optimal algorithm must be a function of the measurement cost. At one extreme, $t_m \to 0$, the total cost to localize a target is dominated by travel time, and the optimal strategy will not travel far and will take many measurements. At the other extreme for high t_m, the optimal strategy can afford to pay for large displacements to gain a minimal number of maximally-informative measurements.

By constraining the final covariance and treating the prior covariance Σ_0 as an "observation" of the target state, the information gain from the sequence of measurements described by S is given by Eq 3.12 as $\Sigma_k^{-1} = \mathbb{F}(S) + \Sigma_0^{-1}$. Taking the trace of this

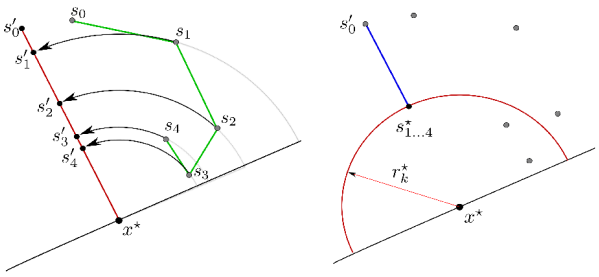

Figure 5.6: An illustration of the sequence S'. An arbitrary trajectory (left) is lower-bounded by a well-structured trajectory S' (right), according to Lemmas 5.6 through 5.7.

equation provides the following relationship, where each α_i and r_i of S are unknown.

$$\frac{1}{\sigma^2_{x,k}} + \frac{1}{\sigma^2_{y,k}} = \frac{1}{\sigma^2_{x,0}} + \frac{1}{\sigma^2_{y,0}} + \sum_{i=1}^{k} \frac{1}{r_i^2 \sigma_s^2} [\sin^2 \alpha_i + \cos^2 \alpha_i] \tag{5.10}$$

The trace shows the net information gain about *both* eigenvalues. By applying the net measurement gain directly to one eigenvalue, we can lower-bound the amount of work required to reduce both eigenvalues. The previous relationship becomes:

$$\frac{1}{\sigma^2_{x,k}} = \frac{1}{\sigma^2_{x,0}} + \sum_{i=1}^{k} \frac{1}{r_i^2 \sigma_s^2} \tag{5.11}$$

Note this is equivalent to setting each α_i to $\frac{\pi}{2}$ as shown in Figure 5.6 (left). The resulting straight-line trajectory is labelled S'. Now we can explore the structure given by S'.

The next lemma shows that S' can be structured such that all measurements are taken from the same location without decreasing the information gain given by Eq (5.11).

Lemma 5.6. *The sequence S' takes all measurements from one location.*

Proof. To find a contradiction, assume not: that S' contains measurements from more than one location from various ranges given as r_i. Let r_{min} be the minimum of all these ranges. The information gain (Eq (5.11)) will be $\frac{1}{r_i^2} \leq \frac{1}{r_{min}^2}$. Since the sequence already pays to travel to r_{min}, the closest position, we could move all measurements to the closest location (at r_{min}) without incurring extra cost but gaining extra information. This contradicts the assumption that S' is optimal. □

Lemma 5.7. *Assume the sequence S' takes $k^\star$ measurements. Then the optimal range from $x^\star$ for taking all measurements is given by,*

$$r_{opt} = \sqrt{k^\star} \cdot \frac{\sigma_{x,0}}{\sigma_s} \sqrt{\frac{\gamma^2}{1-\gamma^2}}$$

incurring a total time cost of,

$$T(S') = k^\star \cdot t_m + r^\star - \sqrt{k} \cdot \frac{\sigma_{x,0}}{\sigma_s} \sqrt{\frac{\gamma^2}{1-\gamma^2}} \tag{5.12}$$

where $r^\star$ is the distance from the starting robot location to $x^\star$.

Proof. Returning to Eq (5.11), it is clear that all r_i are equal from Lemma 5.7. Since the trajectory S satisfies the objective of reducing uncertainty, $\sigma_{x,k}^2$ is upper-bounded by $\gamma^2 \sigma_{x,0}^2$. Substituting this inequality into Eq (5.11) produces the following relationship.

$$r_k = \sqrt{k} \frac{\sigma_{x,0}}{\sigma_s} \sqrt{\frac{1-\gamma^2}{\gamma^2}} \tag{5.13}$$

By assuming $k = k^\star$, the result follows. □

The result of the previous lemmas is the trajectory shown in Figure 5.6 (right). Notice that the range r_{opt} is proportional to the square root of the number of measurements taken. Since $k \geq 1$ it is tempting to simply lower-bound the time requirement by substituting $k = 1$ into Eq (5.12). However, this would unfairly restrict the optimal strategy to travel to a position from which a single measurement would be sufficient. Instead, we must find the trade-off between r_{opt} and k as a function of the system parameters, t_m, γ, and $\sigma_{x,0}$, which determine the optimal number of measurements.

Theorem 5.2. *Let $S_{OFF}^\star$ be the optimal offline, bearing-only (not-necessarily-ambiguous) measurement sequence. If $S_{OFF}^\star$ requires $T(S_{OFF}^\star)$ time to reduce σ_x and σ_y by the constant γ, when centered at the true target location, then $T(S')$ is a lower bound on $T(S_{OFF}^\star)$ as follows:*

$$T(S_{OFF}^\star) \geq T(S') = \max\left[r^\star - \frac{\sigma_0^2}{2 \cdot t_m \sigma_s^2}\left(\frac{\gamma^2}{1-\gamma^2}\right), 0\right] + t_m$$

Proof. Notice Eq (5.12) is a function of k, the unknown number of measurements, and the known problem parameters, γ, $\sigma_{x,0}$, and σ_s. Let σ_0^2 be the larger of the two eigenvalues of Σ_0. We can minimize the cost with respect to k. Taking the derivative of Eq (5.12) and setting equal to zero yields,

$$k = \frac{\sigma_0^2}{4t_m^2\sigma_s^2}\left(\frac{\gamma^2}{1-\gamma^2}\right) \tag{5.14}$$

Substituting this results in a distance traveled of

$$D(S') = r^\star - \frac{\sigma_0^2}{2 \cdot t_m\sigma_s^2}\left(\frac{\gamma^2}{1-\gamma^2}\right)$$

Now observe that in general the starting range to the true target may be less than $r^\star$, requiring no movement. Then from the optimal location, take $k \geq 1$ measurements to find the desired result. □

The closed-form expression for k in Eq (5.14) follows intuition: As the prior uncertainty (σ_0^2) increases, more measurements are required. As the measurement time t_m increases, the optimal strategy reduces k (and subsequently moves closer). As the sensor noise σ_s increases, the optimal strategy takes fewer measurements from closer positions. Based on this lower bound, we compare the cost of our proposed algorithm with that of an optimal offline algorithm.

5.4.2 Comparison with the β-Cautious Strategy

In this section, we show that the proposed algorithm produces a measurement sequence which is, on average, within a constant factor of the optimal offline cost. In what follows, it is convenient to make use of the following constants.

$$N = 4\log_{\left(\frac{\sigma_\beta^2}{\sigma_s^2}\right)}\left(\frac{1}{\gamma}\right) \qquad \text{(Lemma 5.3)}$$

$$C_{dist} = \left(\frac{\sqrt{2}}{\sqrt{\sigma_\beta^2 - \sigma_s^2}} + \frac{\pi\sqrt{\sigma_\beta^2 - \sigma_s^2}}{\sigma_\beta^2}\right) \cdot \left[\frac{1-\sqrt{\gamma}}{1-\frac{\sigma_s}{\sigma_\beta}}\right] \qquad \text{(Theorem 5.1)}$$

$$C_3 = \frac{1}{2\sigma_s^2 t_m}\frac{\gamma^2}{1-\gamma^2} \qquad \text{(Theorem 5.2)}$$

We consider the case when the hypothesis is not very close to the starting location of the robot, given by $\hat{r}_0 > C_3\sigma_0^2$. This assumption is not too restrictive. For example in our application $C_3 \approx 6 \times 10^{-4}$ since $t_m \approx 120$, $\sigma_s \approx \frac{\pi}{12}$, and $\gamma \approx .1$ (as stated in Section 2). In field trials, $\hat{r}_0 \approx \sigma_0 \approx 100m$. In subsequent analysis we also use $\hat{r}_0$ instead of $||s_0 - s_1||$ in the upper-bound, since the range to the hypothesis is always greater than the distance between the starting location and the first measurement.

The robot begins with an estimate of $x^\star$ as $\hat{x}$, a two-dimensional Gaussian, but the optimal offline algorithm has access to $x^\star$. Thus, a direct comparison of the two could produce arbitrarily bad results. One such example is $x^\star \approx s_0$ and $\hat{r}_0 \to \infty$: the β-Cautious strategy travels toward the hypothesis, while the offline algorithm does not. However, such cases occur with very small probability and it is reasonable to expect that on average the costs will be similar. Therefore we take a weighted average (expectation) over possible configurations of the robot and true target, conditioned on the prior hypothesis.

As before, let $T(S)$ be the time cost of a sequence as given by Eq . Let the true target location be $x^\star$. Given the β-Cautious measurement sequence, S_β with cost $T(S_\beta(x^\star))$, we would like to compare to the unknown optimal solution, $S^\star_{OFF}$ with cost $T(S^\star_{OFF}(x^\star))$. We will define the *expected performance ratio* as $\frac{\mathbb{E}_{x^\star}[T(S_\beta(x^\star))]}{\mathbb{E}_{x^\star}[T(S^\star_{OFF}(x^\star))]}$. We derive a bound next.

Theorem 5.3. *Let $x^\star$ be the true target location given a prior estimate $\sim \mathcal{N}(\hat{x}_0, \Sigma_0)$. Let $\hat{r}_0 > C_3\sigma_0^2$ and $\hat{r}_0 > ||s_0 - s_1||$. In expectation over $x^\star$, the time taken by the β-Cautious algorithm is less than a constant times the optimal algorithm:*

$$\frac{\mathbb{E}_{x^\star}[T(S_\beta(x^\star))]}{\mathbb{E}_{x^\star}[T(S^\star_{OFF}(x^\star))]} \leq C$$

with

$$C = \frac{N \cdot t_m + C_{dist}\sigma_0 + \hat{r}_0}{t_m + \hat{r}_0 - C_3\sigma_0^2} \tag{5.15}$$

Proof. Since $T(S') \leq T(S^\star_{OFF})$ (Theorem 5.2), and S' does not change as a function of $\mathcal{Z}$ it suffices to show that

$$\frac{\mathbb{E}_{x^\star}[T(S_\beta(x^\star))]}{\mathbb{E}_{x^\star}[T(S'(x^\star))]} = \frac{\mathbb{E}_{x^\star}[N \cdot t_m + C_{dist}\sigma_0 + ||s_0 - s_1||]}{\mathbb{E}_{x^\star}[\max(r_0^\star - C_3\sigma_0^2, 0) + t_m]} \leq C \tag{5.16}$$

where C does not depend on $x^\star$.

To establish a constant bound, we would like to remove all variables which involve the true target location (a random variable), or the measurement values. Note that the upper-bound established in Theorem 5.1 is not a function of the true target location. It remains to find the lower expected bounds.

Observe that the denominator contains the maximum of two convex functions, which is a convex function. Since the norm $r_0^\star = ||s_0 - x^\star||$ is a convex function, the mean distance to the target is less than the distance to the mean of the prior. Finally, by Jensen's inequality, $\mathbb{E}[f(x)] \geq f(\mathbb{E}[x])$ if the function $f(x)$ is convex. Since we again consider the case of $\hat{r}_0 > C_3\sigma_0^2$, this provides a lower bound as

$$\text{Eq 5.16} \leq \frac{N \cdot t_m + C_{dist}\sigma_0 + \hat{r}_0}{\mathbb{E}_{x^\star}[r_0^\star - C_3\sigma_0^2] + \mathbb{E}_{x^\star}[t_m]} \leq \frac{N \cdot t_m + C_{dist}\sigma_0 + \hat{r}_0}{t_m + \hat{r}_0 - C_3\sigma_0^2}$$

In expectation over the true target location and measurement noise, the β-Cautious costs only a constant factor more than the optimal algorithm which knows the true target location. □

5.4.3 Worst Case Online Cost

We now consider the case of an optimal algorithm operating *without* the access to the true target location. Such an algorithm executes with the same restrictions as the β-Cautious algorithm: it begins with a prior estimate and must react to the value of each measurement i.e., iteratively update the hypothesis using EKF and plan measurement locations. As before, we assume the measurement sequence $\mathcal{Z}$ is chosen by an independent adversary, similar to the analysis in Section , and present a lower bound on the cost of an optimal online algorithm in the worst case.

As seen in Section 5.4.3, the hypothesis may shift as a result of a measurement. To connect this result to the previous theorem, we first show there always exists a measurement sequence in which the hypothesis does not shift.

Lemma 5.8. *If s_i is the sensing location from where the i^{th} measurement is obtained and $\mathcal{N}(\hat{x}_{i-1}, \Sigma_{i-1})$ is the prior target hypothesis, then there exists a measurement z_i such that*

$$||\hat{x}_{i-1} - s_i|| = ||\hat{x}_i - s_i||$$

where $\mathcal{N}(\hat{x}_i, \Sigma_i)$ is the posterior target hypothesis obtained using EKF update.

Proof. The proof follows directly from the EKF update equations given in Eq (3.6) when the residual is zero (i.e., $y_i = 0$). □

The above lemma suggests that for every instance, any algorithm, including the online optimal algorithm, can receive a valid set of measurements where the mean of the hypothesis does not change with the EKF update (the covariance, however, changes). If the adversary can increase the cost by choosing other measurements, then Eq (5.17) is a lower-bound on the worst case cost. Otherwise, it is exactly the worst case cost.

Theorem 5.4. *Let $S^{\star}_{ONL}$ be the optimal online, bearing-only (not-necessarily-ambiguous) measurement sequence. Let $S^{\star}_{ONL}$ require time $T(S^{\star}_{ONL}(\mathcal{Z}))$ to reduce σ_x and σ_y by the constant γ using EKF updates. Then $T(S')$ is also a lower bound on the maximum time required by $S^{\star}_{ONL}$as follows.*

$$\max_{\mathcal{Z}} T(S^{\star}_{ONL}(\mathcal{Z})) \geq T(S') = \max\left[\hat{r}_0 - \frac{\sigma_0^2}{2 \cdot t_m \sigma_s^2}\left(\frac{\gamma^2}{1-\gamma^2}\right), 0\right] + t_m \tag{5.17}$$

Proof. First, by Lemma 5.8, there exists a measurement sequence such that the hypothesis does not shift position. In this case, we are examining the case of a measurement sequence gathering information about a fixed point, $\hat{x}_0$. Then the covariance after all measurements are collected is exactly the same form as that of the FIM, given in Eq 3.12. The full analysis is similar to that of Theorem 5.2. However, in this case, substitute $\hat{x}_0$ for $x^{\star}$ to arrive at the desired value for $T(S')$. □

The presented bound is similar to Theorem 5.2, except the dependence is on initial hypothesis $\hat{r}_0$ instead of the true target location $x^{\star}$. The sequence S', when executed with respect to the true target location, defines a global minimum cost for any algorithm. When executed with respect to the prior hypothesis, it defines a lower-bound on the time taken by any online algorithm which uses an EKF or similar estimators.

5.4.4 Comparison of Worst Case Online Performance

In this section, we define the *performance ratio* as the ratio of the worst case execution times of two measurement sequences. Using the result of Section 5.4.3 and the previous

section, we show that the performance ratio of the β-Cautious Strategy and any other online strategy is bounded above by a constant.

Theorem 5.5. *Given a prior estimate of a target location $\sim \mathcal{N}(\hat{x}_0, \Sigma_0)$, let $\mathcal{Z}$ be the measurements received by an active localization algorithm. Let $\hat{r}_0 > C_3\sigma_0^2$ and $\hat{r}_0 > ||s_0 - s_1||$. For any true target location, the time taken by the β-Cautious algorithm for any system parameters β, t_m, γ, and σ_s is less than a constant times worst case cost of the optimal online algorithm employing an EKF. Furthermore, for our known system values, the time required by the β-Cautious algorithm satisfies,*

$$\frac{\max_{\mathcal{Z}}\ T(S_\beta(\mathcal{Z}))}{\max_{\mathcal{Z}}\ T(S^\star_{ONL}(\mathcal{Z}))} \leq 5.439 \tag{5.18}$$

Proof. $\max_Z\ T(S_\beta(\mathcal{Z}))$ was presented in closed form in Theorem 5.1, where we again let $\hat{r}_0 > ||s_0 - s_1||$. Since S' is a lower bound on the worst case online algorithm, as shown in Theorem 5.4, we have that $T(S') \leq \max_{\mathcal{Z}}\ T(S^\star_{ONL}(\mathcal{Z}))$. Then it suffices to show that

$$\frac{\max_{\mathcal{Z}}\ T(S_\beta(\mathcal{Z}))}{\max_{\mathcal{Z}}\ T(S^\star_{ONL}(\mathcal{Z}))} \leq \frac{N \cdot t_m + C_{dist}\sigma_0 + \hat{r}_0}{\hat{r}_0 - C_3\sigma_0^2 + t_m} \leq 5.439 \tag{5.19}$$

The values for the remainder of the terms (σ_s, γ, and t_m) which determine N, C_3 and C_{dist} will be constant, but depend on the specific system used. We use the known system values from Chapter 2, a starting range equal to the detection range of the tags, a prior uncertainty of similar size, and $\beta = .1$. For reference, $\hat{r}_0 \approx \sigma_0 \approx 100$, $t_m \approx 120$, $\sigma_s \approx \frac{\pi}{12}$, and $\gamma \approx .1$. □

The results presented in Theorem 5.3 show the β-Cautious algorithm is within a constant of the optimal offline strategy on average. Theorem 5.5 shows that no other algorithm will have a significantly lower worst case performance. However, the constants established in Eq 5.15 and Eq 5.18 still depend on system noise, measurement time, and other non-random factors. In the next section, we evaluate the effect of these parameters on the comparisons in simulation.

5.5 Simulations

In this section we conduct numerical studies of the main results presented. First studied

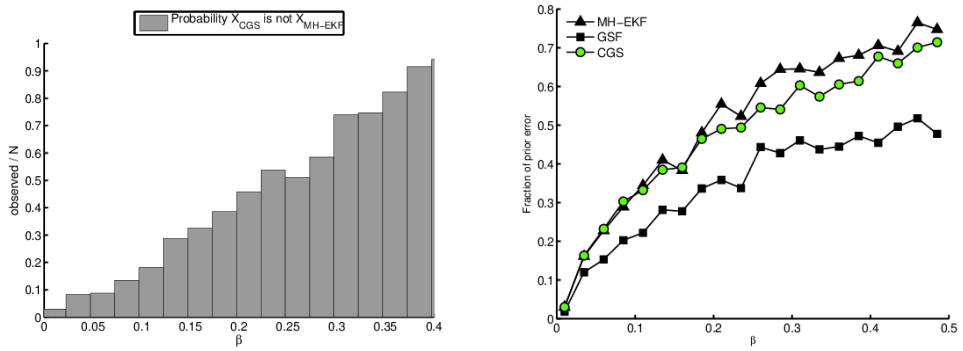

(a) (b)

Figure 5.7: **(a)** The observed probability that the MH-EKF tracks a different hypothesis than the β-Cautious Strategy. Note that for small β, the β-Cautious strategy causes the EKF to track the correct hypothesis more often. **(b)** The normalized error of the final estimate ($||\hat{x}_n - x^\star||/||\hat{x}_0 - x^\star||$) as a function of the β parameter. The median error is shown for the Gaussian Sum Filter, MH-EKF, and β-Cautious Strategy using an EKF. Note that increasing β results in more error, but at less cost as shown in Figure 5.9.

is the effect of Lemma 5.1 which shows that the β-Cautious Strategy chooses measurement locations to minimize the effect of keeping only a single hypothesis. Second, we illustrate the upper-bound presented in Theorem 5.1 as a function of the system parameters and starting conditions. Finally, we illustrate Theorem 5.2 and Theorem 5.3 to show how the performance ratio (time required divided by optimal time) changes with the starting conditions.

Our simulated setup was as follows. The β-Cautious Strategy was implemented as described in Section 5.2. An initial hypothesis was given as $\hat{x}_0 \sim \mathcal{N}(0_{2\times 1}, \sigma_0^2 \cdot I_{2\times 2})$, with $\sigma_0 = 100$. The sensor is initially placed 220 meters away from $\hat{x}$, measurement time was assumed to be 120, and sensor noise σ_s was set to 15 degrees. The true target location, $x^\star$, was repeatedly drawn with replacement from the prior for $N = 1000$ trials. For each such $x^\star$, the algorithm was run, and all measurement locations and values were recorded. Some of the parameters were individually varied to illustrate their effect, as shown in Table 5.1. As discussed in Section 2, these parameters closely match our field implementation.

The first results (Figures 5.7 and 5.8) evaluate the assertions of Section 5.1, namely

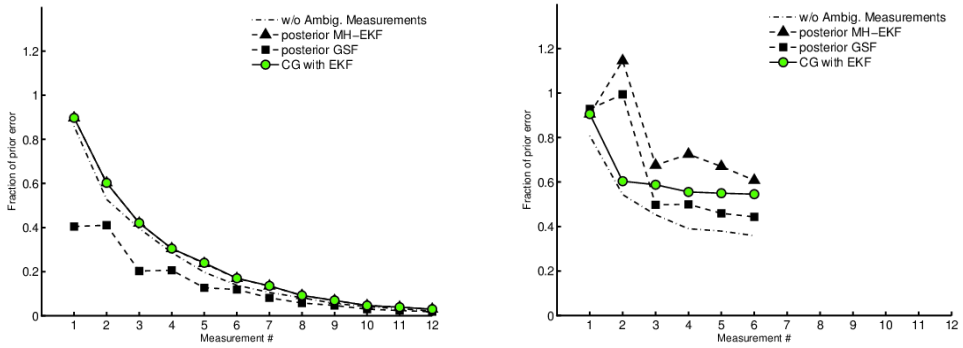

(a) $\beta = .01$ (b) $\beta = .26$

Figure 5.8: Two examples of the effect of the parameter β, comparing the difference in final estimates using an EKF, MH-EKF, and Gaussian Sum Filter. Shown is the median error over 1000 trials, after each measurement, for all three filters, as well as an "omniscient" EKF which was given the correct, un-ambiguous measurements. **(a)** With $\beta = .01$, we notice agreement and small final error. **(b)** With $\beta > .2$, we notice reduced performance in all filters. These observations suggest that the measurement locations corresponding to low values of β are useful for mitigating the effect of ambiguous measurements, as suggested by Lemma 5.1.

Table 5.1: Simulation Parameters

	Range (r_0)	Measure Time (t_m)	Desired Info (γ)	β
Value	220 meters	120 sec	.1	.1
See Fig	Fig 5.10a	Fig 5.10d	Fig 5.9a,5.9b,5.9c,5.10c	Fig 5.9d,5.10b

that by carefully choosing measurement locations for an EKF, we can closely approximate the bi-modal measurement PDF. For this evaluation, we compared the performance of the β-Cautious Strategy with a multiple hypotheses filter. There are two predominant methods for producing a target estimate from multiple hypotheses both of which we implemented for comparison. First, the output could be the most likely of the hypotheses (the target estimate, $\hat{x}_i$ with highest $p(\hat{x}_i|Z)$, for measurement sequence Z). A multiple hypothesis Extended Kalman Filter (MH-EKF) [32] captures this approach. Another interpretation of the hypotheses is available through a Gaussian Sum Filter (GSF, proposed in [79], but also realized in Interacting Mixture Model-based filters [19,80]). Using the GSF and similar methods, the output is the weighted average of all hypotheses. In both cases, we did not implement measurement gating or hypothesis

merging, since these are alternative methods of truncating the PDF (see [32, 76, 77]), and instead maintained all the hypotheses for comparison.

As implied by Lemma 5.1, we expect that decreasing β would reduce the necessity for tracking multiple hypotheses. This can be checked by verifying that a multiple-hypotheses filter does not produce significantly different output when β is small. The β-Cautious Strategy was run as designed (using an EKF to estimate the target state). Depending on the specific setting for β, the algorithm chose an adaptive sequence of measurement locations, of length $k \in [4, 12]$. Using the measurement locations and values, the set of 2^k hypotheses was then created using Eq. (5.1) (during execution the algorithm did not have access to these other hypotheses). The 2^k individual hypotheses correspond to all combinations of "forward" or "backward" measurements for each measurement location. The β-Cautious Strategy, by employing an EKF, tracks one of the 2^k hypotheses directly—corresponding to all "forward" measurements—and discards the rest. Conversely, the MH-EKF will evaluate all the hypotheses, and output highest weighted hypothesis as the target estimate. According to Lemma 5.1, we would expect that small β would correspond to similar output between both algorithms. In Figure 5.7a, we plot the observed probability that the β-Cautious Strategy tracks a hypothesis *different* from the MH-EKF as a function of β. We see that for small values of β, this occurs with very small probability. Also shown is the output of an EKF which has the correct, un-ambiguous bearings as input. As expected, with small β, the un-ambiguous EKF has nearly identical output. These observations confirm the idea that β captures the risk from ambiguous measurements, i.e., of tracking the "wrong" hypothesis.

Another meaningful comparison is the error of the final estimates using all three methods (GSF, MH-EKF, and β-Cautious), which is presented in Figure 5.7b and Figure 5.8. In all simulations, the final covariance was equal, but the error of the estimate was observed to vary with β. Figure 5.7b shows the median error of the final estimate for $\beta \in [.01, .45]$. Note that increasing the caution requirement ($\beta \to 0$) produces less error in the estimate of the target location, even though the covariance does not change. Interestingly *all* filter output was less accurate as β increased, suggesting that the β-Cautious measurement locations are valuable for other filtering techniques, not just the EKF. Figure 5.8 shows the error after each measurement, for two values

of β and all three filtering techniques. In Figure 5.8b, the median decrease (posterior error over prior error) was 40% at best, while it was less than 3% in Figure 5.8a.

As shown in Section 5.4.3, the parameter β has a significant effect on the time required to localize the target, but so do the other system parameters and starting conditions. The focus of the next simulations is to evaluate the effect of these parameters on the maximum time required to localize a target. For each different simulation, one parameter was varied (see Table 5.1). Eq 5.9 is plotted, along with the aggregate observed values for the time to localize the target. In all cases, the theoretical bounds held as shown in Figure 5.9.

The final simulations (Figure 5.10) examine the relationship between the β-Cautious strategy and the optimal algorithm. The distance traveled and number of measurements required was recorded. Shown is the theoretical constant, derived in Section 5.4.2. Below this is the mean observed time $T(S_\beta)$ divided by the mean of the lower bound on the optimal time, $T_{S'}$ from Eq (5.17).

From these trials, and the theoretical results already presented, we conclude that the β parameter captures a tradeoff between the accuracy of the final estimate and the time spent localizing a target. Small β leads to better accuracy for all filters examined, at the cost of increased time spent traveling and taking measurements. Crucially, it was observed that using an Extended Kalman Filter is sufficient to produce final estimates which are consistent and accurate, for small values of β.

The time bound in Theorem 5.1 was predicated on the use of the EKF, through Lemma 5.1 (however the results in Section 5.4.1 apply to any unbiased filter [21]). An interesting future result would be to bound the shift in the hypothesis location for other filtering techniques, allowing similar upper bounds to be established when measurements are planned against the corresponding output. In this work, we have observed that when using the β-Cautious Strategy, the EKF performs as good as more "expressive" filters so long as β is small, thus allowing a closed-form guarantee of the time required to localize the target. In the next section, we will show that our assumptions and results hold during field deployments.

5.6 Field Experiments

After establishing the upper bound in closed form and in simulation and evaluating the consistency of the algorithm, we deployed our system for field trials. Before presenting the results, we give the details of our field implementation.

We conducted two types of experiments. In the first set of trials, we evaluated the sensing model and the upper-bound directly. For these experiments, a transmitting radio tag was placed in a field measuring approximately 64 by 70 meters (Figure 5.12a). We provided a prior target estimate for each trial, and evaluated the cost to localize the target to the desired bounds and the accuracy of the final estimate.

In the first example, shown in Figure 5.12a, the input was a starting hypothesis which encompassed the experiment area (2-σ bounds was 70 meters, with a starting error of 30 meters). The goal of these trials was to establish the correctness of the upper bound and verify that a small number of measurements is sufficient to localize a static target. Using these starting parameters and the system data reported in Section 2, we can derive the expected time using Eq (5.9). Constructing bearing measurements take less than 2 minutes and the chassis velocity is approximately 1 meter per second ($t_m \approx 120$). To achieve a desired final covariance of less than one tenth the original, we expect a travel distance of less than 350 meters, and 4 measurements (based on Eq (5.9)). We found that the experimental results agreed with the theoretical analysis. Specifically, the final covariance was less than 6 meters, one sigma bound, four measurements were required, and the robot traveled less than 70 meters in the given example. The final error of the estimate was less than 4 meters.

We found that in all cases in all experiments, the number of measurements matched the predicted upper bounds and the distance traveled was less than the theoretical limit. This leads us to believe that the theoretical bounds are a good prediction of the performance of the system and produce reliable estimates of the time required to localize one or more nearby targets.

Finally, the algorithm presented will be combined with a robust initialization technique to localize several nearby tags in Chapter 8.

5.7 Discussion

We have examined the problem of using a mobile robot to locate a radio transmitter using a directional antenna. Presented was an active localization algorithm suitable for systems which have non-zero measurement time. In the case of RSSI-based bearing measurements, ambiguity can be mitigated by structuring the measurement sequence carefully. The algorithm was analyzed to show an upper bound on the time cost as a function of the system parameters (sensing noise, measurement time, chassis velocity) and tracking objective (initial uncertainty versus final requested uncertainty). The resulting closed form analysis is amenable to engineering trade-offs and comparisons with other bearing-only active localization algorithms.

This chapter contains the first closed-form lower-bound on the optimal cost of bearing-only localization of static targets. The lower-bound will be useful to algorithm and system designers as a base-line comparison.

To compare the performance of the β-Cautious algorithm directly to the unknown optimal algorithm, we presented simulations and closed form analysis. In the next Chapter, we tighten the lower-bound and are able to provide a means to *compute* the optimal offline strategy, but cannot produce its cost in closed form.

A closed-form representation of the optimal cost was necessary for the comparison to the optimal cost of an online, EKF-based algorithm, which allowed us to present a worst-case bound. Thus, using these results we have shown that our presented algorithm is near optimal when used in the application described.

The algorithm proposed here will be used in Chapter 8, to localize a tight cluster of nearby targets.

The next Chapter will deal with multi-robot extensions. A major challenge when designing a field system for cooperative tracking with multiple robots is communication. The communication constraint complicates the optimal algorithm design: When and where should the robots meet to communicate? Does the optimal multi-robot algorithm enforce communication constraints at all or should the robots proceed independently?

Algorithm 5.1 β-Cautious Strategy$(s_0, \hat{x}_0, \Sigma_0, \beta, \gamma, \sigma_s^2)$

$\sigma_\beta \leftarrow \dfrac{\pi}{2 \cdot \Phi^{-1}(1 - \frac{\beta}{2})}$
$\sigma_{x,0}^2, \sigma_{y,0}^2 \leftarrow$ eigenvalues(Σ_0)
$i \leftarrow 1$
while $\sigma_{x,i} \geq \gamma \cdot \sigma_{x,0}$ or $\sigma_{y,i} \geq \gamma \cdot \sigma_{y,i}$ **do**
    Polar frame at $\hat{x}_{i-1}$ aligned with $\sigma_{x,i-1}$
    $r_i \leftarrow \frac{\sigma_{x,i-1}}{\sqrt{\sigma_\beta^2 - \sigma_s^2}}$
    Let s_i be the closer of $(r_i, \frac{\pi}{2})$ or $(-r_i, \frac{\pi}{2})$.
    Collect measurement z_i from s_i
    $\hat{x}_i, \Sigma_i \leftarrow$ ekf_update$(z_i, \sigma_s, \hat{x}_{i-1}, \Sigma_{i-1})$
    $\sigma_{x,i}^2, \sigma_{y,i}^2 \leftarrow$ eigenvalues(Σ_i)
    $i \leftarrow i + 1$
end while

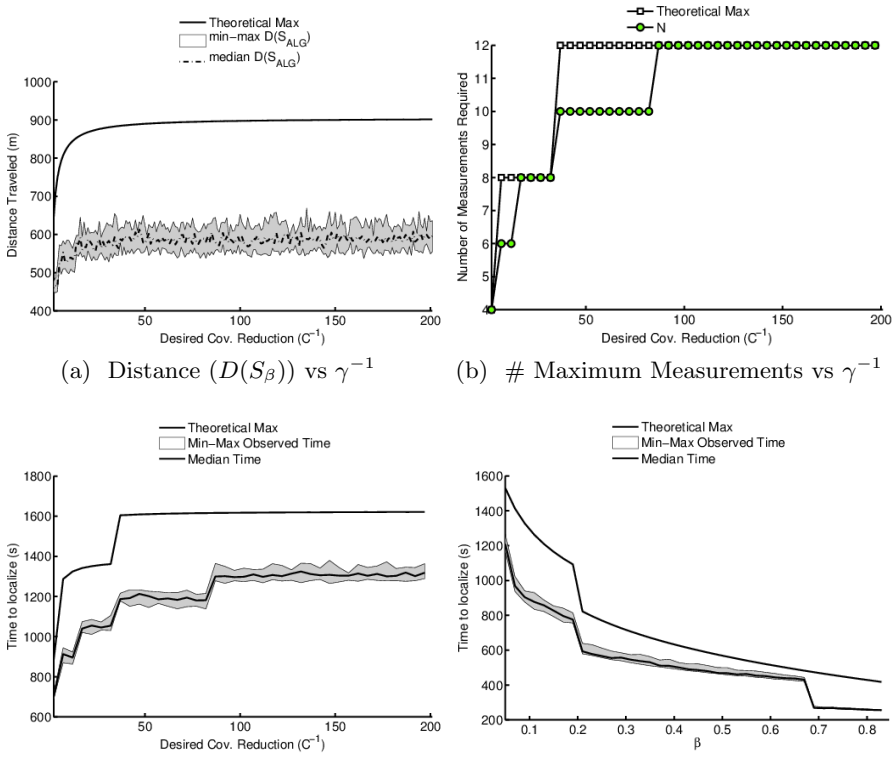

(a) Distance ($D(S_\beta)$) vs γ^{-1}

(b) # Maximum Measurements vs γ^{-1}

(c) Maximum Time ($T(S_\beta)$) vs γ^{-1}

(d) Maximum Time ($T(S_\beta)$) vs β

Figure 5.9: Simulations studies of the possible configurations and the resulting upper bound. We vary the final required uncertainty (γ), and evaluate the costs as shown in Theorem 5.1. **(a)** the distance traveled as γ decreases (corresponding to a more precise final estimate). **(b)** the number of measurements taken. **(c)** the total execution time as γ decreases. In **(d)**, is the tradeoff between increasing the parameter β and the resulting time required to localize the target. Note that the target can be localized more quickly by increasing risk. The discrete drops in time correspond to removing a measurement from the sequence and the remaining reduction in time is from placing the measurements closer together. Both will cause more error in the final estimate, as shown in Figure 5.7b.

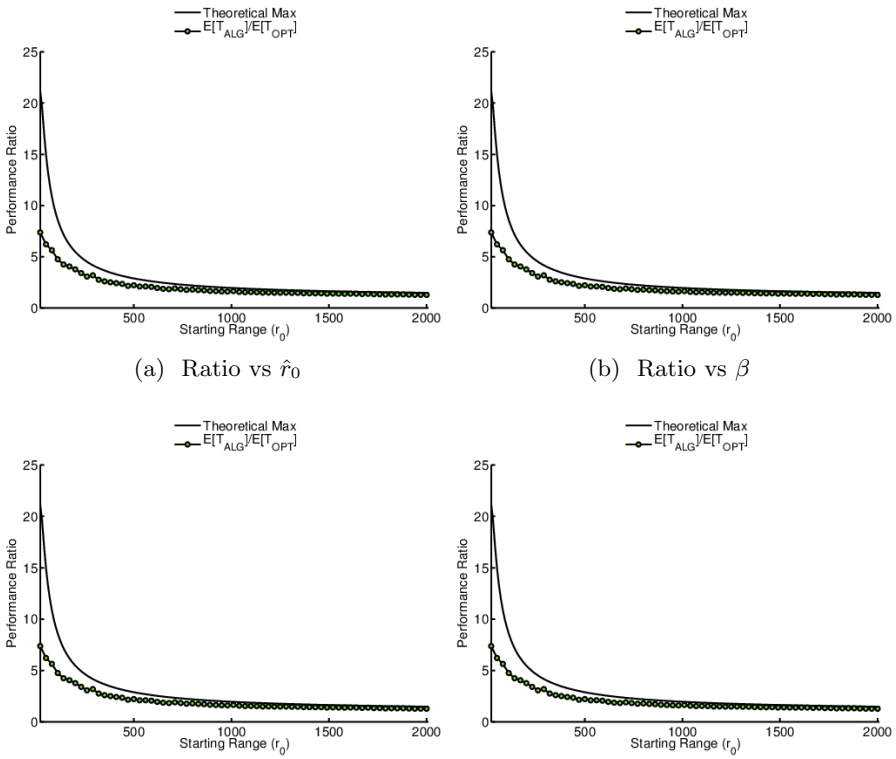

(a) Ratio vs $\hat{r}_0$

(b) Ratio vs β

(c) Ratio vs γ

(d) Ratio vs Measurement time t_m

Figure 5.10: The theoretical performance ratio (Eq (5.15)) and observed performance ratio ($\mathbb{E}[T(S_\beta)]/\mathbb{E}[T(S')]$) as a function of: **(a)** the starting range to the hypothesis, $\hat{r}_0$, **(b)** the desired risk (increasing β), and **(c)** the measurement time (increasing t_m). Note that in some cases the theoretical bounds are quite loose. This results from our analysis: we provide an upper-bound on the worst case. In practice, the worst-case is rarely if ever encountered.

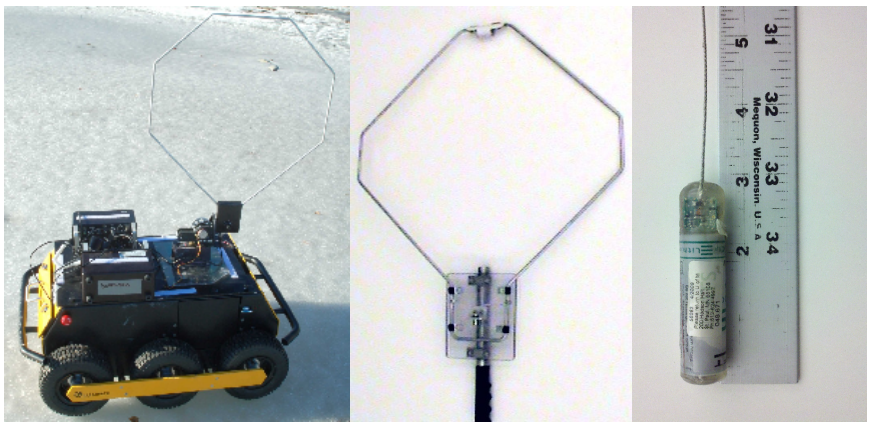

(a) (b) (c)

Figure 5.11: **(a)** The robotic platform employed in field tests. Notice the octagonal antenna used to detect nearby radio transmitters, and the servo-motor used to rotate the antenna. The robot has been tested on multiple lakes in Minnesota, USA, including Lakes Gervais, Staring, Keller, and Phalen. **(b)** The antenna used to gather bearing measurements. The antenna is radially symmetric, producing *ambiguous* bearing measurements. The antenna is approximately 56cm (22 in) in diameter and is mounted on a servo-motor attached to the robotic chassis. **(c)** A radio transmitter which is surgically implanted in invasive fish. Each transmitter (or "tag") has a unique frequency and transmits an uncoded pulse at approximately 1.1 Hz. The tags are nearly 7.5cm (3 in) long.

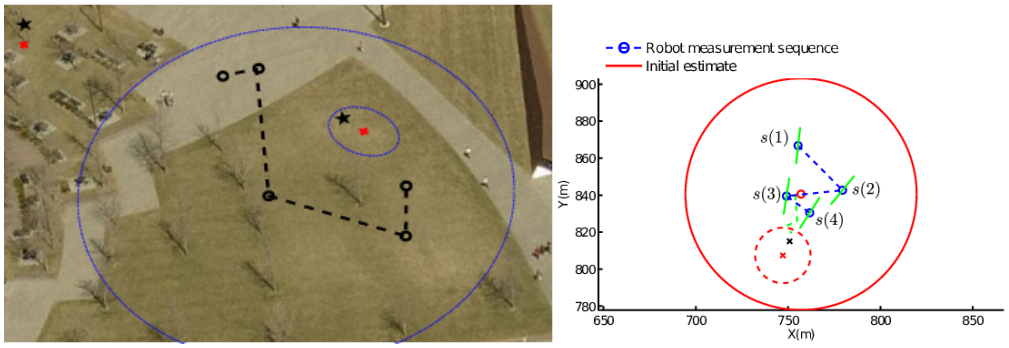

(a) (b)

Figure 5.12: Two single-target field trials. Parameters were $\sigma_\beta^2 = 1$ and $\sigma_s^2 = \left(\frac{\pi}{8}\right)^2$. In both cases, the time for the system to localize the target adhered to the theoretical bounds. **(a)**: The 2 σ uncertainty ellipses are shown for the prior and final estimates. The final error was less than 5 meters after only 4 measurements. The total experiment area was approximately 70 meters by 64 meters. **(b)**: At Lake Gervais, MN. USA. With no prior information, the initial estimate was constructed using the routine described in Chapter 8, producing the large red circle shown. The measurement locations narrowed the uncertainty to the final circle given as a dashed line. The true target location is labelled as a black 'x'.

Chapter 6

Optimal Offline Localization of a Stationary Target with Many Robots

In Chapter 5, we studied the problem of designing active localization strategies for a single robot with a sensor capable of measuring bearings of the radio tags. Extending this strategy to the case of multiple robots is not straightforward, since two or more robots must merge their estimates of the target location by communicating with each other. Furthermore, the communication range of the robots is limited in practice, and an optimal algorithm must include time spent while the robots meet to establish communication. Therefore, we study the problem of active localization for mobile robots subject to distance-based communication constraints.

In this and the next chapter, we provide three main results. First, we extend the existing body of work which analyzes the offline case: planning measurements with respect to a known target location. The optimal algorithm provides a baseline for comparison of system improvements (increased velocity, decreased measurement time, increased numbers of robots, or improved sensing), and the effect on the mission objectives such as time-to-localize. We present optimal offline algorithms and bounds on offline costs for any number of collaborating mobile bearing sensors in Section 6.1.

Second, we extend the optimal offline algorithm to include communication constraints (Section 6.4). While the optimal strategy must include at least one communication exchange to gather all the robots' measurements, we show the optimal strategy might sometimes cause the robots to move out of communication range to take better measurements. Thus, enforcing persistent communication in our setting is potentially suboptimal. This motivates us to study algorithms which allow the robots to break communication when necessary. As a result, they must also include a rendezvous component.

Beginning in Chapter 7, we address the more realistic case: when only a prior estimate of the true target location is known. To solve this *online* problem, we plan measurements to minimize the worst-case cost, even though the prior estimate may be uncertain or even misleading. We present a general method of adapting any offline measurement strategy for use in an online setting. In doing so, the cost is shown to be at most a logarithmic factor more than that of the offline optimal algorithm, as shown in Section 7.1. Our final contribution involves field experiments: We have implemented and tested the online algorithms on the robot system shown in Figure 2.1. We present field deployments in which two networked robots successfully locate a radio transmitter accurately and without requiring significant travel time. The field experiments are presented in Section 7.2.2.

6.1 The Optimal Offline Algorithm

In the offline problem, the true target location ($x^\star$) is known. The goal is to design a minimum-cost measurement strategy S to satisfy the information requirements in Equation (3.24). We study the case with unbounded communication range before introducing communication constraints in Section 6.4. We start by discussing the structure of the matrix $\mathbb{F}$ since the closed-form representation of $\mathbb{F}$ is used to derive the optimal measurement sequences.

Consider a measurement sequence S, and the resulting Fisher Information Matrix, $\mathbb{F}(S)$. Define a coordinate frame, called the Target-Local (TL) frame, centered at $x^\star$. Align the x axis of this frame with the eigenvector corresponding to the maximum eigenvalue of $\mathbb{F}^{-1}(S)$. In the TL frame, all sensor locations are specified in polar coordinates;

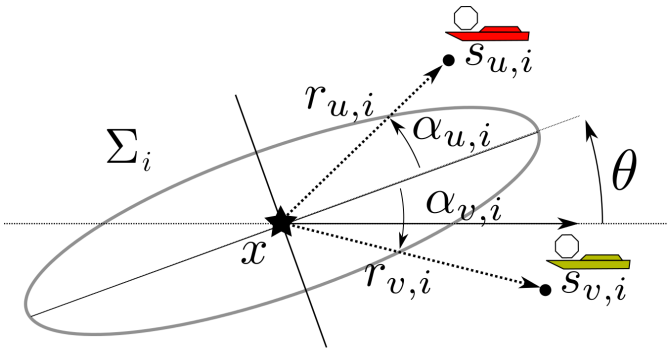

Figure 6.1: The *target-local* coordinate frame. By expressing the measurement locations (black dots) with respect to the frame rotated by θ, $\mathbb{F}$ is a diagonal matrix. The covariance ellipse's eigenvectors are aligned with the frame in which we express sensor locations.

the i^{th} measurement taken by the u^{th} robot is given as $s_{u,i} = (\alpha_{u,i}, r_{u,i})$. α is the angle formed with respect to the x axis, and r is the distance between the sensor location and $x^\star$.

The TL coordinate frame is illustrated in Figure 6.1. In practice, a TL frame is obtained by applying a de-correlating transform, e.g., the Singular Value Decomposition or Eigen decomposition of $\mathbb{F}$ [81]. The FIM has a convenient decomposition as the sum of all FIM from each individual measurement as given below.

$$\begin{aligned}\mathbb{F}_{\text{TL}}(S) &= \sum_{u=1}^{n} \mathbb{F}_{\text{TL}}(S_u) = \sum_{u=1}^{n}\sum_{i=1}^{N_u} \mathbb{F}_{\text{TL}}(s_{u,i}) \\ &= R(\theta) \begin{bmatrix} \sum_{i=1}^{N} \frac{\sin^2(\alpha_i)}{r_i^2\sigma^2} & 0 \\ 0 & \sum_{i=1}^{N} \frac{\cos^2(\alpha_i)}{r_i^2\sigma^2} \end{bmatrix} R(\theta)^T \end{aligned} \tag{6.1}$$

The variable $N = |S|$ is the total number of measurements taken by all robots, and $R(\theta)$ is a transform that rotates coordinates to the TL frame from the world frame. In the TL coordinate frame, two useful properties of $\mathbb{F}(S)$ become evident.

First, the eigenvalues are simply the diagonal elements. Thus,

$$\underline{\lambda}\mathbb{F}(S) = \sum_{i=1}^{N} \frac{\sin^2(\alpha_i)}{r_i^2\sigma^2} \tag{6.2}$$

and

$$\bar{\lambda}\mathbb{F}(S) = \sum_{i=1}^{N} \frac{\cos^2(\alpha_i)}{r_i^2\sigma^2}. \tag{6.3}$$

Note, if (6.2) is greater than (6.3), then the axes of the frame are switched so that (6.2) is less than (6.3). In general, the off-diagonal elements of $\mathbb{F}(S)$ are given by $\sum_{i=1}^{N} -\frac{\sin(2\alpha_i)}{r_i^2\sigma^2}$. When $\mathbb{F}(S)$ is diagonalized this sum must equal 0, i.e.,

$$\sum_{i=1}^{N} -\frac{\sin(2\alpha_i)}{r_i^2\sigma^2} = 0. \tag{6.4}$$

Second, the value of θ can be adjusted without affecting the eigenvalues, implying the following useful lemma.

Lemma 6.1. *All measurement locations can be rotated around the true target location without affecting the eigenvalues of* $\mathbb{F}$*.*

Proof. Changing the orientation of the world frame with respect to the covariance ellipse (θ in Equation 6.1) has no effect on eigenvalues since rotations are orthogonal transforms. □

The remainder of the section is devoted to algorithms to find the optimal number of measurements and the correct assignment of robots to measurement locations.

6.2 Optimal Active Localization Using a Single Robot

In this section, we solve the special case of Problem 1 when $n = 1$. The derivation proceeds as follows. In Lemma 6.2, we show that the optimal one-robot trajectory has only two measurement locations. Lemma 6.3 establishes the optimal second location as a function of the first measurement location. The section ends by describing a method of searching for the optimal first measurement location.

Lemma 6.2 (Two Measurement Locations are Necessary and Sufficient)**.** *There exists an optimal one-robot, offline, bearing-only measurement sequence consisting of exactly two measurement locations.*

Proof. First note that there must be at least two measurement locations to satisfy $\underline{\lambda}\mathbb{F} > 0$. For contradiction, suppose not and consider Equation 6.4 with only one measurement location. Since $\sin(2\alpha) = 2\sin(\alpha)\cos(\alpha)$, Equation 6.4 implies that one of Equation 6.2 or Equation 6.3 is equal to zero, contradicting the assumption that both eigenvalues are greater than zero.

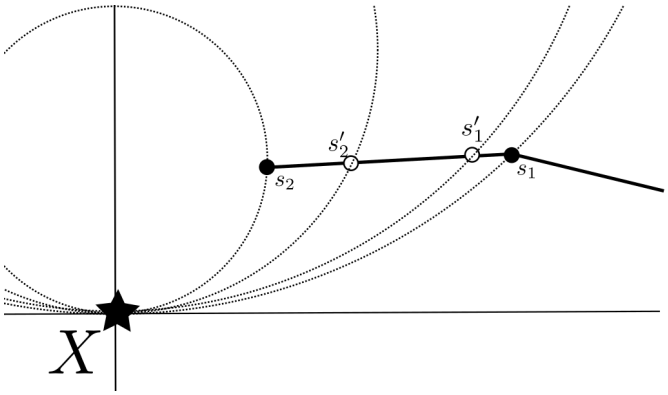

Figure 6.2: An illustration of Lemma 6.2. Three or more measurement locations are sub-optimal in the case of a single robot. Two measurement locations s_1 and s_2 can be moved closer together to produce a lesser-cost trajectory with the same information. This process can be repeated until the pair of measurement locations is collapsed to the same point.

To complete the proof, suppose there are three or more distinct measurement locations in the optimal sequence. Let $S = \{s_1, s_2, s_3\}$ be three consecutive measurements from this trajectory. Consider the diagonalized $\mathbb{F}$ resulting from the trajectory. Since $N \geq 3$, there is a pair of measurement locations (s_1, s_2) with either (i) $\alpha_1 \geq 0$ and $\alpha_2 \geq 0$ or (ii) $\alpha_1 < 0$ and $\alpha_2 < 0$. We will show that if three distinct measurement locations exist, the cost is not optimal. From Equation (6.2), we see

$$\underline{\lambda} = \sum N_i \frac{\sin^2(\alpha_i)}{r_i^2 \sigma^2}, \tag{6.5}$$

where N_i is the number of measurements taken at location s_i.

The locus of measurement locations yielding the same value for Equation (6.2) is defined by the circular contour of the form $r_i = C \sin \alpha_i$. See Figure 6.2.

If the pair is on the same contour, we can reduce the sequence cost by taking $N_1 + N_2$ measurements from one location, with no effect on the information gains—a

contradiction of the assumption of optimality of the original trajectory. If not, then one measurement is "more informative" than another. Let $N_2 \frac{\sin^2(\alpha_2)}{r_2^2} \geq N_1 \frac{\sin^2(\alpha_1)}{r_1^2}$ (the proof for the opposite case is similar). This implies s_1 lies "inside" the circular contour of s_2. Thus, s_2 could be moved closer to s_1, thereby increasing the information. By the triangle inequality, the cost of the path from previous measurement locations to s_1 then to s_2 is no longer than before. Since the sequence now has more information than required, s_1 can be moved closer to s_2, producing a trajectory with lesser cost, but with the same information as the supposed optimal solution—a contradiction of the optimality of the original trajectory. □

From both locations, there may be many measurements taken. For the moment, assume that the correct measurement counts N_1 and N_2 are known. We will later show how to search over possible values for N_1 and N_2. The following lemma provides a relationship between the two measurement locations.

Lemma 6.3 (Structure of One-Robot Trajectory)**.** *There exists an optimal solution with the first measurement location on the line* $\overline{s_0 x^\star}$*. Furthermore, given the first measurement location,* s_0*, and measurement counts for the two measurement locations,* N_1 *and* N_2*, the second measurement location must satisfy,*

$$\sin^2 \alpha_2 = \lambda_d \frac{r_2^2 \sigma^2}{N_2} + \lambda_d \frac{r_1^2 \sigma^2}{N_1} - \lambda_d^2 \frac{r_1^2 r_2^2 \sigma^4}{N_1 N_2} \tag{6.6}$$

and

$$r_2^2 = N_2 \frac{N_1 \sin^2 \alpha_2 - \lambda_d \sigma^2 r_1^2}{N_1 \lambda_d - \lambda_d^2 \sigma^4 r_1^2}. \tag{6.7}$$

Proof. Given a starting location s_0, the goal is to find the optimal measurement locations, s_1 and s_2. Note that there exists an optimal algorithm with the first measurement location, s_1 placed on the line between s_0 and $x^\star$. If it was not, rotating both s_1 and s_2 (adjusting θ as stated in Lemma 6.1) would reduce the time to travel between s_0 and s_1 without affecting the eigenvalues or cost to visit s_2 from s_1.

The eigenvalues of the resulting FIM can be found using the quadratic formula. For any 2×2 matrix A with trace $\mathrm{tr}(A)$ and determinant $\det(A)$, the eigenvalues λ satisfy

$$\lambda(A) = \frac{1}{2}\mathrm{tr}(A) \pm \frac{1}{2}\sqrt{\mathrm{tr}(A)^2 - 4 \cdot \det(A)}. \tag{6.8}$$

When considering the optimal sequence, both $\mathrm{tr}(\mathbb{F})$ and $\det(\mathbb{F})$ are positive. Fix the x axis of the coordinate frame to the line $\overline{s_0 x^\star}$. Then $\alpha_1 = 0$, and it is possible to solve for α_2 and r_2 using the fact that

$$\det(\mathbb{F}) = \sum_{i=1}^{N_1 \cdot N_2} \frac{\sin^2 \alpha_2}{r_1^2 r_2^2 \sigma^4} \text{ (c.f. Equation. 6 [82])}. \tag{6.9}$$

Since $\underline{\lambda}$ is equal to the desired λ_d, solving the previous yields

$$\sin^2 \alpha_2 = \lambda_d \frac{r_2^2 \sigma^2}{N_2} + \lambda_d \frac{r_1^2 \sigma^2}{N_1} - \lambda_d^2 \frac{r_1^2 r_2^2 \sigma^4}{N_1 N_2} \tag{6.10}$$

and

$$r_2^2 = N_2 \frac{N_1 \sin^2 \alpha_2 - \lambda_d \sigma^2 r_1^2}{N_1 \lambda_d - \lambda_d^2 \sigma^4 r_1^2}. \tag{6.11}$$

□

The values of r_2 and α_2 from Lemma 6.3 describe a curve as shown in Figure 6.3 (for differing values of r_1, and λ_d).

The optimal second measurement location is the closest point on the resulting curve described by Equations 6.10. Because the curve is convex (for a given r_1, N_1, and N_2) there exists a unique point on the curve closest to the first measurement location. Finding the optimal trajectory reduces to searching for the optimal range, r_1, and measurement counts, N_1 and N_2.

The cost of the sequence as a function of the two measurement locations is

$$\begin{aligned} C_{\text{one-robot}} =& t_m(N_1 + N_2) + d(s_0, x^\star) - r_1 \\ &+ \sqrt{(r_2 \sin \alpha_2)^2 + (r_1 - r_2 \cos \alpha_2)^2}. \end{aligned} \tag{6.12}$$

Minimizing this cost over N_1 and N_2 can be done by enumeration using a table of size $N \times N$, with $N = N_1 + N_2$. The table size is bounded since $N \leq \frac{d(s_0, x^\star)}{t_m} + 2$ and N is a positive integer. If $N > \frac{d(s_0, x^\star)}{t_m}$, the robot spends more time measuring than would be required to travel to the true target location. From close to $x^\star$, any

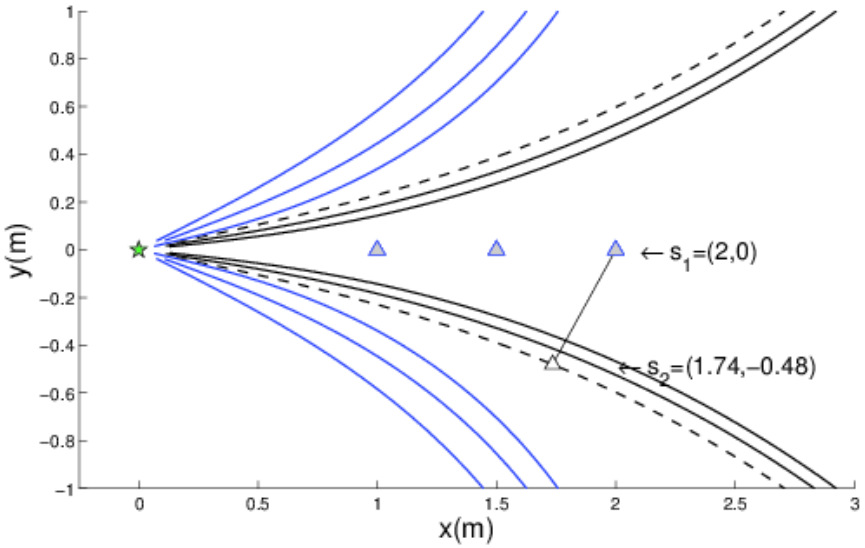

Figure 6.3: Examples of the contours described by Equation (6.10) and (6.11) for a target at $(0,0)$ (shown as a star), $r_1 \in \{1, 1.5, 2\}$ and λ_d set to .01 (black lines of lesser curvature) or .05 (blue). σ_s was 1 and N_1 was 1. For example, if the robot first travels to the position $s_1 = (2,0)$ and takes one measurement then it can take all remaining measurements from anywhere on the dashed curve (e.g., s_2 as labelled) to ensure both eigenvalues of $\mathbb{F}$are greater than λ_d.

two measurements that are not collinear with the target are sufficient to achieve any information objective since $r_1 = r_2 \approx 0$ (Equation (6.2)). Each entry in the table corresponds to a minimization of Equation (6.12) over r_1, which is accomplished using finite-difference methods. The one-robot trajectories shown in Figure 6.4 were calculated for values of $\lambda_d \in \{1, 2, 4, 6, 12\}$.

To summarize, the optimal one-robot trajectory can be found using Algorithm 6.1. For brevity, we have omitted boundary checking (e.g., $0 < r_1 \leq d(s_0, x^\star)$) and initialization. As stated, the minimization on Line 6.1 is done using a finite difference approximation to gradient descent.

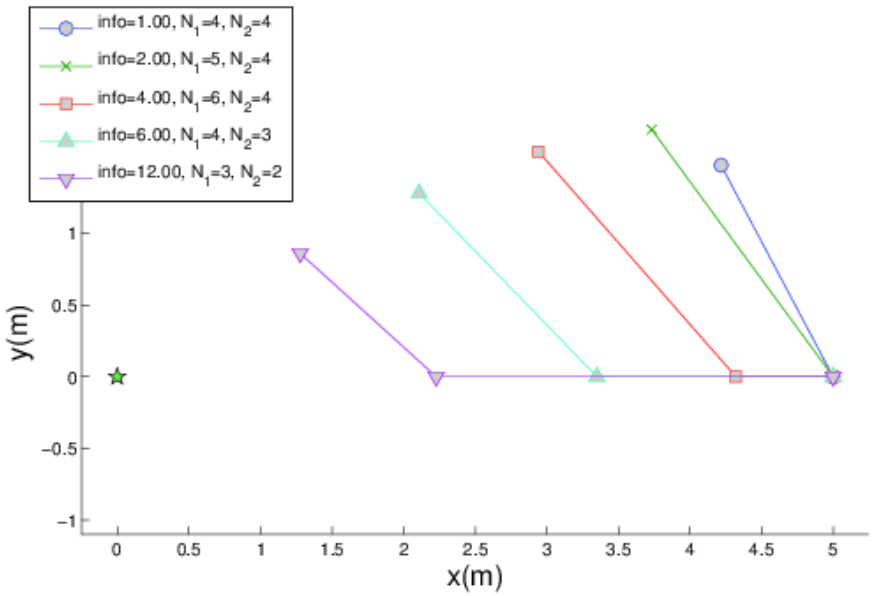

Figure 6.4: These optimal one-robot offline trajectories corresponding to values of $\lambda_d \in \{1, 2, 4, 6, 12\}$. Note the robot begins at location $(5, 0)$ and moves along the x-axis to the first marked location.

6.3 Optimal Active Localization with Two Robots

This section details the cost of using two robots and gives an algorithm for deriving the optimal deployment in Algorithm 6.2. Theorem 6.1 shows that the two-robot strategy, with slight modification, is also optimal for many pairs of robots collaborating to locate static targets. Finally, in Section 6.4 a method to incorporate communication constraints is given.

First, we show that an optimal two-robot deployment is symmetric. We say that a strategy is symmetric if, for any measurement location at location (α_v, r_v), there exists another measurement with $\alpha_u = -\alpha_v$ and $r_u = r_v$.

Lemma 6.4 (Symmetric Trajectories)**.** *There exists an optimal symmetric two-robot measurement strategy i.e., for robots u and v,*

$$\forall i : \alpha_{u,i} = -\alpha_{v,i} \text{ and } r_{u,i} = r_{v,i}. \tag{6.13}$$

Proof. Consider any optimal measurement sequence, $S^\star$, consisting of two trajectories,

Algorithm 6.1 One-Robot Offline Solution

Input: $\sigma, s_0, x^\star, \lambda_d$
Output: s_1, s_2, N_1, N_2

Initialize guess for r_1^1
$N_{max} \leftarrow \frac{d(s_0,x^\star)}{t_m} + 2$
$M, R, A \leftarrow N_{max} \times N_{max}$ matrix
for $t = [2, \infty)$ and r_1 not converged **do**
    for each row i and column j of M **do**
        $N_1 \leftarrow i$ and $N_2 \leftarrow j$
        $A_{i,j} \leftarrow \arg\min_{\alpha_2}$ Equation (6.12) subject to Equation (6.10)
        $R_{i,j} \leftarrow$ evaluate Equation (6.11)
        $M_{i,j} \leftarrow$ evaluate Equation (6.12)
    end for
    $C^t \leftarrow \min_{i,j} M$
    $r_1^{t+1} \leftarrow r_1^t - c \cdot \frac{C^t - C^{t-1}}{r_1^t - r_1^{t-1}}$ for small c
end for
$i^\star, j^\star \leftarrow \arg\min_{i,j} M$
$N_1 \leftarrow i^\star, N_2 \leftarrow j^\star$
$\alpha_2 \leftarrow A_{i^\star,j^\star}$
$r_2 \leftarrow R_{i^\star,j^\star}$
$s_1 \leftarrow (0, r_1), s_2 \leftarrow (\alpha_2, r_2)$

one for each robot, $S_u^\star$ and $S_v^\star$. Suppose $S_u^\star$ and $S_v^\star$ are not symmetric. Construct a symmetric, equivalent trajectory as follows. Let S_u' and S_v' be the same robot trajectories, but flipped about the line $\overline{s_0 x^\star}$, as shown in Figure 6.5. The two options for symmetric trajectories are either $S_u^\star$ and S_u' or $S_v^\star$ and S_v'. We will show that at least one must satisfy $\underline{\lambda} \geq \lambda_d$. Consider that

$$\lambda_{min}\left(\mathbb{F}(S_u^\star) + \mathbb{F}(S_v^\star)\right) = \lambda_d. \tag{6.14}$$

By Weyl's theorem (Section 6.7 [18]),

$$\lambda_{min}\left(\mathbb{F}(S_u') + \mathbb{F}(S_v') + \mathbb{F}(S_u^\star) + \mathbb{F}(S_v^\star)\right) = 2\lambda_d. \tag{6.15}$$

Since each measurement location, i, has a mirrored location, j, we have $r_i = r_j$ and $\alpha_i = -\alpha_j$, which implies Equation (6.4). Thus, $\mathbb{F}(S_u') + \mathbb{F}(S_v') + \mathbb{F}(S_u) + \mathbb{F}(S_v)$ is a

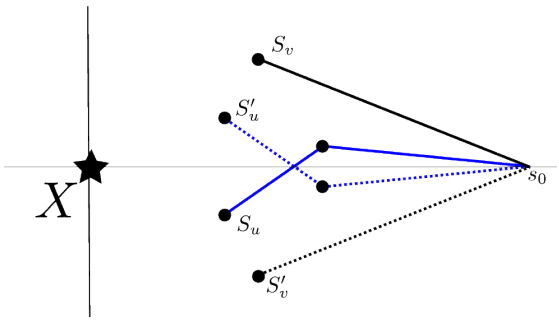

Figure 6.5: The steps of the proof of Lemma 6.4. First, the optimal two-robot strategy, $S^\star = \{S_u + S_v\}$, is "mirrored" about the line $\overline{x^\star s_0}$. Since the information from the two pairs of symmetric strategies, $S'_u + S_u$ or $S'_v + S_v$, is twice the required information, it is clear that one of the two pairs produces the required information.

diagonal matrix, implying

$$\begin{aligned} 2\lambda_d =& N_{u,1}\frac{\sin^2\alpha_{u,1}}{r_{u,1}^2\sigma^2} + N_{v,1}\frac{\sin^2\alpha_{v,1}}{r_{v,1}^2\sigma^2} \\ &+ N'_{u,1}\frac{\sin^2\alpha'_{u,1}}{r'^2_{u,1}\sigma^2} + N'_{v,1}\frac{\sin^2\alpha'_{v,1}}{r'^2_{v,1}\sigma^2}. \end{aligned} \tag{6.16}$$

Then, either,

$$N_{u,1}\frac{\sin^2\alpha_{u,1}}{r_{u,1}^2\sigma^2} + N'_{u,1}\frac{\sin^2\alpha'_{u,1}}{r'^2_{u,1}\sigma^2} \geq \lambda_d \tag{6.17}$$

$$\text{or, } N_{v,1}\frac{\sin^2\alpha_{v,1}}{r_{v,1}^2\sigma^2} + N'_{v,1}\frac{\sin^2\alpha'_{v,1}}{r'^2_{v,1}\sigma^2} \geq \lambda_d. \tag{6.18}$$

Thus, at least one of the symmetric trajectories produces a Fisher Information Matrix with both eigenvalues at least λ_d. □

The proof of the previous lemma suggests further structure in the optimal sequence as shown by the following lemma.

Lemma 6.5. *There exists an optimal two-robot measurement sequence with one measurement location per robot.*

Proof. Suppose not. To find a contradiction, construct the symmetric sequence as described in Lemma 6.4. By symmetry, both robots have the same number of measurement locations in their sequences.

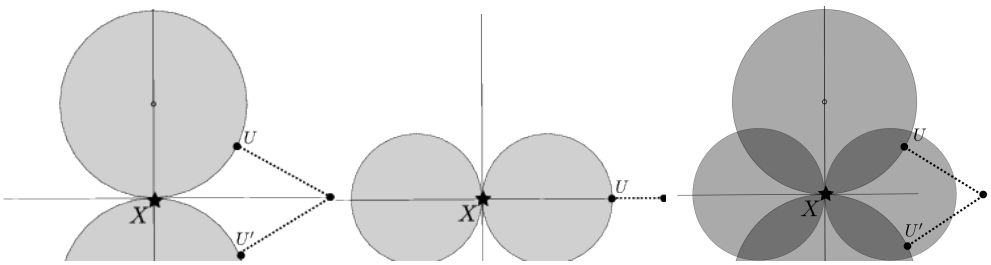

Figure 6.6: An illustration of the constraints on the measurement sequences. (a) by Equation 6.2, (b) by Equation 6.3, and (c), the intersection. Note the radius in (b) is never greater than the radius in (a). Assuming the other measurements are placed, the last measurement U, must fall in the regions specified, while traveling the least. The dotted line adjoining U and the starting location illustrates the shortest path.

If both robots have more than one measurement location to visit and the trajectories cross the x axis, then it is less costly to redistribute the measurements such that neither trajectory crosses the x axis. That is, let all measurements above the x axis (with positive α) be assigned to one robot, and all below (negative α) to the other. Now neither of the trajectories cross the x axis. Of the measurement locations assigned above the x axis, choose any two: s_1 and s_2. Following the same arguments used in Lemma 6.2 (illustrated in Figure 6.2), the two measurement locations can be collapsed down to a single location. Repeating this process for all pairs in both trajectories produces only two measurements: one for each robot. □

In a symmetric trajectory with two robots, u and v, and with one measurement location each, we can reduce Equation (6.2) by noting $|\alpha_1|$, N_1, and r_1 are equal for both robots u and v.

$$\lambda_d = N_u \frac{\sin^2 \alpha_u}{r_u^2 \sigma^2} + N_v \frac{\sin^2 \alpha_v}{r_v^2 \sigma^2} = 2 \cdot N^\star \frac{\sin^2 \alpha}{r^2 \sigma^2}, \tag{6.19}$$

where $N^\star$ is the optimal value for $N_u = N_v$.

For a fixed σ, λ_d, and $N^\star$, the previous equation describes a pair of circles in polar coordinates as shown in Figure 6.6. Thus, for any $N^\star$, the optimal measurement location lies on the circle of radius $r_\lambda = \frac{1}{2}\sqrt{\frac{2N^\star}{\lambda_d \sigma^2}}$, which lies tangential to the x axis at $x^\star$, the

true target location. Since the cost to travel to the perimeter of a circle has a unique minimum, the optimal symmetric trajectory follows in closed form for each possible integer value of $N^\star$.

Thus, the two-robot optimization problem reduces to finding the correct value of $N^\star$. Both robots are responsible for $N^\star$ measurements, and are constrained by Equation (6.19), $\frac{\lambda_d}{2} = N^\star \frac{\sin^2 \alpha}{r^2 \sigma^2}$. The minimum cost for each robot satisfying Equation (6.2) is given by the cost to travel to the boundary of the circle of radius r_λ and take $N^\star$ measurements.

$$C = \sqrt{d(s_0, x^\star)^2 + \frac{N^\star}{2\lambda_d \sigma^2}} - \sqrt{\frac{N^\star}{2\lambda_d \sigma^2}} + N^\star t_m \tag{6.20}$$

To complete the optimization, a table of size $1 \times \lceil \frac{d(s_0, x^\star)}{t_m} \rceil$ is used to search for the optimal value of $N^\star$. The i^{th} cell of the table represents the evaluation of Equation (6.20) with $N^\star = i$. The index of the cell containing the minimum value is the optimal number of measurements for a single robot. With the number of measurements solved, Equation (6.19) can be used to find the trajectories. The result is illustrated in Figure 6.7. The process described in this section is formalized in Algorithm 6.2.

Algorithm 6.2 Two Robot Offline Solution

Input: $\sigma, s_0, x^\star, \lambda_d$
Output: s_u, s_v, N

1: $N_{max} \leftarrow \frac{d(s_0, x^\star)}{t_m} + 2$
2: $M \leftarrow N_{max} \times 1$ vector
3: **for** each row i of M **do**
4: $\quad N \leftarrow i$
5: $\quad C_i \leftarrow$ Equation (6.20)
6: **end for**
7: $N \leftarrow \arg\min C$
8: $r_\lambda = \frac{1}{2}\sqrt{\frac{2N}{\lambda_d \sigma^2}}$
9: $s_u \leftarrow$ closest point on circle of radius r_λ centered at $(0, r_\lambda)$
10: $s_v \leftarrow$ closest point on circle of radius r_λ centered at $(0, -r_\lambda)$

The proposed algorithm produces the optimal two-robot trajectory. For completeness, it can be shown that the algorithm can be used to find the optimal sequence for

k pairs of robots as well. This is done as follows. First, for $n = 2k$ robots, the optimal two-robot measurement locations are found by using Algorithm 6.2 with sensor noise $\sigma' = \sigma\sqrt{\frac{1}{k}}$. Then, k robots are sent along the two paths. The correctness of this adaptation is proven next.

Theorem 6.1 (Optimality of Algorithm 6.2 for n Robots)**.** *Let there be $n = 2k$ robots for some positive integer k. Computing the optimal two robot measurement strategy using sensor noise, $\sigma' = \sigma\sqrt{\frac{1}{k}}$ produces the optimal n robot measurement strategy.*

Proof. It must be shown that there exists an optimal symmetric n robot strategy to generalize the two-robot algorithm. Let $S^\star$ be an optimal set of n trajectories, one for each robot. Similar to Lemma 6.4, we can mirror the trajectories and choose the "most informative" of the n pairs of trajectories as follows. Recall for each pair, S_u and S'_u, $\alpha_u = -\alpha'_u$, $r_u = r'_u$, $N_u = N'_u$, and the FIM produced by the pair satisfies $\underline{\lambda}(\mathbb{F}(S_u)+\mathbb{F}(S'_u)) = 2N_u\frac{\sin^2\alpha_u}{r_u^2\sigma^2}$. At least one of the n pairs satisfies $N\frac{\sin^2\alpha}{r^2\sigma^2} \geq \frac{\lambda_d}{n}$ since the summation of information from all pairs of trajectories satisfies $\sum_{i=1}^{n} 2N_i\frac{\sin^2\alpha}{r_i^2\sigma^2} = 2\lambda_d$. Thus, any optimal n robot trajectory has identical cost and information gains as a symmetric n robot trajectory when n is even.

Let S_u and S'_u be the pair of trajectories selected in the previous step. Now, repeat the steps of Lemma 6.5 to collapse the set of measurement locations for down to two: one for S_u and another for S_v. Since the optimal strategy consists of two symmetric paths with one measurement location, as before, we can solve for only one of them in closed form. In this case, the path derived will be travelled by $k = \frac{n}{2}$ robots, however.

To calculate the $\frac{n}{2}$ robot optimal trajectory, simply repeat the steps of the two-robot algorithm, but notice that each "measurement" is actually $\frac{n}{2}$ robots measuring simultaneously. Thus, each measurement produces a factor $\frac{n}{2}$ more information, which is equivalent to scaling down the variance of the sensor noise by the same factor. □

6.4 Near-Optimal Active Localization with Distance-Constrained Communications

We now move on to the case when communication among all the robots is required to form a final estimate of the target location. In this section, we describe an extension to

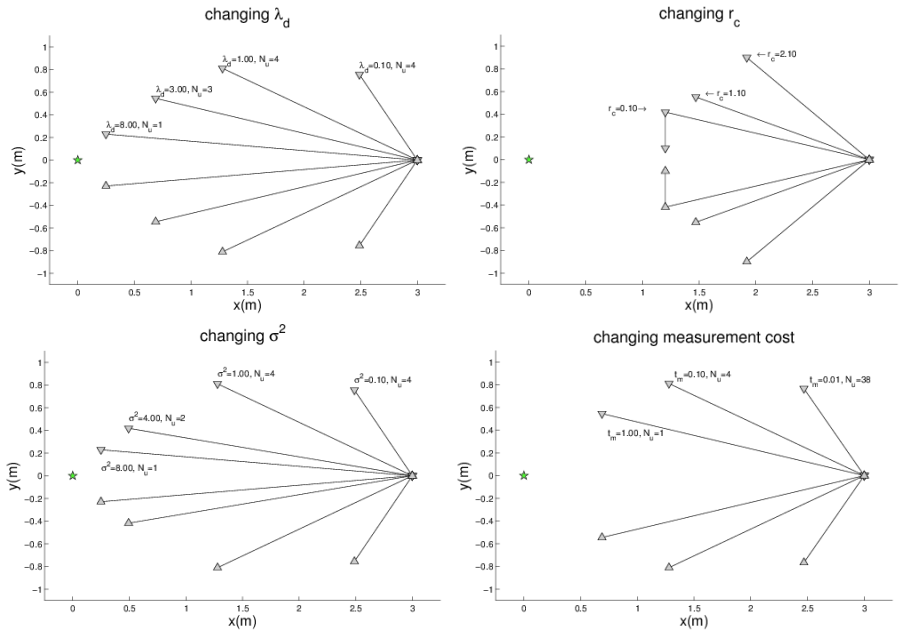

Figure 6.7: Optimal two-robot trajectories for various system parameters. In all figures the robots started at location $(3, 0)$ and the true target was at $(0, 0)$. Communication constraints were only considered in the top right figure and all other parameters were held fixed. Top-left: $\lambda_d \in \{.1, 1, 3, 8\}$. Top-right: $r_c \in \{2.1, 1.1, .1\}$. When $r_c = .1$, the robots rendezvous after measuring. When $r_c = 2.1$ the output is the same as the result from unbounded r_c. Bottom-right: $t_m \in \{.01, .1, 1\}$ Note that as t_m increases, the optimal algorithm travels to more informative locations so that fewer measurements are required. Bottom-left: $\sigma \in \{.1, 1, 4, 8\}$. Note that changing the sensor noise produces the same effect as requiring more information (compare left two figures).

the previous algorithm for the case when the robots have limited communication range. First consider the case of two robots that must be within distance r_c to communicate. A natural strategy is simply to execute the optimal unconstrained algorithm (e.g., Algorithm 6.2), then have all robots move towards the centroid of the robots' positions until communication is possible among all robots. Figure 6.8 illustrates this strategy as the solid line. However, it may be more time-efficient to simply move to s'_u, which places the robots in communication range during measurements (as illustrated by the dotted line). However, the second option requires the robots to travel further before taking the same number of measurements. Algorithm 6.3 expands Algorithm 6.2 to incorporate this tradeoff.

While easy to use in practice, it is not clear if Algorithm 6.3 is always optimal or extends to arbitrary numbers of robots. For example, when many robots are used, it may be more cost effective to form a long "chain" of robots, allowing the ends of the chain to spread out to informative locations, while the middle robots periodically establish links between the distant robots. However, in Theorem 6.2, we will show that no other strategy can do significantly better than the symmetric strategy given in Algorithm 6.3. The result of Theorem 6.2 will allow derivation of a near-optimal, online, and communication-adaptive algorithm in the next section. Finally, in light of Theorem 6.1, Algorithm 6.3 is useful for any number of pairs of robots.

Assuming α_u, N_u, and r_u can be found, expansion of Equation (6.20) produces the following equation.

$$\sqrt{d(s_0, x^\star)^2 + r_u^2 - 2d(s_0, x^\star) r_u \cos(\alpha_u)} + N_u t_m \\ + \min(r_u \sin(\alpha_u) - \frac{1}{2} r_c, 0) \tag{6.21}$$

Using this new cost function, the previous two-robot algorithm changes to the following.

Note that as $r_c \to \infty$, the output matches the result from the previous section. The next result shows that Algorithm 6.3 is close to the optimal cost.

Theorem 6.2 (Algorithm 6.3 is a Two Approximation)**.** *Algorithm 6.3 produces a measurement strategy of cost less than twice that of the optimal communication-constrained measurement strategy.*

Proof. Let C be the cost of Algorithm 6.3 when $r_c \to \infty$. By Theorem 6.1, C is the optimal cost for even numbers of robots. Let $C_r^\star$ be the cost of the optimal strategy

Algorithm 6.3 Two-Robot Communication-Constrained

Input: $\sigma, s_0, x^\star, \lambda_d, r_c$
Output: s_u, s_v, N
1: $N_{max} \leftarrow \frac{d(s_0,x^\star)}{t_m} + 2$
2: **for** $i \in [1, N_{max}]$ **do**
3: $\quad N \leftarrow i$
4: $\quad A_i \leftarrow \arg\min_\alpha$ Equation (6.21)
5: $\quad C_i \leftarrow$ evaluate Equation (6.21) with A_i
6: **end for**
7: $i^\star \leftarrow \arg\min C$
8: $N \leftarrow i^\star$
9: $\alpha \leftarrow A_{i^\star}$
10: $r_\lambda = \frac{1}{2}\sqrt{\frac{2N}{\lambda_d \sigma^2}}$
11: $s_u \leftarrow (r_\lambda \sin(\frac{\pi}{2} - \alpha), r_\lambda \cos(\frac{\pi}{2} - \alpha))$
12: $s_v \leftarrow (r_\lambda \sin(\frac{\pi}{2} - \alpha), -r_\lambda \cos(\frac{\pi}{2} - \alpha))$

for any communication radius r and the same number of robots. Then $C \leq C_r^\star$ since adding communication constraints can only increase the cost of the strategy. Let R be the cost for all robots to rendezvous after taking the measurements defined by Algorithm 6.3. Clearly $R < C$ since the cost to rendezvous is at most the cost to move back to the starting location. Then $C \leq C_r^\star \leq C + R$ implies that $C_r^\star < 2 \cdot C$. Thus, Algorithm 6.3 produces a measurement strategy of cost at most twice that of the optimal communication-constrained measurement strategy. □

6.5 Discussion

The offline algorithms presented here require a repeated minimization of convex functions (See Line 6.2 in Algorithm 6.3). Interestingly, due to the symmetry of the offline, multi-robot optimal solution, only one measurement location must be found regardless of the number of robots. Thus, the computational complexity of optimizing N robot trajectories is the same regardless of N. However, up to $\frac{d(s_0,x^\star)}{t_m}$ solutions must be evaluated (See Line 6.2 in Algorithm 6.2). For our application, $t_m \approx 100$ and the time to travel to the true target is only a few minutes. Thus, we typically evaluate less than 20 solutions before finding the optimal. Furthermore, Equation 6.20 is convex in $N^\star$ and

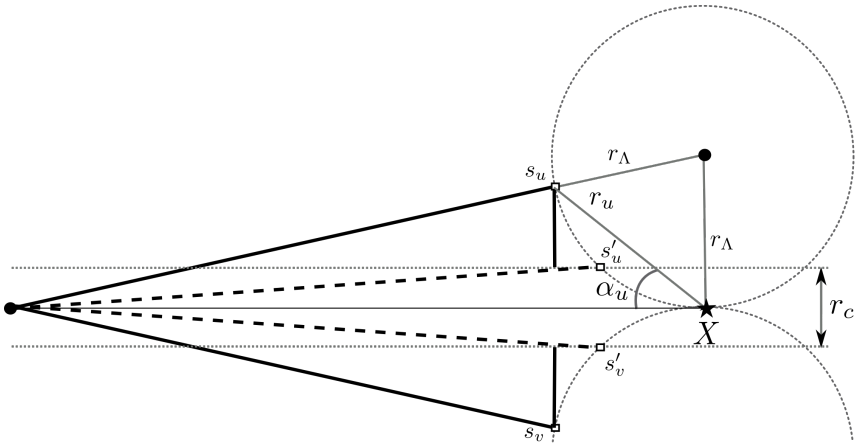

Figure 6.8: An illustration of two different choices for communication-constrained measurement locations. s_u and s_v represent the output of Algorithm 6.2. From these locations, the robots can move directly toward each other to communicate. Alternatively, they can move to s'_u and s'_v, and remain in communication during measurement. Algorithm 6.3 finds the optimal placement of symmetric measurements to minimize the cost while including the rendezvous cost.

thus Newton-like methods could be applied for further speedup.

In an online setting, the true target location is unknown but the objective is the same: For any true target location, the measurement sequence must satisfy $\underline{\lambda}\mathbb{F}(S) > \lambda_d$ even though the PDF representing the distribution of possible target locations changes with each measurement. To remain competitive with the optimal case, an online measurement strategy should not allocate too much time moving towards a distant target estimate if it is highly likely to change given a few measurements. In the next Chapter, we rely on the fact that Algorithm 6.3 is simple to implement and build an adaptive algorithm for real-world localization problems.

Chapter 7

Offline to Online Algorithms and Near-Optimal Localization of a Single Target

The last chapter established an algorithm which can position a robot (or many robots) to gather informative measurements about a *known target*. In this chapter, we address the more realistic case: when only a prior estimate of the true target location is known. To solve this *online* problem, we plan measurements to minimize the worst-case cost, even though the prior estimate may be uncertain or even misleading. We present a general method of adapting any offline measurement strategy for use in an online setting. In doing so, the cost is shown to be at most a logarithmic factor more than that of the offline optimal algorithm, as shown in Section 7.1. Our final contribution involves field experiments: We have implemented and tested the online algorithms on the robot system shown in Figure 2.1. We present field deployments in which two networked robots successfully locate a radio transmitter accurately and without requiring significant travel time. The field experiments are presented in Section 7.2.2.

7.1 The Online Algorithm

In this chapter, we present a conversion of the offline strategy presented in the previous section into a near-optimal online strategy. In the online setting, algorithms do not have access to the true target location $x^\star$. Instead, we start with an estimate in the form of a prior PDF. It is important to note that the goal is still to find the required amount of information with respect to the true target location irrespective of the initial estimate.

Given an estimate of $x^\star$, one possible extension to the offline algorithm is to choose the most likely point in the PDF to be $x^\star$, then execute the offline algorithm with respect to this point. For example, if the target estimate is a two-dimensional Gaussian, then the most likely point is the mean, $\hat{x}$. However, the true target location may be close to the robots' initial location, while $\hat{x}$ may not, resulting in much more work than is necessary.

Instead, consider x, the *closest* point of the current PDF with "high enough" probability. For example, x could be the closest point lying within the $3-\sigma$ bound of a two-dimensional Gaussian, which accounts for 99.7 percent of the probability mass. Given the high likelihood of the true target being inside the $3-\sigma$ bound, it is "safe" to assume the optimal algorithm must travel at *least* to the closest point within this $3-\sigma$ bound. The $3-\sigma$ bound of a 2D Gaussian distribution is an ellipse, but in general, any convex shape containing the desired amount of probability mass can be used.

More formally, we adapt the previously discussed offline algorithms to an online version as follows. Let the *offline* two-robot algorithm be described by the function $\mathcal{A}(s_0, x^\star, r_c, n, \lambda_d, t_m)$ with cost $C(s_0, x^\star, r_c, n, \lambda_d, t_m)$ for n robots starting at location s_0 with communication range r_c and measurement time t_m.

At each step, i, form a convex shape R_i containing the desired probability mass (e.g., the $3-\sigma$ bounds of the Gaussian prior). Then, locate the point in the interior of the shape closest to the robot's starting location, label it x, execute $\mathcal{A}(s_0, x, r_c, n, \lambda_d, t_m)$, and pay cost $C(s_0, x, r_c, n, \lambda_d, t_m)$. The gathered measurements are used to update the hypothesis, a new x is selected from the posterior PDF, and the centroid of the robots' positions is assumed to be the robots' starting location.

We call this algorithm `MULTI-STEP`, and illustrate the steps for a Gaussian target estimate in Algorithm 7.1. The remainder of this section shows that repeated calls to

$\mathcal{A}$ produces near-optimal costs with high probability. Specifically, the cost is at most a logarithmic factor worse than optimal assuming the true target is contained in all convex regions chosen at each time step.

In practice, we use a filtering algorithm to update the PDF after the robots take measurements of the bearing to $x^\star$. We require some technical assumptions about the starting locations of the robots and the filtering method used. As mentioned, at each step of the algorithm, we use a region R_i to contain the possible locations for $x^\star$. The methods used in [6] ensure the robots begin outside a suitable region. In Lemmas 7.1 and 7.2, as well as Theorem 7.1, we require that the robots begin outside the region and that the true target will fall within the region with probability $1-\epsilon$. This condition is satisfied if the filter used is *consistent*. Third, we require that this probability is independent of the region chosen (i.e., $P(x^\star \in R_i)$ is independent from $P(x^\star \in R_j)$ for all $i \neq j$). This last requirement is satisfied if each estimate of the target location is conditioned only on the measurements received and the measurements have independent noise [19]. In practice, we can employ a batch-processed, maximum likelihood estimator [19] which satisfies the last two requirements.

The rest of the section proceeds as follows. First, Lemma 7.1 shows the cost of each *individual* invocation is bounded. Then, Lemma 7.2 proves an upper bound on the number of calls to $\mathcal{A}$ required to localize any target to required precision. This will produce the bound presented in Theorem 7.1.

Algorithm 7.1 `MULTI-STEP`$(s_0, \hat{x}_0, \Sigma_0, r_c, \lambda_d, t_m, n)$

$\Sigma_i \leftarrow \Sigma_0$
$\hat{x}_i \leftarrow \hat{x}_0$
while $\bar{\lambda}(\Sigma_i) > \frac{1}{\lambda_d}$ **do**
  $R_i \leftarrow$ circle of radius $3 \cdot \sqrt{\bar{\lambda}(\Sigma_i)}$ at point $\hat{x}_i$
  $x_d \leftarrow$ closest point on R_i
  $s_{u,i}, s_{v,i} \leftarrow \mathcal{A}(s_i, x_d, r_c, n, \lambda_d, t_m)$
  $Z \leftarrow$ Collect measurements from s_u and s_v.
  $\hat{x}_i \leftarrow$ Update target estimate using Z
  $s_i \leftarrow$ centroid of $s_{u,i}$ and $s_{v,i}$
end while

In the following lemma, let $C(x)$ be the cost of the call to $\mathcal{A}(s_0, x)$ for target estimate x and starting location s_0. Let $\mathcal{A}$ be a γ-approximation to the optimal solution i.e.,

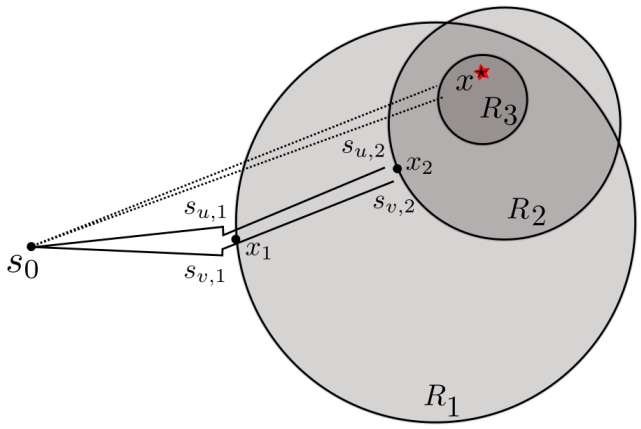

Figure 7.1: An illustration of the two-robot `MULTI-STEP` algorithm (solid paths) and the optimal $\mathcal{A}$ algorithm (dashed paths). The robots begin at s_0. The optimal choice is to move directly to $x^\star$, but we are unsure of the location of $x^\star$. Thus, we form a convex region R such that the probability $x^\star$ is in R is high. At each step of the `MULTI-STEP` algorithm, we do less work than $\mathcal{A}(s_0, x^\star)$ by Lemma 7.1. Since the number of $\mathcal{A}$ executions is bounded by Lemma 7.2, we do not do significantly more work than optimal by Theorem 7.1.

$C(x^\star) \leq \gamma C^\star$ where $C^\star$ is the *optimal offline cost*.

Lemma 7.1 (Bounded Subroutine Cost)**.** *Let $\mathcal{R}$ be a convex region such that $P(x^\star \in \mathcal{R}|Z) = 1 - \epsilon$, where Z is the set of measurements obtained by all previous steps. Let x be the closest point in $\mathcal{R}$ to the robots' starting location, s_0. Then the cost of running $\mathcal{A}$ with input x satisfies $C(x) \leq \gamma C^\star$ with probability equal to $1 - \epsilon$.*

Proof. By definition, x is the closest point in R to the robots' starting location, and so $d(s_0, x^\star) \geq d(s_0, x)$ We can prove that $C(x) \leq C(x^\star)$ by contradiction. If $C(x^\star) < C(x)$ we could take all the measurements taken with respect to $x^\star$ and place them in the same configuration around x. Now, both invocations spend the same time measuring. However, traveling to sensor locations with respect to x would take no more time than traveling to sensor locations near $x^\star$, since $d(s_0, x) \leq d(s_0, x^\star)$ by assumption. This contradicts the assumption that $C(x^\star) < C(x)$. Since $C(x) \leq C(x^\star)$ and $C(x^\star) \leq \gamma C^\star$, it follows that $C(x) \leq \gamma C^\star$. □

Thus, the cost of each invocation of $\mathcal{A}$ is bounded. However, it may take arbitrarily many calls to $\mathcal{A}$ to reduce the uncertainty adequately, producing an unbounded cost

compared to the optimal algorithm. The following result shows the number of calls is small compared to optimal, assuming the regions R_i contain the true target.

Intuitively, we will establish that all measurements are taken inside the $K-\sigma$ bound of the *true* covariance, with K possibly large, but bounded. The true covariance (CRLB) is proportional to $\sqrt{\frac{1}{\underline{\lambda}\mathbb{F}}}$ at each measurement step. We will show the information gained at each step is inversely proportional to the range from the true target, and the range is inversely proportional to the *current* information. Thus, the information gained by each measurement is proportional to the sum of the information already obtained. That is, each measurement step produces a constant-factor increase in $\underline{\lambda}\mathbb{F}$.

Lemma 7.2 (Number of Calls to $\mathcal{A}$)**.** *The* `MULTI-STEP` *algorithm requires* $\mathcal{O}(\log_b \lambda_d)$ *calls to the optimal offline algorithm, where* $b = \mathcal{O}\left(1 + \frac{1}{\sigma^2}\right)$.

Proof. In what follows, S is the set of all measurement locations visited during an execution of `MULTI-STEP`, and S_i is the measurement locations chosen by the i^{th} call to $\mathcal{A}$. The FIM of all previous measurement steps up to and including the i^{th} step is denoted $\mathbb{F}_i$. Let `MULTI-STEP` use T calls to $\mathcal{A}$. Then $\underline{\lambda}\mathbb{F}_T = \underline{\lambda}\mathbb{F}(S, x^\star) \geq \lambda_d$ (we drop the $x^\star$ in further analysis).

Recall from Equation 6.1 that

$$\mathbb{F}_T = \mathbb{F}(S) = \sum_{i=1}^{T} \mathbb{F}(S_i). \tag{7.1}$$

By Weyl's theorem (Section 6.7 [18]),

$$\underline{\lambda}\mathbb{F}_T = \underline{\lambda}\mathbb{F}(S) \geq \sum_{i=1}^{T} \underline{\lambda}\mathbb{F}(S_i). \tag{7.2}$$

The right hand side of Equation 7.2 represents the information gains from each of the T measurement steps. Now consider the i^{th} measurement step and the resulting $\mathbb{F}$.

$$\underline{\lambda}\mathbb{F}_i \geq \underline{\lambda}\mathbb{F}(S_i) + \underline{\lambda}\mathbb{F}_{i-1} \tag{7.3}$$

$$\geq \sum_{j=1}^{N} \frac{\sin^2 \alpha_j}{r_j^2 \sigma^2} + \underline{\lambda}\mathbb{F}_{i-1} \tag{7.4}$$

where the second equation follows from Equation 6.1 expanded for all N measurements taken during the i^{th} step. From Lemma 6.2 we know that $N \geq 2$ measurements are taken.

Let R_i be the i^{th} region chosen by `MULTI-STEP`. We will assume that R_i contains the true target location and is convex. Since each region is convex, and the measurement locations chosen by $\mathcal{A}$ are symmetric about the line $\overline{s_0 x}$ (Figure 7.1), there is no point in the intersection of all the regions which is collinear with the measurement locations chosen. So, for all of the T sets of measurement locations chosen by `MULTI-STEP`, we have

$$\underline{\lambda}\mathbb{F}(S_i) = \sum_{j=1}^{N} \frac{\sin^2 \alpha_j}{r_j^2 \sigma^2} > 0 \tag{7.5}$$

implying that each step provides positive progress of $\underline{\lambda}\mathbb{F}_i$ to λ_d.

To lower-bound the rate of convergence let

$$K = \max_i r_i \sqrt{\underline{\lambda}\mathbb{F}_i}. \tag{7.6}$$

By definition, for all steps i, $r_i \leq \frac{K}{\sqrt{\underline{\lambda}\mathbb{F}_i}}$. In light of Equation 7.5 and substituting Equation 7.6 into Equation 7.4 we see

$$\begin{aligned}
\underline{\lambda}\mathbb{F}_i &\geq \underline{\lambda}\mathbb{F}(S_i) + \underline{\lambda}\mathbb{F}_{i-1} \\
&\geq \sum_{j=1}^{N} \frac{\sin^2 \alpha_j}{K^2\sigma^2} \underline{\lambda}\mathbb{F}_i + \underline{\lambda}\mathbb{F}_{i-1} \\
&\geq \frac{\beta}{K^2\sigma^2} \underline{\lambda}\mathbb{F}_{i-1} + \underline{\lambda}\mathbb{F}_{i-1} \\
&\geq \left(1 + \frac{\beta}{K^2\sigma^2}\right) \underline{\lambda}\mathbb{F}_{i-1}
\end{aligned}$$

where for brevity β was chosen to be $\min_i \sum \sin^2 \alpha_i$. If `MULTI-STEP` makes $N \geq 1$ calls to $\mathcal{A}$, then

$$\begin{aligned}
\underline{\lambda}\mathbb{F}_N &\geq \underline{\lambda}\mathbb{F}_0 \left(1 + \frac{\beta}{K^2\sigma^2}\right)^N \\
N &\leq \log_b(\underline{\lambda}\mathbb{F}_N) - \log_b(\underline{\lambda}\mathbb{F}_0)
\end{aligned} \tag{7.7}$$

with $b = \left(1 + \frac{\beta}{K^2\sigma^2}\right) > 1$. □

It is worth noting that the previous lemma establishes the cost of the `MULTI-STEP` algorithm as a function of the desired *uncertainty*, rather than the range to the true target

or other uncontrollable variables. Our final result follows: We show that the cost of using MULTI-STEP($\hat{x}$) is less than a log factor worse than the optimal offline algorithm, $\mathcal{A}(x^\star)$ with high probability.

Theorem 7.1 (Cost Bounds)**.** *With probability,* $(1-\epsilon)^{\log_b \lambda_d - \log_b \underline{\lambda}\mathbb{F}_0}$*, the ratio of the cost of the* MULTI-STEP *algorithm to the optimal offline algorithm satisfies* $\frac{\textit{MULTI-STEP}(\hat{x}(0))}{\mathcal{A}(x^\star)} = \mathcal{O}(\log_b \lambda_d - \log_b \underline{\lambda}\mathbb{F}_0)$*, where* $b = \mathcal{O}\left(1 + \frac{1}{\sigma^2}\right)$*,* $\underline{\lambda}\mathbb{F}_0$ *is the "prior" information (if available),* λ_d *is the desired information, and* $0 < \epsilon < 1$*.*

Proof. By Lemma 7.2 MULTI-STEP makes $\mathcal{O}(\log \lambda_d - \log \underline{\lambda}\mathbb{F}(0))$ calls to $\mathcal{A}$, and by Lemma 7.1 each of these costs is less than a scalar multiple of the optimal cost. Thus, the first result follows.

When the regions are selected to independently contain the true target location with probability $1-\epsilon$, the probability all regions contain the target is $(1-\epsilon)^N$, for N regions. Given the value of N from Lemma 7.2, the probability follows as stated. □

We have shown that an optimal *offline* algorithm can be converted to an online algorithm by carefully selecting a conservative (nearby) point to serve as a proxy for the true target location. The method is general to any offline optimal algorithm or any filtering method, provided an independent convex region can be described which contains the true target with high probability. In the next section we verify the results of Theorem 7.1 in simulations before testing the MULTI-STEP algorithm in field experiments.

7.2 Implementations and Experiments

We now explore the results of Theorem 7.1 through simulations and experiments. Our goal is to verify the logarithmic behavior of the bound presented in the previous section and test the effectiveness of the algorithm in locating radio-tags in real-world environments.

7.2.1 Simulations

We explore the effects of the ratio of prior information to desired precision through simulations. In each simulation, we provide a prior estimate of the target location with

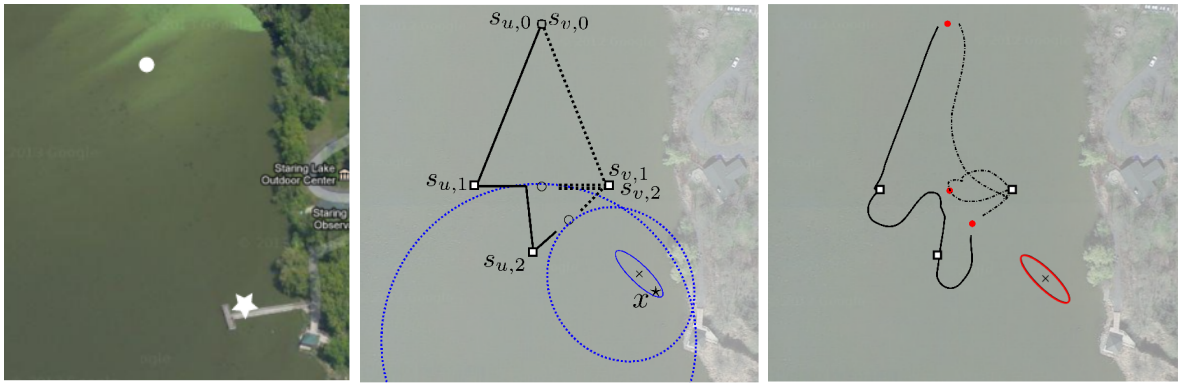

(a) The experiment area. (b) The execution steps of the algorithm. (c) The robot paths overlaid.

Figure 7.2: Experiment results from Lake Staring, Minnesota, USA. **(a)**: The experiment area. The true target (and camera in [1]) were placed on the docks near the bottom right corner (labelled with a star). The robots began near the top-middle (circle). **(b)**: The two calls to Algorithm 6.3 produced the dark paths shown, and reduced the uncertainty (the blue circles). The final actual uncertainty was the solid ellipse. **(c)**: More execution details. The solid red circles are the points where the robots exchanged information. The figure covers an area approximately 200m vertically by 150m horizontally.

circular covariance and eigenvalues $\frac{1}{\underline{\lambda}^{\mathbb{P}_0}}$ and execute the `MULTI-STEP` algorithm until the uncertainty converges to the desired $\frac{1}{\lambda_d}$.

We repeatedly test the performance ratio by sampling a true target location from the prior PDF and executing Algorithm 6.3 using the true target location, and `MULTI-STEP` on the hypothesis. To give a real-world sense of scale to the simulations, note our choice represents a starting hypothesis (three-sigma bound) which grows to encompass a 254 square kilometer area, while requiring a final estimate which is as accurate as a commercial GPS fix (i.e., a few meter uncertainty).

The results are presented in Figure 7.3. The x-axes of the figures show the ratio $\frac{\lambda_d}{\underline{\lambda}^{\mathbb{P}_0}}$ (desired gain in information). The ratio of prior uncertainty to final uncertainty is the inverse of this. According to Theorem 7.1, we expect the curve to be bounded by $\log \lambda_d$.

First, we present the actual number of calls the `MULTI-STEP` algorithm makes to the $\mathcal{A}$ subroutine. We notice a logarithmic trend to the ratios, as expected. These results

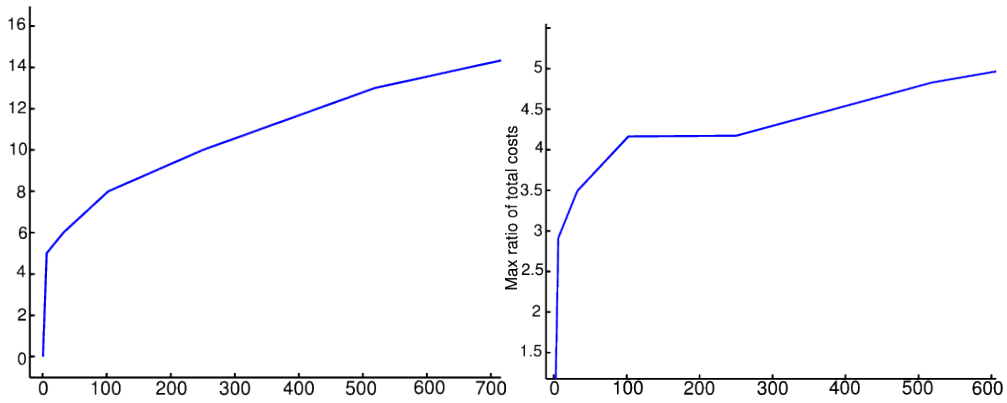

(a) Number of calls to $\mathcal{A}$ (b) Ratio of costs

Figure 7.3: The aggregate results of numerical studies as a function of the starting and final information. Left: the number of calls to $\mathcal{A}$. Right: the ratio of costs of online algorithm to optimal offline algorithm. Shown is the maximum value encountered during simulations.

are shown in Figure 7.3a. The number of calls is not necessarily reflective of the ratio of the costs between our online algorithm and the optimal offline algorithm, since the total distance traveled for each call will decrease.

To explore this, we present the ratio of the *actual* cost in Figure 7.3b from the same trials. The actual cost is given by the maximum distance traveled plus the maximum time spent measuring. We expect the cost ratio to significantly change, depending on the relative positions of the true target location, hypothesis location and uncertainty, and the starting robot positions. In Figure 7.3b we present the worst-case ratio of costs encountered during simulations for each prior hypothesis. Interestingly, the worst-case ratio of costs was less than 7 in these trials, which was less than the number of calls to the $\mathcal{A}$ subroutine. This suggests, in practice, the cost of our online algorithm could be closer to the optimal offline algorithm than is suggested by the theoretical results since each subsequent invocation seems to cost less than the previous one.

7.2.2 Field Experiments

As described in the introduction, we are building a working multi-robot system to search for invasive fish in lakes. To test the suitability of the algorithm to real-world conditions, we have implemented the algorithm for field trials on lakes in Minnesota,

USA. We report five field experiments which show the feasibility of the algorithm in practice.

The experiments were run in Lake Staring, Minnesota, USA (shown in Figure 7.2) in 2012 and 2013. The transmitting tag was deployed at a known location in the environment, and the robots executed the `MULTI-STEP` algorithm. In our prior work on this system, we described a method for reliably constructing a consistent, bounded-uncertainty prior estimate of the target location [6], and so we assume a prior is available during the bearing-only localization phase.

The boats began 140 meters from the target and executed the algorithm given in Section 7.1. To exchange measurements the robots used an ad-hoc wireless network. An example of the final result is shown in Figure 7.2c, as a blue square. We show the algorithm steps in Figure 7.2b, and the actual robot paths in Figure 7.2c. After each measurement, the boats transmitted measurement values over the wireless network. We used a low power network which could not communicate more than 10-20 meters reliably. In each of the five experiments, the robots traveled a combined distance of one kilometer and localized the target to within 10 meters of its measured location. Note the position of the tag's location was accurate to within 5 meters due to GPS error. In all cases, the localization took the expected two steps to locate the target. The final expected error (distance of the final mean of the estimate from the true target mean) was 11.2, 7.1, 1.3, 10.1, and 23.9 meters across the five trials. We provide a video of the localization process at [1].

7.3 Discussion

We have used the insights provided by the optimal offline algorithms in Section 7.1 to develop an online active localization strategy suitable for field deployments. We proved that the performance of the online strategy is within a logarithmic factor of the optimal strategy. We verified the theoretical bounds through simulations studies and presented a working field implementation in our intended operating environment. In field trials, two communicating robots were able to repeatedly locate a radio transmitter.

In this and the previous chapters we have assumed that a prior estimate of the target is available. In the next two chapters we deal with how to structure such an estimate,

and extend the localization problem to include multiple targets.

Chapter 8

Initialization and Localization for Clusters of Targets

As discussed in Chapter 1, the overall, high-level objective for our carp-tracking robots is as follows: Given a list of N frequencies (one per tagged fish), each of which can be detected by the robot at a unique range r_i, localize each target to a desired accuracy in bounded time. As mentioned, we partition this problem in two separate phases: (i) *Search* phase where the objective is to find a location for the robot within the sensing range of each target, and (ii) *Localization* phase where the robot uses bearing measurements to reduce the uncertainty in the target's estimate.

In [16], we presented a method for searching the lake for a position from which the robot could detect a nearby tag. During field tests of this system, we found that the localization routine was sensitive to the accuracy of the initial estimate. Constructing a consistent, reasonably certain prior estimate in limited time has proven to be a difficult task. The problem becomes further challenging because the sensing ranges of individual tags can vary based on the depth of the fish, the age of the tag, and other environmental factors. For example, Figure 8.1 shows a field trial where the robot could not complete the triangulation due to an incorrect initialization. The target was initialized with a 2D Gaussian distribution centered at the location where the robot first moved into the sensing range of the tag, with a variance based on empirical estimates of the sensing range. However, the variance was set too low and as such the initial estimate was not

consistent. During triangulation, the robot moved to a location which fell outside the sensing range of the target, and the final estimate was wrong. The robot successfully triangulated the same tag in another run where the initial estimate (not shown for clarity) was consistent. This indicates the importance of starting with a good initial estimate.

The problem discussed in this chapter is that of establishing a subroutine which can:

1. Initialize a consistent estimate of the target location,
2. Map a region from which bearing measurements are likely to succeed,
3. Exploit clustering behavior of the fish to locate nearby targets efficiently.

The method proposed is what we term a *local search*. The robot will, after detecting a nearby tag, search for the extend of the region from which the signal strength is high enough to take bearing measurements. This will enable a safe transition to the localization phase. For details on how the bearing-only localization proceeds, see Chapter 5.

The chapter proceeds as follows: After presenting the details of the search strategy and its analysis in Section 8.2, we evaluate the strategy through simulations (Section 8.3), and present results from a field experiment (Section 8.4). The field trial demonstrates that our proposed initialization strategy is effective, and promising for large-scale future experiments. We believe our proposed approach of search, initialization, and localization should be applicable for other applications where one or more robots are tasked with accurately locating one or more targets in bounded time.

8.1 Motivation

In this section, we present the details of our system and then discuss some intuitive methods for addressing the problem under consideration.

In our previous trials we observed that the tags' radio signal is undetectable unless we are within 100-200 meters. This provides a natural task partitioning: *Search* and *Localization* [16]. The goal of the search phase is to cover the regions of the lake that are likely to contain tagged fish and move the robot to within sensing range of each tag. We

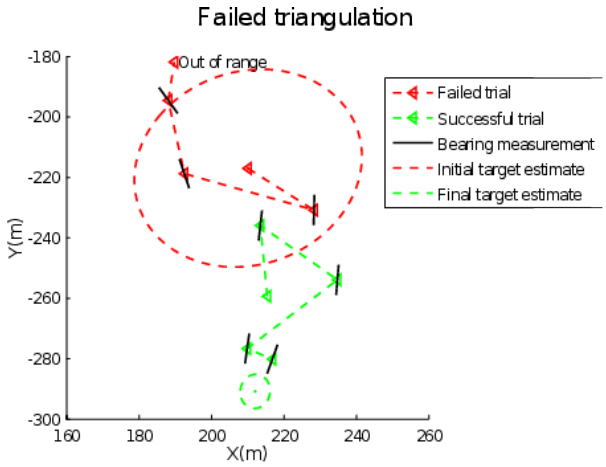

Figure 8.1: Failed triangulation due to incorrect initialization for trials conducted on Lake Staring, MN. The initial estimate for the first trial was inconsistent and resulted in the localization to diverge and move the robot out of the tag's sensing range. During a second trial, with a consistent initial estimate, the target was successfully localized.

then switch to *Localization* where the goal is to obtain multiple bearing measurements to localize the tag to a desired precision. Once a target is localized, the robot can resume its search for other tags. During the search phase, we simply wait for a detection of a non-zero RSSI value, which takes significantly less time than obtaining a full bearing measurement.

The localization subroutine described in Chapter 5 takes time proportional to the area of initial uncertainty and the distance between the initial estimate and the robot. In simulation and experiments this method performs well, but only if the initial estimate of the target is consistent and not significantly uncertain. Obtaining an initial estimate of the target location with bounded uncertainty is challenging, as we discuss next.

8.1.1 The Initialization Problem

Before the localization algorithm can be deployed to precisely estimate tag locations, we must initialize a prior estimate as input. We briefly present some intuitive methods we have tried and discuss why they fail.

Measurement-based. As often recommended in bearing-only tracking literature, a small number of bearing measurements can be collected and processed in a batch.

(a) A typical search path. (b) Ambiguous measurements

Figure 8.2: Examples of search patterns (Figure 8.2a) and ambiguous bearing measurements (Figure 8.2b). High sensor noise, ambiguity and unknown sensing range makes it difficult to transition from search to localization.

Given a set of k measurements $\mathbf{Z} = \{z_1, \cdots z_k\}$, we maximize the likelihood, $p(\mathbf{Z}|x)$ over target locations x. In practice, limited sensing range and long measurement time make this strategy infeasible. Also, consider Figure 8.2b. The two dark regions show areas which are likely to contain the true target and we cannot easily determine which hypothesis is the origin of the measurements ($\hat{x}$ or $\hat{x}'$). A third measurement, taken from a large baseline could disambiguate the two. However, a large baseline is likely to move the robot outside the sensing range of the target, producing no information while paying the full cost of a bearing measurement. Another solution could be to take a fixed number of measurements around the initial detection point. Again, the long bearing measurement time makes this an expensive strategy which must be repeated for each nearby tag. Further, it is not clear how these additional measurement locations should be chosen to guarantee a good estimate of the target.

Initial hypothesis. In contrast to the above, we can initialize a hypothesis by taking two measurements as shown in Figure 8.2b. By drawing a wedge surrounding each measurement to represent its uncertainty, we can obtain an intersection representing the target hypothesis. We can fit a Gaussian distribution to this intersection area and use as an initial estimate. This is not robust in practice, since the intersection can be unbounded. Additionally, we have two intersection areas leading to two initial hypothesis. As such, this method provides no guarantees about initial estimate uncertainty or

range.

Signal-strength based. We can attempt to use the signal strength to resolve the ambiguity of each measurement. The robot could travel toward one hypothesis and measure the signal strength. We expect the signal strength to increase if the robot travels towards the correct hypothesis. In practice, we found this strategy to be sensitive to sensor noise from the unknown and possibly complex spatial signal strength patterns. We found that for small movements near the edge of the sensing range this method was unreliable.

Each of these initialization methods fails to provide a guarantee of time cost, uncertainty, or consistency of the estimate. In the next section, we describe our solution to this problem which relies on a local search strategy.

8.2 Local Search

The goal of the local search is two-fold: (1) determine whether an aggregation exists nearby and which targets are contained within the aggregation, and (2) form good initial estimates (mean and covariance) for each target in the aggregation. The initialization phase begins as soon as the robot first detects a non-zero RSSI from a radio tag while on the search path (Figure 8.3a).

We assume that the detected tag X is at the center of a sensing circle C_X of radius r. Our objective is to establish an initial estimate of X and r. In this section, we first present our local search initialization strategy for a single target (i.e. X). Then, we bound the worst-case and average-case time required for this strategy. The strategy is extended to the case of an aggregation of multiple tagged fish following.

8.2.1 Single-Target Local Search

Note that both X (the origin of C_x) and r are unknown. By finding three points on the perimeter of C_X we can solve for X and r. To find these points, the local search proceeds as follows:

1. From the point of first detection (O), the robot moves in a fixed direction with respect to the global frame (e.g., North or angle α).

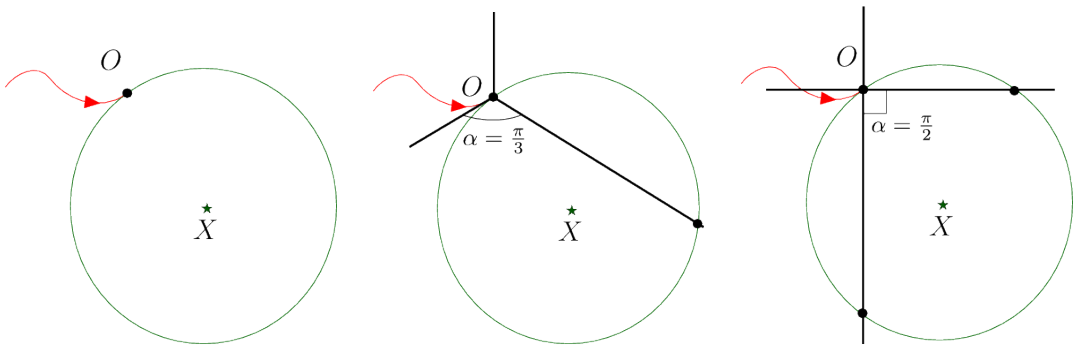

Figure 8.3: (a) While on its coverage path (curved arrow), the robot, at O, detects a non-zero signal for some frequency X. (b) The initialization strategy determines the sensing circle for X by moving along search paths as shown until X is not detectable again. Shown is a case where three search paths fail to uniquely identify the sensing circle. (c) An example of a Four-path search.

2. When the robot can no longer detect the target X (position A in Figure 8.4) it reverses direction and returns to O.

The line segment traversed in these two steps is called as a *search path*. To analyze the time cost of this strategy, we establish the minimum number of search paths needed to find at least three points on the boundary of C_X. We can see that at least four equally spaced search paths are necessary and sufficient from Figure 8.3b.

We now establish the cost of using four search paths to find X and r. The analysis follows Figure 8.4. Let angle OAX be θ. By design, the angle AOB is $\frac{\pi}{2}$. The distance $|AB|$ is $2r$ and segment OA has length $2r\cos\theta$ while OB has length $2r\sin\theta$. Assume the robot moves with velocity v. Each of these lines must be traversed twice, for a total required time of,

$$T_{\text{single}} = \frac{4r}{v}\cos\theta + \frac{4r}{v}\sin\theta + 4\cdot\epsilon \tag{8.1}$$

where ϵ is the time taken to recognize the robot has left C_X, turn around, and re-enter C_X. Note that θ is unknown and can take any value between 0 and 2π, depending on the relative orientation of the target position with respect to the first search direction. To obtain the worst-case cost, we maximize the cost function with respect to θ. A straightforward derivation shows the cost is maximum when $\theta = 45$ degrees for a

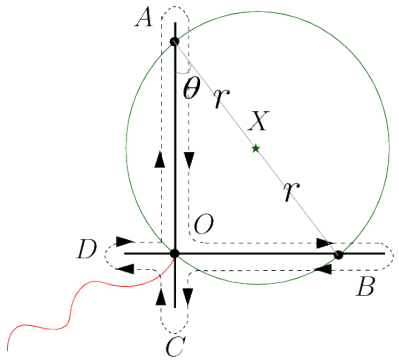

Figure 8.4: The robot continues along an arbitrary but fixed direction until it cannot detect the signal from X (at position A). The robot then returns to O and repeats the same strategy along a perpendicular line (B). In general, the O can lie in the interior of the sensing circle, hence the robot also searches along C and D

maximum cost of,

$$\max_{\theta} \quad T_{\text{single}} = 2^{\frac{5}{2}} \frac{r}{v} + 4 \cdot \epsilon \tag{8.2}$$

The expected search time, assuming θ is uniform in the range $[0, 2\pi]$ is $\vec{E}[T_{\text{single}}] = 2\frac{r}{v} + 4\epsilon$.

8.2.2 Multi-Target Local Search

To extend the local search strategy to multiple targets, we need a model for fish aggregations. While common carp are relatively broadly dispersed during summers, they tend to form tight aggregations under ice-covered lakes in winters [83–86]. For example, while average distances between radio-tagged carp during summers are 300-500 meters, in winters, these distances decrease to 50-100 meters [83]. In some cases, entire populations of carp, usually thousands of fish, have been shown to aggregate in areas that are only 100×100 meters in size [83]. We formalize the notion of an aggregation using the following definition.

Definition 1. *Let $\mathcal{L} = \{X_1, \cdots, X_i, \cdots, X_N\}$ be a set of tagged fish, r_i be the sensing radius of X_i, and $r^\star = \min_i r_i$. $\mathcal{L}$ is called an aggregation if, $\forall i, j, ||X_i - X_j||_2 < r^\star$*

Under this definition, we cannot directly use the local search strategy for a single target for multiple targets. Figure 8.5a illustrates an example case where the four search

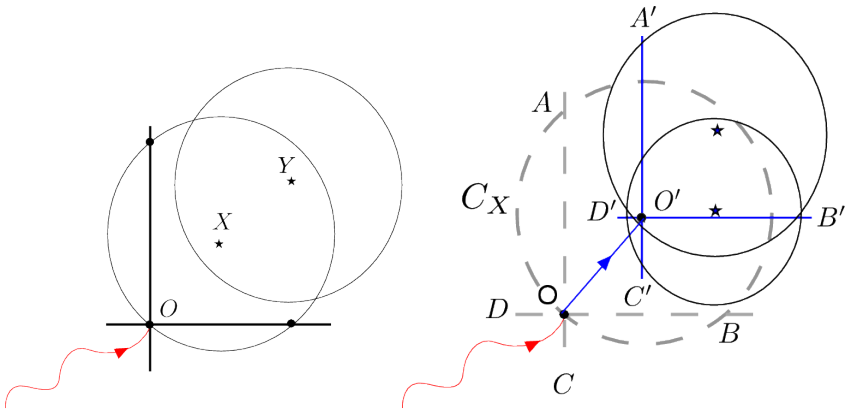

(a) (b)

Figure 8.5: (a) The single target search fails to intersect all the sensing circles in the case of an aggregation. (b) An example of searching for an aggregation using two separate search steps. The robot first finds the boundary of C_X (dashed), centered at O'. Then, after moving to O', searches along four paths to identify the boundaries of each sensing circle.

paths do not intersect the sensing circle of Y present in the aggregation.

By Definition 1, for any target x, the distance to all other targets to x is less than $r^\star$. Returning to the case of one target shown in Figure 8.4, we see that four search paths can provide an estimate of a target location as the center of the estimated sensing disk. In general, since we don't know which fish are contained in the aggregation, it might be necessary to search for all frequencies. As a practical step, we make the assumption that the true location of the first fish X is close to the center O' of the estimated sensing circle. This allows us to move to O' and determine which fish are nearby. We can then perform another multi-path search to map the boundaries of all nearby frequencies (see Figure 8.5b). We call the resulting algorithm *Four-Path*.

Assuming we begin a search from the target location X, we can show that four paths are sufficient to detect the boundaries of each sensing circle in the aggregation. Consider Figure 8.6, which illustrates the possible configurations of the rest of the targets with respect to the first. We have three cases:

- The target Y is aligned with the search path starting at O', and we detect two points of C_Y. This case has a unique solution: Y is at $\frac{1}{2}|XA'|$ along XA'.

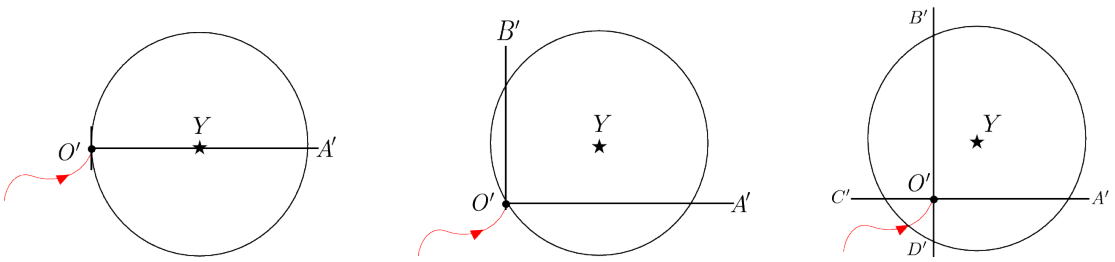

Figure 8.6: In general, the starting location of local search can lie anywhere on the boundary or interior of the sensing circle. In each case, we obtain a different number of points as shown. For all cases, we can determine the sensing circle uniquely.

- O' is on the boundary of C_Y. In this case we detect three points O', A', and B'. We can solve C_Y directly.
- O' is inside the circle C_Y. We can detect four points at A', ...,D', and solve the sensing circle C_Y using least-squares fitting.

Each search path begins at $O' \approx X$. The robot moves until it cannot detect any nearby tags. By Definition 1, this can be a maximum of $2r$ in any direction (traveled twice) for a total cost of $16\frac{r}{v} + 4 \cdot \epsilon$. A total of five targets are required to achieve the worst-case cost. Adding this to the worst-case cost of the initial search, plus the maximum displacement between the points O and O' gives,

$$T_{\text{multi}} = 17\frac{r}{v} + 2\tfrac{5}{2}\frac{r}{v} + 4 \cdot \epsilon. \tag{8.3}$$

8.2.3 Discussion

The cost shown by Equation (8.3) may seem large. For example, given our winter-time system, v is approximately 2 meters per second and, for comparison, assume r is near 100 meters. Thus the total cost is approximately 19 minutes for the worst-case 5 targets. While we are not concerned with the aggregation displacing in this time, this may cause unnecessary drain on the limited operational life of the robot. To put this in context, compare this to the cost of taking two bearing measurements to initialize each target individually. Recall that a bearing measurement takes approximately 1-2 minutes. At least two measurements are required, resulting in 10-20 minutes for 5 targets, not counting the time to displace between measurement locations. By amortizing the cost

of a local search on a per-target basis, it is clear the search-based strategy will incur a lower cost to initialize larger aggregations.

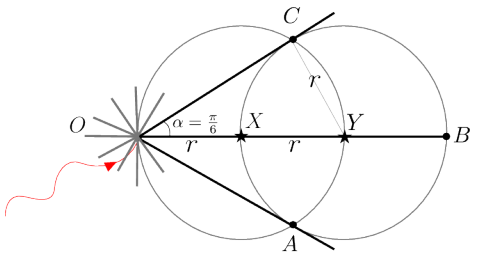

Figure 8.7: To extend the single target local search strategy, we need at least twelve search paths (separated by less than $\frac{\pi}{6}$) to intersect each sensing circle at least thrice.

To see the relative advantage of a two-phase search, consider the work required by a single-phase search. That is, upon detecting a non-zero signal strength, we could search along $K > 4$ search paths and attempt to intersect each nearby sensing circle. The necessary number of search paths can be found as follows. Refer to Figure 8.7. In this example two targets, X and Y are arranged along the x axis with respect to the starting location O. Assume the first search path moves along the x axis and the next search path is offset by an angle α. Then, to intersect the circle C_Y we require $2r \sin \alpha = r$. Solving, we get $\alpha = 30$ degrees, i.e., $K \geq 12$ search paths over 360 degrees. We call the resulting algorithm *Twelve-Path*. Note, unlike the Four-Path strategy, we must sample the entire list of frequencies in the lake over each of the twelve paths because we do not know until we are finished which tags belong to the aggregation. Hence the time taken to sample a frequency, and the total number of targets in the lake affect the cost of this strategy.

Because the distribution of the targets both in and between aggregations plays a large role in the *expected* search time, we compare these strategies in simulations.

8.3 Simulations

In the analysis presented in the previous section we assumed the time required to sample a frequency (t) was negligible. In practice, we may periodically stop the robot while sampling the frequencies to avoid radio interference from the electric drives, which takes some time. Second, we assumed the same sensing range r for all tags, when in practice it

can be different for each tag. Finally, we evaluated the cost to initialize the targets in a single aggregation. In general, there can be more than one aggregation in the lake, each possibly containing different numbers of tagged fish. In this section, we investigate the role of the time spent in sampling the frequencies, the effect of multiple aggregations on total cost, and the effect of different sensing ranges on the time to initialize all targets.

We conducted simulations as follows. To evaluate a varying sensing range, r is drawn uniformly at random between $[50, 100]$m for each tag. We vary the number of aggregations from $1 - 10$ (with at least one fish each). The remaining fish are assigned randomly. The direction in which the robot enters the detection disk of the first target for each aggregation is also drawn uniformly at random between 0 and 2π radians. The velocity of the robot is given as v and is assumed fixed.

We compare Twelve-Path and Four-Path strategies presented in the previous section. Recall that the Twelve-Path (Figure 8.7) strategy moves along twelve search paths from the point of first detection, while sampling on the entire list of frequencies present in the lake. The Four-Path strategy (see Figure 8.5b) estimates the sensing circle for first tag detected, moves to the center of this estimated circle, samples all frequencies once to detect the list of frequencies present in the aggregation, and then moves along four search paths to estimate the sensing disks for only the subset of tags detected in the aggregation. Both produce an estimate of the sensing range and position of each nearby tag.

In Figure 8.8, we compare the mean, min and max time taken for executing both strategies for 50 iterations, as a function of the aggregation size M with total number of fish, $N = 10$. The sampling time per frequency is $t = 0.03$ sec (we obtain similar results for other choices of sampling time). We observe that the Four-Path strategy takes less time, as compared to the Twelve-Path strategy.

Figure 8.9 shows the time taken by the Four-Path strategy when size of one aggregation is increased (as opposed to the number of aggregations in Figure 8.8). For lower sampling time, we observe that the time to travel over the search paths dominates the time to sample for various frequencies. Since the distance traveled by the robot doesn't change significantly with increasing number of fish in the aggregation (by Definition 1), we see that the time taken scales well.

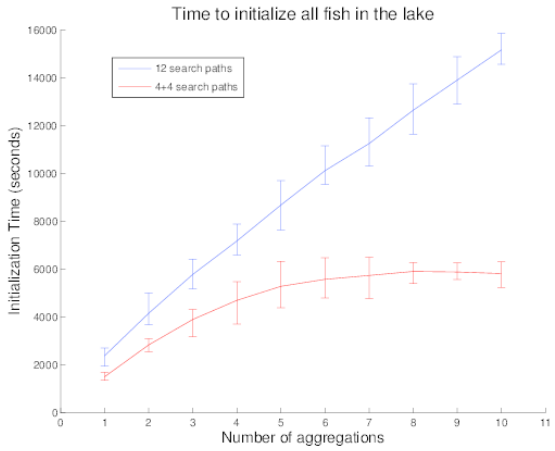

Figure 8.8: Simulation comparing the time taken to initialize all 10 fish in the lake, as the number of aggregations varies. The Four-Path strategy performs better than the Twelve-Path. The bars indicate the minimum and maximum times, and the trend line plots the mean time of 50 instances.

8.4 Experiments

We implemented our initialization strategy on the mobile chassis shown in Figure 1.1. Three tags were deployed on Lake Gervais, MN, and their true locations were recorded for comparison (see Figure 8.10). The robot first detected the tag with frequency 48341 at the location marked START in Figure 8.10a. The robot then executed the Four-Path strategy. After completing the first phase of the Four-Path strategy, we fit a circle to the points where we stopped detecting the signal for 48341 as shown. This circle was used as the 3-σ uncertainty ellipse of a 2D Gaussian distribution with the center of the circle used as the mean for initializing the estimate for this tag. The robot then traveled to the center of this circle and sampled the list of frequencies to detect nearby tags. The robot detected signals for frequencies 48931 and 48999 (48999 was due to radio interference and not an actual tag–the Localization strategy received no valid measurements and discarded this estimate).

The robot then executed the second phase of the Four-Path strategy, where it searched for frequencies detected at the center of the initial circle as shown in Figure 8.10b. The corresponding hypothesis for all tags are shown relative to the true locations. Using this initial hypothesis, the robot then executed the active localization

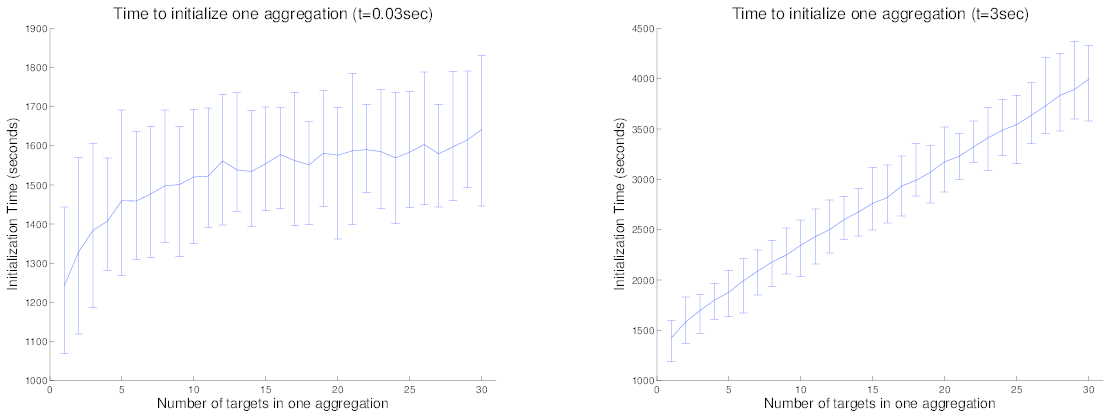

(a) $t = 0.03$ sec. (b) $t = 3$ sec.

Figure 8.9: Mean, minimum and maximum time taken as the number of fish increases in one aggregation for the Four-Path strategy. For lower sampling time, the time to travel dominates and thus scales well for larger aggregations.

algorithm described in Chapter 5. Figure 8.10c shows the execution of this localization algorithm, the measurement locations selected for each tag (triangles), and the bearing measured (black lines).

The final estimates for the two actual tags in the aggregation after five measurements (48341 and 48931) are shown using the 3-σ uncertainty ellipse. Figure 8.10d shows the GPS location of the tags along with the initial and final estimates. The final covariance for 48341 had eigenvalues 56m^2 and 168m^2 (corresponding to an error ellipse with radii 7m and 12m), starting from an initial covariance with eigenvalues 1380m^2. The final covariance for 48931 had eigenvalues 49m^2 and 127m^2 (radii 7m and 11m), starting from an initial covariance with eigenvalues 1758m^2. The final error for 48341 and 48931 were 27m and 23m respectively.

8.5 Discussion

This chapter dealt with the proper initialization of targets from the moment they are first detected, paving the way for a multi-target localization of aggregated targets. The complicated interplay of target distribution, sensing range, measurement noise, and ambiguous measurement model makes each phase independently interesting.

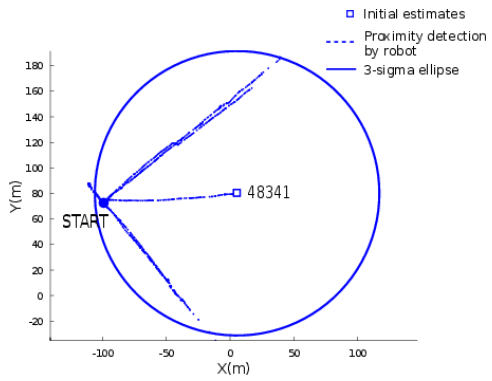

(a) First Local Search (Section 8.2.1)

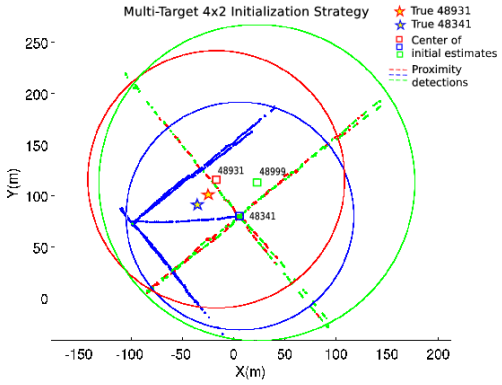

(b) Aggregation Search (Section 8.2.2)

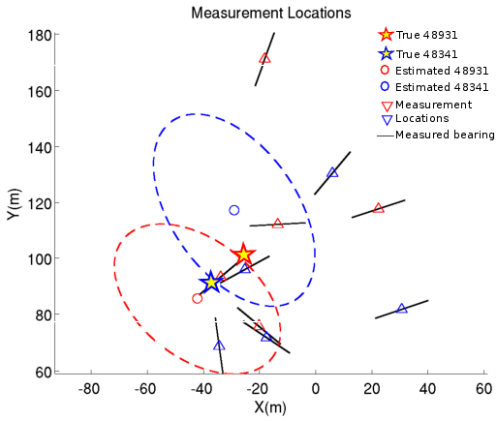

(c) Localization Output

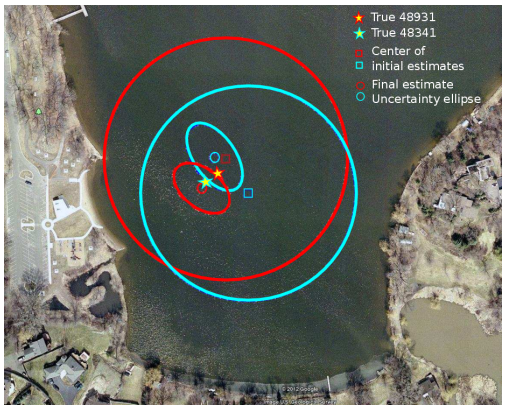

(d) Final Estimates vs True

Figure 8.10: A successful experiment demonstrating the local search strategy and localization steps.

While the algorithm developed worked well in combination with the single-target localization strategy from Chapter 5, no strong theoretical guarantees were provided with respect to the optimal algorithm. In the next chapter, we will present a method for localizing many stationary targets regardless of their configuration, and with much stronger guarantees about optimality.

Chapter 9

Guaranteed Localization for Many Targets

The previous chapters divided the problem of localizing targets into two phases. First, a search phase brought the robot close to the target and initialized a prior estimate of its location. Then, a dedicated localization phase which used bearing measurements and adaptive, online strategies to choose measurement locations.

In this chapter, we consider merging the two problems. If the targets are known to be in an area, one method of dealing with the localization problem is to take sufficient bearing meausements so that a target in any location can be localized. Just as the search phase used a coverage algorithm to ensure the targets could be detected, in this chapter we form a coverage problem to ensure that each target is localized.

We focus on a novel version of this general coverage problem in which the robot can collect only bearing measurements. Therefore, it must collect multiple measurements and estimate the targets' positions. The problem we study is to compute a coverage path as well as sensing locations along the path as shown in Figure 9.1. The goal is to guarantee that the uncertainty in each position estimate does not exceed a given bound while minimizing the data collection time.

We build off the work of Tekdas et al. [87] who studied the problem of placing stationary bearing sensors. Specifically, the authors studied the problem of placing a minimum number of sensors to guarantee that the uncertainty everywhere in the

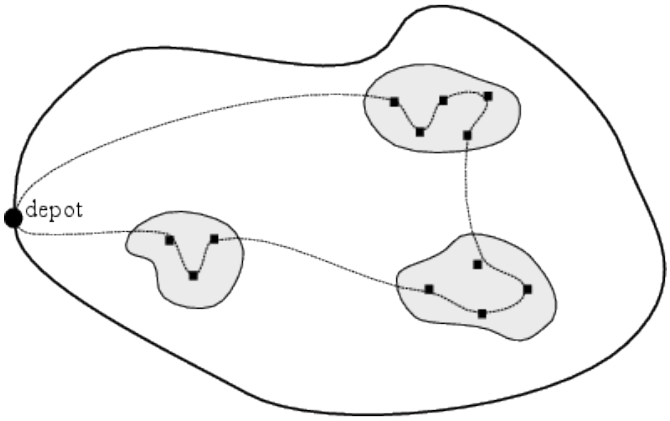

Figure 9.1: Gathering Bearing Data: Shaded areas are the input regions which need to be searched. The goal is to compute measurement locations (squares) and a tour (dashed line) along them so that no matter where the targets are, the uncertainty in localizing them is small.

workspace is below a given threshold $U^\star$. They presented an algorithm which places $3k$ sensors and achieves $5.5U^\star$ uncertainty everywhere in the workspace where k is the optimal solution.

We study the problem for the case of a single, mobile bearing-only sensor trying to locate targets dispersed across an arbitrary but bounded subset of the plane.

We proceed as follows. In Section 9.1, we provide the basics of bearing-based target localization and present the uncertainty measure used. In Section 9.2, we present the data gathering strategy and analyze its performance. In Section 9.3, the uncertainty measure and sensor placement algorithm are validated in simulation. Next, in Section 9.4, we test the placement algorithm and sensor noise model in real-world field experiments.

9.1 Preliminaries

9.1.1 Uncertainty Model

Triangulation is commonly used in estimating the location of a target from two bearing measurements. The accuracy of the estimation depends on the target-sensor geometry and the environment. A common method to measure the uncertainty of the estimate

is to use the geometric dilution of precision (GDOP). Consider two measurements from locations s_1 and s_2 for a target at location w. It is well known that the uncertainty is proportional to:

$$U(s_1, s_2, w) \propto \frac{d(s_1, w)d(s_2, w)}{|sin\measuredangle s_1 w s_2|} \tag{9.1}$$

where $d(s_i, w)$ denotes the distance between robot s_i and target location w. See e.g. [64].

The GDOP function can be extended to obtain the uncertainty in estimating the target's position for a given noise level in the bearing measurements by using the Fisher Information Matrix (FIM) [52]. Let I_θ denote the FIM for a given target-measurement geometry. The square roots of the eigenvalues of I_θ^{-1} denote the lengths of the axes of the target covariance. The determinant of the FIM can be regarded as a computable measure of the area of the ellipse. Given two bearing measurements for a target w, the determinant of the FIM is given as [52]:

$$det(I_\theta) = \frac{1}{\sigma^4} \frac{sin^2\measuredangle s_1 w s_2}{d(s_1, w)^2 d(s_2, w)^2} \tag{9.2}$$

where σ is the standard deviation of the noise in the bearing measurements. Since the determinant is the product of the eigenvalues, taking the reciprocal of both sides, followed by taking their square root yields:

$$\begin{aligned} \lambda_1\lambda_2 &= \frac{1}{\sigma^4} \frac{sin^2\measuredangle s_1 w s_2}{d(s_1, w)^2 d(s_2, w)^2} \\ \frac{1}{\lambda_1\lambda_2} &= \frac{d(s_1, w)^2 d(s_2, w)^2}{sin^2\measuredangle s_1 w s_2} \sigma^4 \\ \frac{1}{\sqrt{\lambda_1\lambda_2}} &= \frac{d(s_1, w)d(s_2, w)}{|sin\measuredangle s_1 w s_2|} \sigma^2 \end{aligned} \tag{9.3}$$

If we multiply both sides by π, the left hand side will give the area of the uncertainty ellipse, whose axes are of length $1/\sqrt{\lambda_1}$ and $1/\sqrt{\lambda_2}$. Hence, for a given noise level σ, the uncertainty becomes

$$U_\sigma(s_1, s_2, w) = \frac{d(s_1, w)d(s_2, w)}{|sin\measuredangle s_1 w s_2|} \pi\sigma^2 \tag{9.4}$$

9.1.2 Problem Statement

Let $\mathcal{T} \subseteq \mathbb{R}^2$ be a given set of candidate target locations. $\mathcal{T}$ can be an arbitrary, potentially disconnected, subset. In the fish tracking application, $\mathcal{T}$ can be the entire

lake or a collection of regions where the fish are likely to be. A single robot equipped with a bearing sensor is charged with taking sensor measurements. The noise in bearing measurements is assumed to be mutually independent and normally distributed with zero mean and σ^2 variance. Each measurement takes τ time units which can be zero.

A *data gathering tour* S is a set of ordered measurement locations $S = \{s_1, s_2, \ldots s_n\}$. The cost of S is given by

$$cost(S) = \sum_{i=0}^{n-1} d(s_i, s_{i+1}) + n\tau \tag{9.5}$$

The first term in Eq. 9.5 corresponds to time spent in traveling whereas the second term corresponds to the total measurement time. To simplify the notation, we define $s_0 = s_n$. For any given point x, we define $U_\sigma(S, w)$ as $\min_{s,s' \in S} U_\sigma(s, s', w)$ – i.e. the uncertainty achieved by the best pair in S.

In this paper, we study the following problem:

Problem 2. *Given an environment $\mathcal{T}$, initial position s_0 and measurement error variance σ^2, compute a data gathering tour S such that cost(S) is minimized,* and *for each location $w \in \mathcal{T}$, there exist $s_i, s_j \in S$ such that $U_\sigma(s_i, s_j, w)$ is less than a given threshold $U^\star$.*

Our main result is an algorithm which computes a tour whose cost is at most 28.9 times the optimal cost while guaranteeing that the localization uncertainty is at most $5.5U^\star$. In obtaining this result, we use the following results from previous work which will be used in the analysis.

The sensor placement scheme in [87] proceeds as follows: Given the environment $\mathcal{T} \subseteq \mathbb{R}^2$, an uncertainty threshold $U^\star$, and a bearing noise variance σ^2, Algorithm 9.1 determines the locations of the sensors. Throughout the paper, let $D(x, a)$ be a disk centered at x with radius a.

The authors then show the following result:

Lemma 9.1 ([87])**.** *For any $x \in \mathcal{T}$ and any $y \in D(x, 2R)$, $U(S(x), y)$ is less than $5.5U^\star$.*

The second result we will use is related to a variant of the well-known Traveling Salesperson Problem (TSP) known as TSP with Neighborhoods (TSPN). In a geometric

Algorithm 9.1 *PlaceSensors*

Input: $\mathcal{T}$, $U^\star$ and σ^2
1: $R \leftarrow \sqrt{U^\star/(\pi\sigma^2)}$
2: $R' \leftarrow 2R/\sqrt[3]{4}$
3: $\mathcal{S} \leftarrow \emptyset$
4: $\mathcal{D} \leftarrow \emptyset$
5: **while** $\mathcal{T} \neq \emptyset$ **do**
6: Pick an arbitrary point x in $\mathcal{T}$
7: $D(x, R) \leftarrow$ a disk with radius R around x
8: $C(x, R') \leftarrow$ a circle centered at x with radius R'
9: $s_i \leftarrow$ a point on C at angle $(i-1)2\pi/3$, $i = 1, 2, 3$
10: $S(x) \leftarrow \{s_1, s_2, s_3\}$
11: $\mathcal{D} \leftarrow \mathcal{D} \cup D(x, R)$
12: $\mathcal{S} \leftarrow S \cup S(x)$
13: $\mathcal{T} \leftarrow \mathcal{T} \setminus D(x, 2R)$
14: **end while**
Output: $\mathcal{S}$ and $\mathcal{D}$

version of TSPN, we are given n uniform disks. The goal is to compute the shortest tour which visits at least one point in each disk.

Lemma 9.2 ([88]). *Let $\mathcal{D}$ be a set of n disjoint disks with radius R. Any tour τ of $\mathcal{D}$ satisfies $|\tau| \geq \frac{n}{2}\alpha R$ where $\alpha = 0.4786$ and $n \geq 3$.*

9.2 Gathering Bearing Data

Our algorithm *GatherData* proceeds as follows: Given the environment $\mathcal{T}$ and the uncertainty threshold $U^\star$, we first run the Algorithm *PlaceSensors* (Algorithm 9.1) to obtain sensor locations given by $S = \cup S(x)$ where $x \in \mathcal{T}$. *GatherData* computes a TSP tour of these points and outputs them in the order given by the tour.

In general, picking sensing locations independent of the tour can yield arbitrarily bad results. We show that by picking the sensor locations carefully, we can bound the deviation from the optimal tour. The full analysis is available in [89].

Let OPT be the optimal solution for gathering data under the cost function given in Equation 9.5. We show that the cost of the resulting tour is within a constant factor of the cost of OPT.

Theorem 9.1. *Let SOL be the cost of the tour generated by* GatherData. $SOL \leq (1 + \frac{2\beta}{\alpha})OPT = 28.9OPT$ *where* $\beta = 6.6687$, $\alpha = 0.4786$ *and OPT is the optimal data gathering tour.*

9.3 Simulations

In this section we validate the sensor model and the subroutine *PlaceSensors* in simulations. For this purpose, we evaluate simulated instances for varying bearing noise $\sigma = \{\pi/36, \pi/18, \pi/12, \pi/9\}$ radians and uncertainty thresholds $U^\star = \{4, 8, 16, 32, 64, 128\}$. In each simulation, a target location is chosen uniformly at random within the measurement area defined by a circle with radius $2R = 2\sqrt{U^\star/(\pi\sigma^2)}$. The sensors are placed according to *PlaceSensors*. Each sensor obtains a single noisy measurement. An iterative batch estimator is used to find the maximum likelihood estimate of the target's location. The estimation process is described in Chapter 3.

This process is repeated 1000 times. For each scenario, we compute the mean area and estimation error. The uncertainty area is calculated as $\pi\sqrt{det(\Sigma)}$, for covariance Σ, which is the area of the uncertainty ellipse.

A sample scenario with $U^\star = 32$ and $\sigma = \pi/12$ is shown in Fig. 9.3a. Each sensor location is shown as a blue solid circle. A black square denotes true target position and a red cross is the estimate. The uncertainty area is shown by a red ellipse. For this scenario, Fig. 9.3b shows the uncertainty ellipses for 1000 random target locations with $U^\star = 32$ and $\sigma = \pi/12$. Only 4 samples out of 1000 exceed the threshold value of $5.5U^\star = 177$. In those four samples, high measurement noise had placed the target estimate outside of the circle. Thus, the estimated uncertainty for the target hypothesis was large.

Statistical results are as shown in Fig. 9.4a and 9.4b. It is observed that for a given uncertainty threshold $U^\star$, the resulting average uncertainty area becomes almost constant with increasing noise. The average uncertainty area is far below the threshold $5.5U^\star$, which verifies Lemma 9.1. According to Fig. 9.4b, estimation error gets more noise-sensitive when the uncertainty threshold increases. For instance, while the slope of the average estimation error is approximately 2 when $U^\star = 4$, the slope is 4 for $U^\star = 128$.

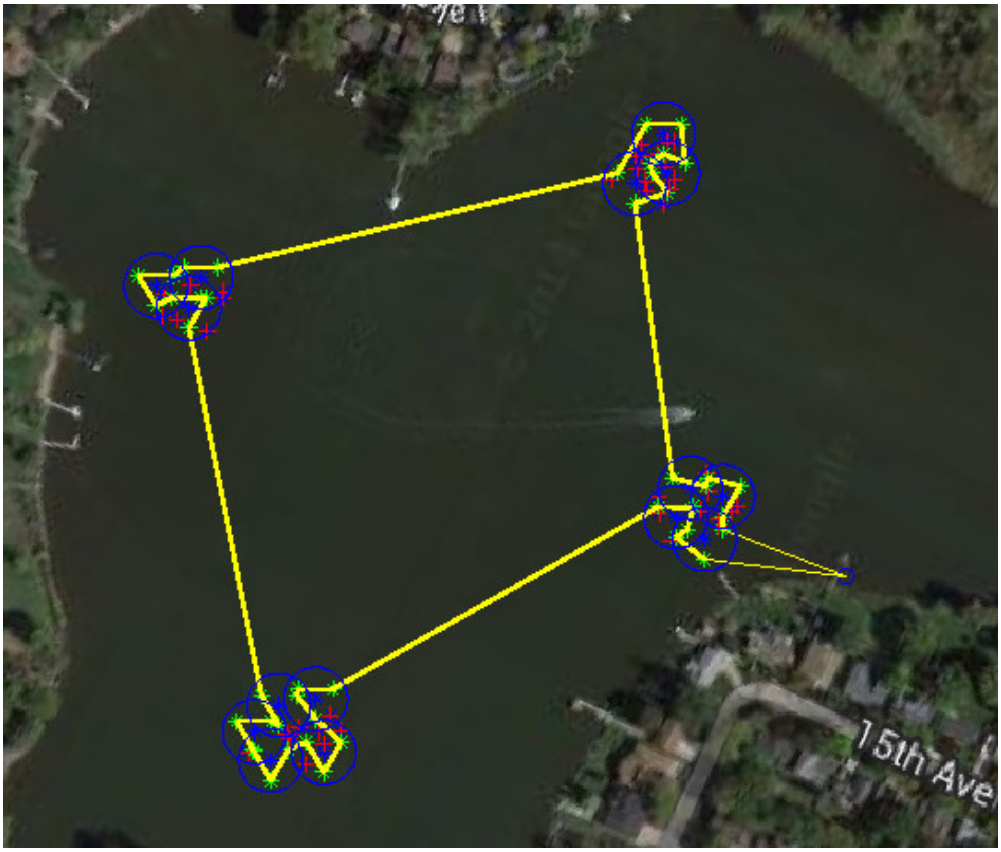

Figure 9.2: A simulated example tour generated by the algorithm. The four areas are known to contain targets, and a sensing tour is computed to localize all the targets. Theorem 9.1 shows that the tour of the measurement locations is near optimal, and Lemma 9.1 shows that any target in the area will be localized to desired uncertainty. The green crosses are computed measurement locations, the yellow path is the tour, and the red crosses are the target locations.

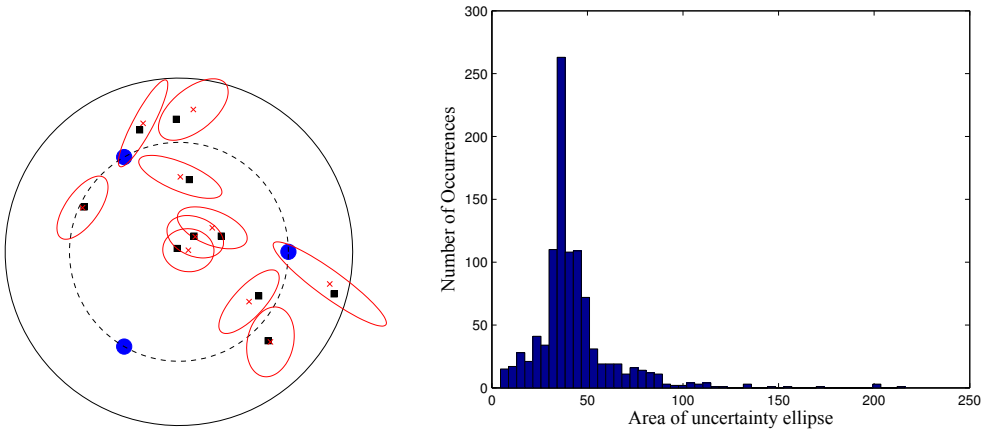

(a) (b)

Figure 9.3: (a) A sample scenario with $U^\star = 32$ and $\sigma = \pi/12$. Each measurement location is shown by blue solid circle. Black squares denote true target positions. Red crosses are the positions of the estimates. Uncertainty areas is shown as red ellipses. (b) Number of occurrences of areas of the uncertainty ellipses for 1000 random target locations with $U^\star = 32$ and $\sigma = \pi/12$.

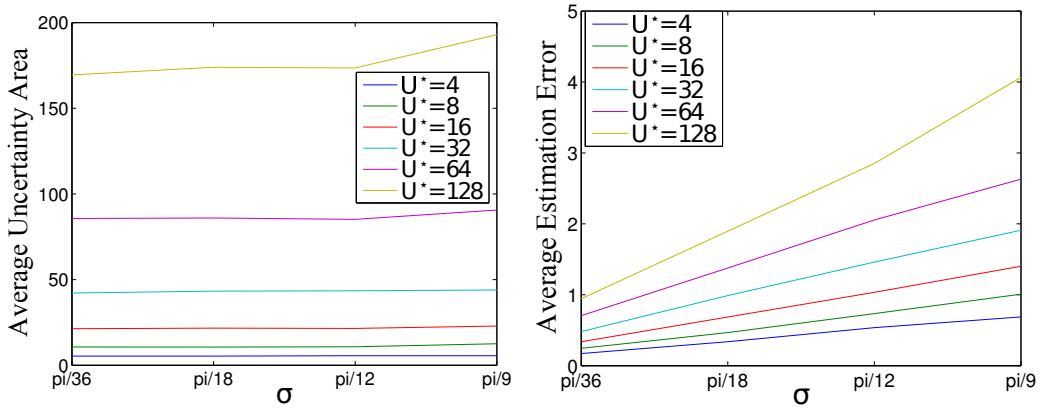

(a) (b)

Figure 9.4: (a) Average uncertainty area and (b) average estimation error for varying the uncertainty threshold $U^\star$ and the measurement noise σ.

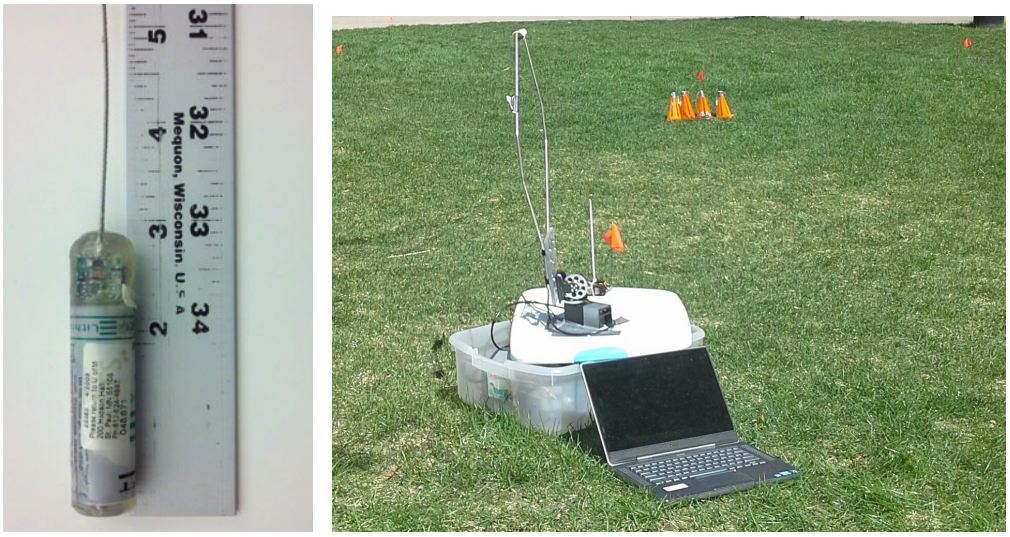

(a) A radio transmitter. (b) The field experimental setup.

Figure 9.5: (a) A tag sends an uncoded transmission on a specific frequency once per second. (b) The antenna is shown in the foreground, and radio transmitters were placed in the field nearby. A direction-sensitive antenna is rotated to estimate the bearing to the transmitting radio tag. The signal strength is strongest when the plane of the antenna loop is roughly aligned with the tag.

9.4 Field Experiments

9.4.1 Sensing Model Validation

Our study is motivated by a real-world application: tracking radio-tagged invasive fish with a radio antenna system. As mentioned, the fish in question tend to aggregate in stationary groups. Thus, the goal of our field test is to verify the radio tags shown in Figure 9.5a can be located using estimates of bearings constructed from three radio antennas. The sensor, a direction-sensitive radio antenna connected to a pan-tilt servo, was developed for the robotic system described in Chapter 2 and is shown detached from the system in Figure 9.5b.

First, we did systematic experiments in a grassy field so as to evaluate the overall performance of the approach. For this purpose, we divide the environment equally into square cells with edges of 5-meter length as shown in Figure 9.7, hence we have 25 locations for radio tags. 7 tags with different frequencies are placed at each corner of

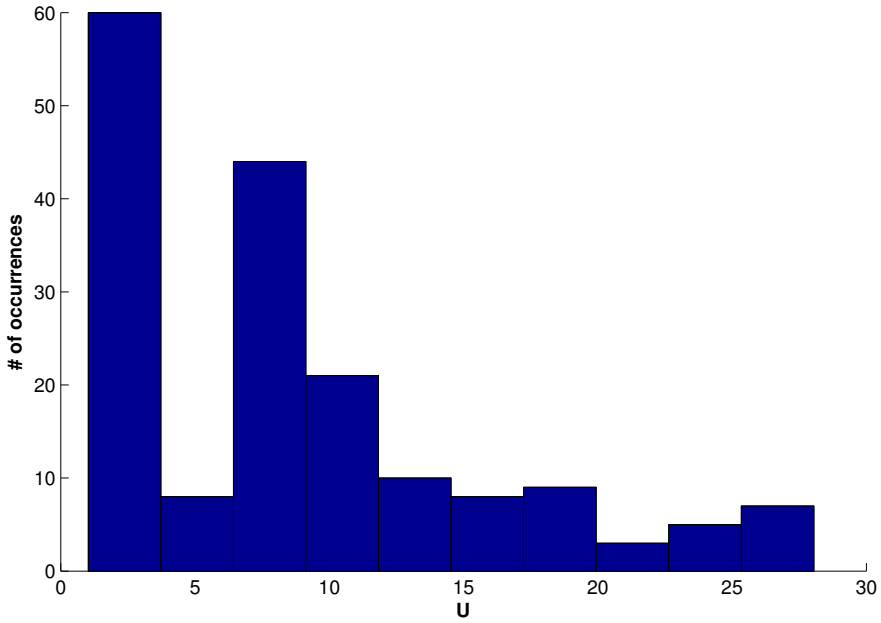

Figure 9.6: Number of occurrences of areas of the uncertainty ellipses for the experiment results with $U^\star = 2.5$ and $\sigma = \pi/18$.

the cells. We have assumed the measurement noise of $\sigma = \pi/18$ rad, and the uncertainty U is set to 2.5. Using Lemma 9.1, the radius of the circle on which three sensors are located is calculated as $R' = 6$ meters, the radius of the measurement area within which the uncertainty is less than $5.5U$ is equal to $2R = 10$ meters. Three measurements are taken for each radio tag from three sensor locations on a circle of radius $R' = 6$ meters.

The estimated target positions are plotted in Figure 9.7 along with the measured ground-truth locations. The sensor locations are shown as blue circles, target estimates are black x's. For each target position inside the circle with radius $R = 10$ meters, the uncertainty U is less than $5.5U^\star$.

9.4.2 Lake Experiments

We report results from a set of tests conducted on two different days at Lake Staring in MN, USA. The robot (OceanScience QBoat) shown in Figure 9.8 was used in the experiments. The boat was augmented with an on-board laptop and motor control

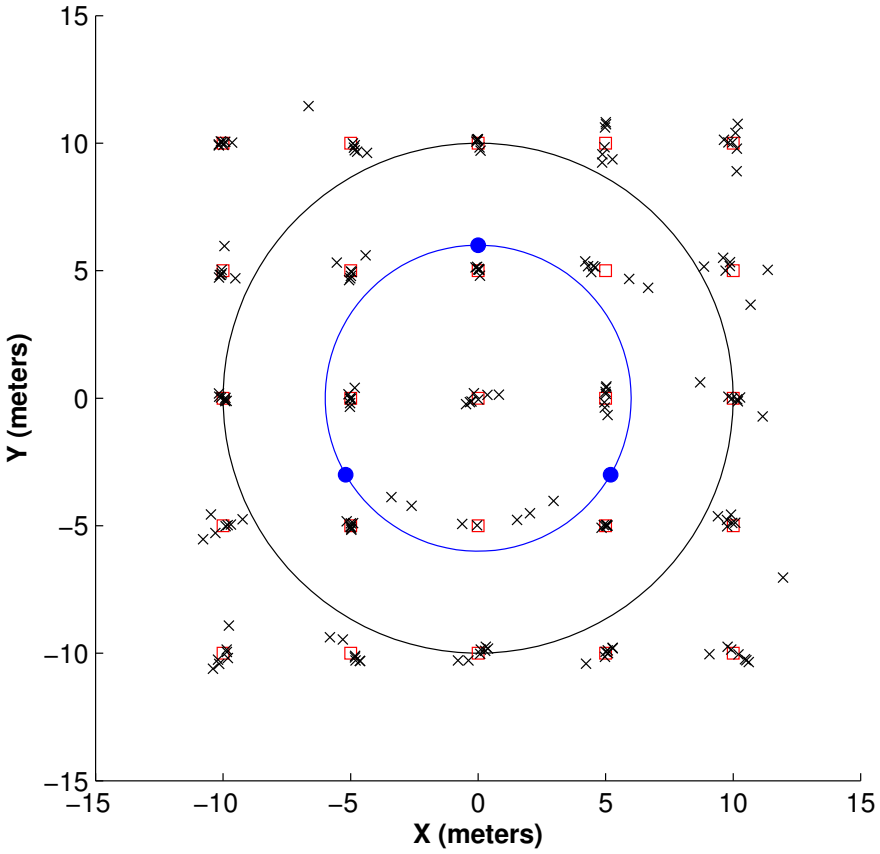

Figure 9.7: Actual and estimated positions for the field experiment results. Each measurement location is shown by a blue solid circle. Red squares show true target positions and black crosses show estimate positions.

Figure 9.8: Lake experiment: gathering bearing data on a windy day.

board for autonomous navigation, and a pan-tilt servo, antenna, and real-time spectral analyzer to produce bearing measurements. It is 2 meters in length and has an average speed of 1 meter per second.

The tags were deployed at a known location within a measurement area. Due to the wind affecting the boat's navigation and cloud cover affecting GPS signals, the uncertainties on the localization will increase. Hence, the uncertainty threshold $U^\star$ was set to 4.5 in the first day experiment. Under these conditions, the radius of the measurement area is equal to 14 meters. Figure 9.9 shows one of the trials. In these experiments, the boat started navigating to its measurement locations (square symbols) from the location shown as the star. The cross symbol represents the estimated target position and the diamond symbol shows the true target location. The uncertainty U is about 19.3, which is less than $5.5U^\star$.

We have also conducted experiments with two measurement regions on the second day. This day was even windier (Figure 9.8 shows a snapshot). Therefore, the measurement noise σ was changed from $\pi/18$ to $\pi/12$ and the uncertainty threshold $U^\star$ was set to 20. One of these experiments can be seen in Figure 9.10. The targets were localized with an error of approximately 6 meters.

In conclusion, the simulation results indicate that the proposed approach enables us to analyze the relationship between the bearing noise σ and uncertainty threshold $U^\star$. Given a fixed $U^\star$, the estimation performance is robust to the change in the bearing noise. The practical applicability of the proposed approach has been also tested in a

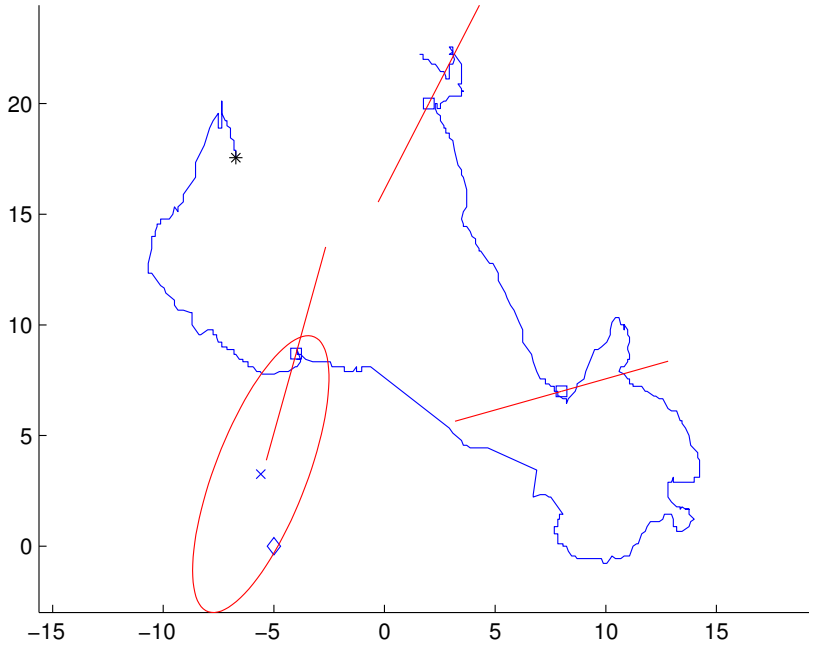

Figure 9.9: Actual and estimated positions for a lake experiment result. The measurement locations are denoted by square. While the diamond denotes true target position, the cross estimate position.

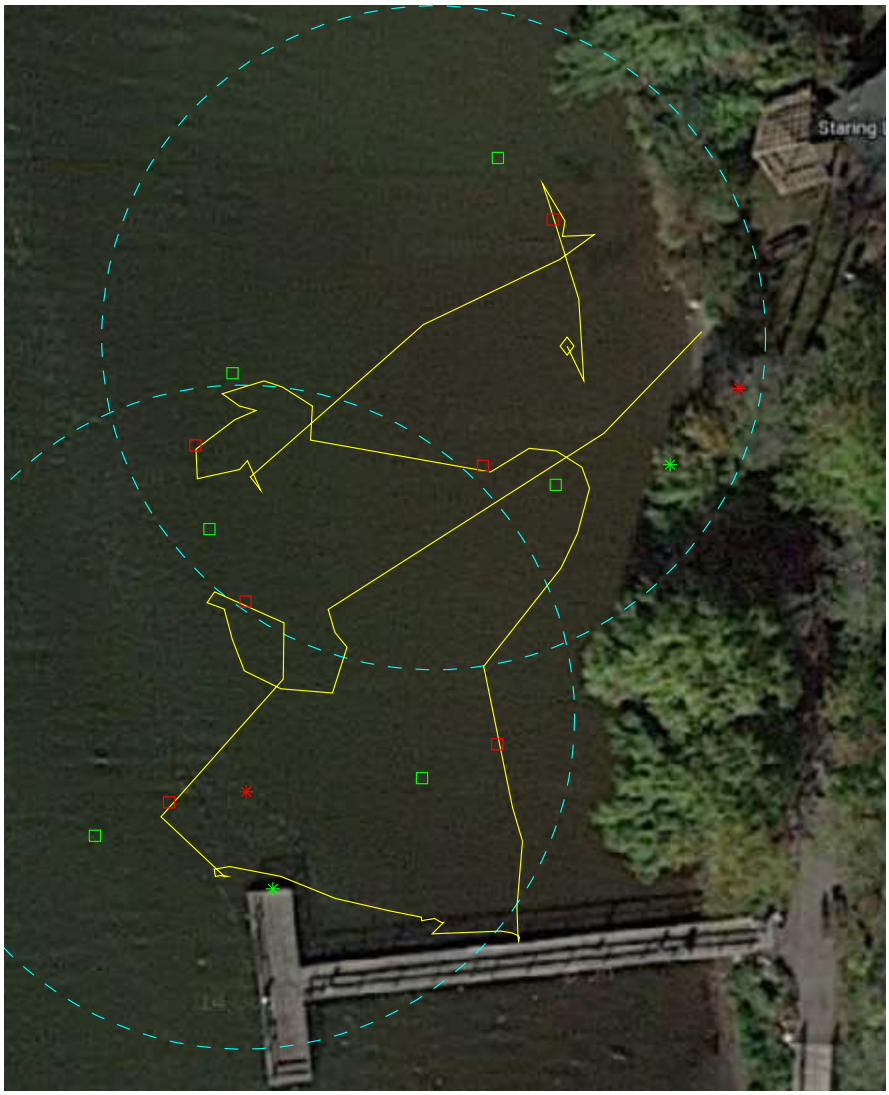

Figure 9.10: Two measurement regions. Green and red squares denote the desired and actual measurement locations, respectively. While green stars denote true target positions, red stars estimate position. The boat began from the location labeled with the yellow diamond and followed the yellow trajectory. The boundary of the measurement regions is denoted by dashed line.

series of experiments with an autonomous boat. The experiments have demonstrated the effectiveness of the proposed approach even under other uncertainties such as wind and GPS errors.

9.5 Discussion

We have presented an algorithm which can localize many targets, regardless of their spatial distribution. In contrast to the previously discussed methods, which take a number of measurements proportional to the desired precision and number of targets, the coverage version scales with the size of the environment. Thus, this method would be particularly effective if the targets were tightly clustered in a small area. Furthermore, being an offline algorithm, with no adaptive component, the execution time is known at deployment.

Our optimality guarantee takes the form of a constant factor approximation such that the cost of gathering data is within factor 28.9 of the optimal solution and the uncertainty is within a factor 5.5. These two factors can be traded off to guarantee, for example, the same level of uncertainty with the optimal solution at the expense of increased cost. We leave the analysis of this trade-off for future work.

Chapter 10

Tracking Adversarial Targets in the Open Plane

For the remainder of the thesis we will consider a target moving through the environment. In addition, we now depart from the information-theoretic formulations of the previous chapters. In this chapter and the next, we will study the effect of bearing information on pursuit-evasion games. In a typical pursuit-evasion game, a pursuer tries to capture an evader who in turn tries to avoid capture. Earlier pursuit-evasion games were studied as recreational mathematics problems. For example, in the lion-and-man game presented in [72] a lion tries to capture a man in a circular arena. In recent years, pursuit-evasion games have received significant attention due to their applications in robotics and related fields [69].

Modeling tracking problems as pursuit-evasion games is advantageous because we may not have good models for how the targets move. By modeling the targets as adversaries that are trying to escape and designing corresponding pursuit strategies, we can develop tracking strategies which work regardless of the motion of the target.

Furthermore, we consider adversarial sensing. In this model, the evader may "adjust" the bearing measurement received by a limited value. By considering adversarial sensing, tracking strategies are made robust against sensor biases or incorrect sensing models.

For such pursuit strategies to be practically applicable, they must work under realistic sensing models. Unfortunately, traditional formulations assume idealized measurements. For example, consider the lion-and-man game in which a lion tries to capture a man in a circular arena [72]. The players have equal maximum velocities. The lion knows the exact location of the man at all times. In contrast, in most robotics settings the location of the target is not available. In our fish tracking application, the pursuer can measure only the bearing rather than the exact location. Moreover, the measurements are uncertain: if we rotate the antenna 2α degrees between consecutive measurements and obtain the angle with the highest signal value, our estimate of the bearing can be off by up to α degrees.

Therefore, we focus on pursuit-evasion games in which the pursuer can obtain only uncertain bearing measurements. In this chapter, we look into the simple setting of chasing the evader in the open plane. When the players have the same speed, the best the pursuer can do is to maintain the initial distance between the players by moving toward the evader along the line connecting them. The evader can ensure that the separation is maintained by moving away from the pursuer in the same direction. The pursuer can execute this strategy even if he obtains only bearing measurements (rather than the exact location of the evader). In Section 10.1, we show that if there is any uncertainty in bearing measurements, the evader can increase the distance between the players. Specifically, we show for any pursuer strategy, there exists an evasion strategy which guarantees that the distance between the players increases indefinitely.

10.1 Open Plane Pursuit

In this section we describe the evader's strategy to win the open-plane pursuit. We first cover the game model. Let the position of the evader and pursuer at the beginning of turn (time step) t be $e(t)$ and $p(t)$ respectively. Each turn proceeds as follows. First, the pursuer measures the angle $b(t) = b^\star(t) + \alpha(t)$, where $b^\star(t)$ is the true bearing to the evader and $\alpha(t)$ is the offset applied by the evader, subject to $|\alpha(t)| \leq \alpha$. The pursuer then chooses the next location $p(t+1)$ subject to $||p(t+1) - p(t)|| \leq 1$. The strategy by which the pursuer chooses its next location is given by the deterministic policy $\pi : (P, B) \rightarrow p(t+1)$, where $P = \{p(1), p(2), \cdots, p(t)\}$ is the previous pursuer

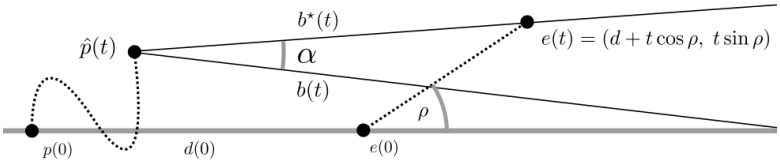

Figure 10.1: The evader's simulation, which is used to find the final pursuer's location after time T, given measurement sequence B. The evader path is shown along with one possible pursuer path. The true bearing ($b^\star(t)$) and offset bearing ($b(t)$) are solid lines.

positions, and $B = \{b(1), b(2), \cdots, b(t)\}$ is all the measurements received by the pursuer up to time t. Next, the evader moves to $e(t+1)$ where $||e(t+1) - e(t)|| \leq 1$.

It is worth noting that we allow the evader to have full knowledge of the policy chosen by the pursuer. Since the pursuer is deterministic, this gives the evader the power to predict the pursuer's actions as a function of the measurement history. We show that there is no pursuer policy which can capture the evader regardless of the evader strategy.

10.1.1 Evader Strategy

We will show that for any deterministic pursuer policy π, the evader can specify a trajectory and measurement sequence to increase the distance between the pursuer and the evader. Let π_p be the pursuer's specified strategy. The evader strategy proceeds in rounds, each lasting for time T (to be derived shortly).

The evader will first simulate a possible measurement sequence, B, and observe the output of the policy $\pi_p(P, B)$ (i.e., the pursuer's trajectory). Based on the pursuer's trajectory, the evader will choose a trajectory to follow, but will use the same measurement sequence, B, used in the simulation step. Since the pursuer's response is a function of only the measurements, the evader can follow a different trajectory without altering the pursuer response, as long as the measurements remain the same.

As shown in Figure 10.1, let the line $\overline{p(0)e(0)}$ be the x axis of a coordinate frame which remains fixed for the current round. Let $d(0)$ be the separation between $p(0)$ and $e(0)$ at the beginning of the round. There are two parameters to the simulation, a constant T_α and ρ. Here, $T = T_\alpha \cdot d(0)$ is the length of the round and is specified by

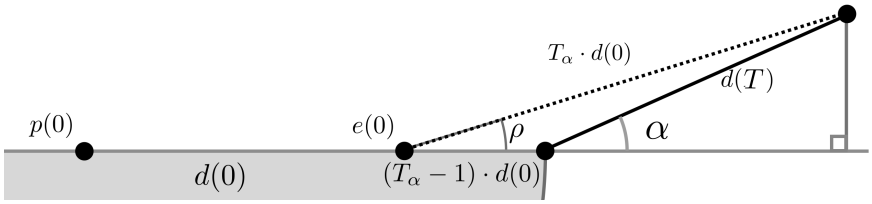

Figure 10.2: The pursuer starts location $p(0)$ and the evader at $e(0)$ separated by distance $d(0)$. After time T, the pursuer is in a closed disc C of radius T centered at $p(0)$. The key component of the evader strategy is to generate two motions which produce the same set of bearing measurements. Since the pursuer's strategy is deterministic (as a function of the bearing measurement), the evader knows which half of C the pursuer ends in (above or below the line $\overline{p(0)e(0)}$). If the pursuer is anywhere in the lower half of C, (shaded portion), the evader will be at location $e(T)$ (the other case is symmetric). The closest position the pursuer can take is at $p^\star(T)$, and the ending distance between the players is given by $d(T)$.

the evader. The constant ρ is an acute angle (offset from $\overline{p(0)e(0)}$) which is less than α. The constant T_α is given as follows (and is derived in Theorem 10.1). The value of the constant T_α was chosen to maximize the final distance at the end of the round (as a function of α). Note that $d(0) > r > 1$ since the evader is not captured and $T_\alpha > 1$ implying each round lasts at least a full turn. The constant T is not necessarily an integer, but rounding up T to the nearest integer does not weaken Lemma 10.3, since it is proven the distance between the players increases monotonically.

$$T_\alpha = \left(1 - \sqrt{\frac{1}{2 + 2\cos\alpha}}\right)^{-1}. \tag{10.1}$$

Given T_α, we solve for ρ (Figure 10.2) using the triangle formed by the points $e(0)$, $p^\star(T)$, and $e(T)$. This yields

$$\rho = \pi - \sin^{-1}\left((1 - T_\alpha^{-1})\sin\alpha\right). \tag{10.2}$$

The specific steps of the simulation are given in Algorithm 10.1, and illustrated in Figure 10.1. The evader will calculate the pursuer's simulated location, $\hat{p}$ as a function of the declared strategy π_p for $T = T_\alpha \cdot d(0)$ steps. To construct an input measurement for each turn, the evader will first find $b^\star(t)$, the orientation of the line $\overline{\hat{p}(t)e(t)}$, where $e(t) =$

Algorithm 10.1 Evader Strategy: $\pi_e(\alpha, d, \pi_p)$

$T_\alpha \leftarrow \left(1 - \sqrt{\frac{1}{2 + 2\cos\alpha}}\right)^{-1}$
$\rho \leftarrow \pi - \sin^{-1}\left((1 - T_\alpha^{-1})\sin\alpha\right)$ ▷ Departure angle
$\hat{p}(1) \leftarrow (0, 0)$ ▷ Simulated pursuer location
$B \leftarrow \emptyset$ ▷ Generated bearing measurements
$T \leftarrow T_\alpha \cdot d$ ▷ Optimal round length
for all $t \in [1, T)$ **do** ▷ **Simulation Step**
    $b^\star \leftarrow$ **orientation of the line connecting** $\hat{p}(t)$ **and the point** $(d + t\cos\rho, t\sin\rho)$
    $B(t) \leftarrow b^\star - \alpha$
    $\hat{p}(t+1) \leftarrow \pi_p(\hat{P}, B)$
end for
if $\hat{p}(T)$ **on or below** $\overline{pe}$ **then** ▷ **Evader response**
    for all $t \in [1, T]$ **do**
        $e(t) \leftarrow (d + t\cos\rho, t\sin\rho)$
        Give measurement $B(t)$
    end for
else
    for all $t \in [1, T]$ **do**
        $e(t) \leftarrow (d + t\cos\rho, -t\sin\rho)$
        Give measurement $B(t)$
    end for
end if

$(d + t\cos\rho, t\sin\rho)$ for each turn $t \in [1, T]$. Then, the sequence $B = \{b(1), \cdots, b(T)\}$ is given by $b^\star(t) - \alpha$ for all time up to T.

At the end of the simulation, the evader knows the pursuer's final location, $\hat{p}(T)$ as a response to the measurement sequence B. The goal of the evader's strategy is to move to a final position $e(T)$ which is on the opposite side of $\overline{pe}$ as the final pursuer position, $\hat{p}(T)$. We separate the result into two cases, and show in both cases the desired result is guaranteed.

Case 1. *The final simulated pursuer position, $\hat{p}(T)$, is on or below the line $\overline{pe}$.*

In this case the evader will move along the path specified by $e(t) = (d + t\cos\rho, t\sin\rho)$, and generate bearing measurements B. Since the input does not change from the simulation, $p(T)$ will be $\hat{p}(T)$, and the final position of the evader will be $(d + T\cos\rho, T\sin\rho)$.

Case 2. *The final simulated pursuer position, $\hat{p}(T)$, is above the line $\overline{pe}$.*

In this case, the evader will follow a different trajectory, E' which is the reflection of E about $\overline{pe}$ i.e., $e(t)$ is the point $(d + t\cos\rho, -t\sin\rho)$ for all $t \in [1, T]$. Assuming B does not change, the pursuer will again follow the simulated output, $\hat{p}$, and arrive at $p(T)$ at the end of the round. Both pursuer and evader are on the opposite side of $\overline{pe}$. We now show the bearing measurements B, do not need to change while the evader is moving along the path E'. To proceed, we need the following structural lemma.

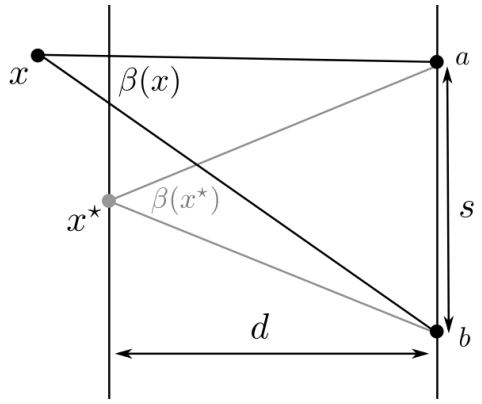

Figure 10.3: An illustration of Lemma 10.1: The angle $\widehat{axb}$, labelled $\beta(x)$, is maximized at the distance d along the perpendicular bisector of a and b.

Lemma 10.1. *As shown in Figure 10.3, let ℓ_1 and ℓ_2 be two parallel lines separated by perpendicular distance d. Place any two non-coincident points on ℓ_2, a and b, separated by distance $s > 0$. Now consider a third point at distance d or greater from ℓ_2, x. The function $\beta(x)=\widehat{axb}$ is maximized at $x^\star$, which is at distance d along the perpendicular bisector of a and b.*

Proof. The function $\beta(x)$ is the angle between the two points a and b from the point x, as shown. First, notice if x is anywhere *left* of the line, ℓ_1, we can move the point toward the centroid of a and b and strictly increase the angle $\beta(x)$. Thus, the point maximizing $\beta(x)$ is on the line ℓ_1.

Without loss of generality, let a be at the point $(d, \frac{s}{2})$ and b be at $(d, -\frac{s}{2})$, and let the coordinates of the point x be $(0, y)$.

$$\beta(x) = \tan^{-1}\left(\frac{\frac{s}{2} - y}{d}\right) + \tan^{-1}\left(\frac{\frac{s}{2} + y}{d}\right) \tag{10.3}$$

It can be verified the maximum of the function occurs when $y = 0$, corresponding to the point x being along the perpendicular bisector of a and b. □

We are now ready to prove that the evader can take either trajectory, E or E', and still generate the same measurement sequence B.

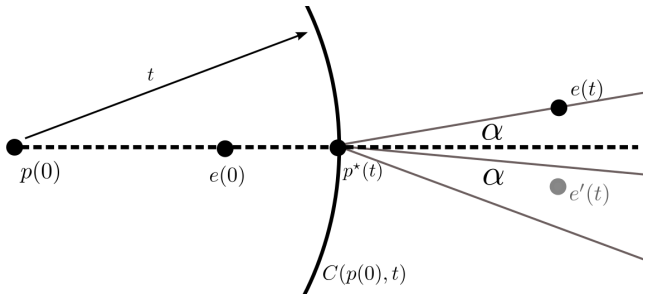

Figure 10.4: An illustration of Lemma 10.2: An evader at position e or e' can generate the measurement $b(t)$ because the angle $\widehat{ep^\star e'}$ is less than 2α.

Lemma 10.2. *Let E' be the sequence of evader positions given by $\{(d+t\cos\rho, -t\sin\rho) : t = [1,T]\}$, and E be the sequence of evader positions given by $\{(d + t\cos\rho, t\sin\rho) : t = [1,T]\}$. The bearing measurement sequence B described in Algorithm 10.1 can be generated by an evader following either E or E'.*

Proof. As shown in Figure 10.4, the pursuer at every time step is inside the circle denoted by $C_p(t)$ of radius t centered on $p(0)$. Let $\beta(t)$ be the angle $e(t)\widehat{p(t)e'}(t)$. By Lemma 10.1, the position $p(t)$ which maximizes the angle $\beta(t)$ is at the intersection of the x axis and the boundary of $C_p(t)$. We call this point $p^\star(t)$ and the corresponding angle $\beta^\star(t)$.

Let the distance between $p^\star(t)$ and the line $\overline{e(t)e'(t)}$ be $d(t)$. For all $t \in [1,T]$ the following holds.

$$d(t) = d(0) + t(\cos\rho - 1) \tag{10.4}$$

Note the minimum value is at $t = T$ and $d(T) > 0$ by design. The separation between $e(t)$ and $e'(t)$ is,

$$s(t) = |e(t) - e'(t)| = 2t\sin\rho \tag{10.5}$$

which is maximized when $t = T$. The angle, $\beta^\star(t)$ satisfies the following.

$$\beta^\star(t) = 2 \cdot \tan^{-1}\left(\frac{s(t)}{2d(t)}\right) \tag{10.6}$$

Recall $\tan^{-1}(x)$ is monotone in x and the argument $\frac{s(t)}{2d(t)}$ is maximized at $t = T$. Therefore $\beta^\star(t)$ is maximized when $t = T$. By inspecting Figure 10.2 we see,

$$\beta^\star(t) = 2 \cdot \tan^{-1}\left(\frac{d(T)\sin\alpha}{d(T)\cos\alpha}\right) \tag{10.7}$$

which implies $\beta^\star(T) = 2\alpha$, or $\beta(t) \leq 2\alpha$ for all $t \in [1, T]$.

Consider the measurements B from the evader's simulation (Algorithm 10.1). Recall each $b(t)$ was given by the angle to the point $e(t)$ from $p(t)$, minus α. We have just proven that the angle $e(t)\widehat{p(t)e'}(t)$ is less than 2α for any $p(t)$, as illustrated in Figure 10.4.

Thus, the angle between $b(t)$ and $e'(t)$ is less than α for all $p(t)$. Therefore, an evader at $e'(t)$ can use an offset less than α to generate the same measurement $b(t)$ for all $t \in [1, T]$. □

The previous lemmas show that the evader can always end the round on the opposite side of $\overline{p(0)e(0)}$ as the pursuer. Thus, without loss of generality, the ending configuration is as shown in Figure 10.2. We are now ready to prove the first main result of the paper: That each application of the evader's strategy yields a constant-factor increase in the distance between the pursuer and the evader.

Lemma 10.3. *For any deterministic pursuer strategy, π_p, an evader distance $d(0)$ away with maximum bearing offset α, using Algorithm 10.1 produces a final separation after time T satisfying $d(T) = \eta \cdot d(0)$ with $\eta > 1$ when $\alpha > 0$.*

Proof. The proof follows directly from the configuration of the players at the end of the round. As shown in Figure 10.2,

$$[T_\alpha d(0)]^2 = [d(T)\sin\alpha]^2 + [(T_\alpha - 1)d(0) + d(T)\cos\alpha]^2 \tag{10.8}$$

After some manipulation, we solve for $d(T)$ as a function of $d(0)$ as follows.

$$d(T) = d(0)\left[\sqrt{\cos^2\alpha(T_\alpha - 1)^2 + 2T_\alpha - 1} - \cos\alpha(T_\alpha - 1)\right] \tag{10.9}$$

We call the term in brackets in the previous equation η, and note $T_\alpha > 1$ by design making $\eta > 1$ for any positive α. □

We now consider *repeated* applications of the evader's strategy e.g., after playing for a long time. Since each round increases the separation between the players by a constant factor, and the length of the round is also proportional to the separation at the start of the round, we expect a logarithmic number of rounds played before any time t. We combine the logarithmic number of rounds played before a given time t, with the exponential increase to prove the following: the distance will increase at a rate proportional to the time t.

Theorem 10.1. *For any deterministic pursuer strategy, π_p, an evader using repeated applications of the strategy given in Algorithm 10.1 increases the distance to the pursuer, $d(t)$, at a linear rate. At the end of t turns playing, the distance satisfies the following at the end of each evader round.*

$$d(t) \geq \gamma \cdot t + d(0) \tag{10.10}$$

$$\text{with } \gamma = \sqrt{\frac{2}{1+\cos\alpha}} - 1 \tag{10.11}$$

Proof. Given the result of Lemma 10.3, we see the first round takes time $T_\alpha d(0)$, and produces $d(1) = \eta d(0)$. Continuing, the i^{th} round takes time $T_\alpha \cdot d(i-1)$, and produces end-of-round separation $d(i) = \eta d(i-1)$. Or, after expansion back to the first round, $d(i) = \eta^i d(0)$.

For any time t, which falls at the end of N rounds, the following holds.

$$t = \sum_{i=0}^{N} T_\alpha \cdot (\eta^i d(0)) \tag{10.12}$$

Which implies $N = \log_\eta \left(1 + t\frac{\eta-1}{T_\alpha \cdot d(0)}\right)$. At the end of these N rounds, the separation is,

$$d(t) = d(0)\eta^N \tag{10.13}$$

$$= d(0)\eta^{\log_\eta\left(1+t\frac{\eta-1}{T_\alpha\cdot d(0)}\right)} \tag{10.14}$$

$$= d(0) + t\frac{\eta-1}{T_\alpha} \tag{10.15}$$

Note the constant η contains both T_α and α. It can be verified that the choice of T_α given in Eq (10.1) maximizes $\frac{\eta-1}{T_\alpha}$ when $\alpha \in (0, \frac{\pi}{2}]$, and produces a rate of increase as given in the theorem statement. □

The analysis in this section showed that the pursuer cannot maintain the distance to an evader if it does not know the precise direction to the evader. In the next section we show that the evader can use the extra distance to win another classical pursuit-evasion game played in closed environments.

10.2 Discussion

In this chapter, we showed that by manipulating the bearing information available to the pursuer, the evader can forever increase the distance between the players.

In the next chapter, we will consider another classical game in which the players maneuver inside a bounded area: the Lion and Man game. We will show that the distance-increasing algorithm that the evader used in this chapter can enable it to win the Lion and Man game as well, provided the area is large enough to do so.

Chapter 11

Tracking and Capturing Adversarial Targets in Bounded Environments

The previous chapter showed that a pursuer cannot hope to maintain the distance to an evader with equal speed if the pursuer only has bearing information about the evader. In this chapter, we consider a second classical pursuit-evasion game. We study the lion-and-man game in a circular arena. In this game, a pursuer and evader with equal speeds maneuver in a bounded environment. The pursuer's goal is to move to within a specified distance of the evader. If the pursuer is aware of the evader's exact location, it is easy to see that the pursuer can get closer and closer to the evader by moving toward it. This is because the evader has to move away from the pursuer to maintain separation which is not possible indefinitely in a bounded arena. Every time the evader turns, the distance between the players decreases. This greedy strategy can be executed even when the pursuer can obtain only bearing measurements. However, with any sensing uncertainty the outcome is not as simple. We show that the size of the environment, relative to the sensing uncertainty α, determines the winner of the game. In this chapter, we show that if the environment is large enough, the evader wins. However, if the environment is small enough (or the sensor noise is reduced sufficiently), the game tips back in favor of the pursuer.

11.1 The Lion and Man Game

We now investigate the effect of uncertain bearing measurements in the context of the classical Lion-and-Man game. The game is played in a circular arena. At the beginning of the game, the pursuer specifies a starting location $p(0)$ followed by the evader choosing a starting location $e(0)$. We use the shorthand notation $|a|$ to denote the distance between the center of the playing environment and the point a.

As in the open-plane pursuit, the game proceeds in turns. First, the pursuer obtains a measurement, i.e. the angle to the evader, $b(t)$. As before, due to uncertainty, $b(t) = b^\star(t) + \alpha(t)$ where $b^\star$ is the orientation of the line through the two players, adjusted by $\alpha(t)$, an angle of the evader's choosing up to absolute value α. The pursuer moves to a point contained inside the arena and within the step size. We again assume the pursuer must choose a deterministic strategy π_p which is a function of the bearing measurements and his prior locations.

Due to the sensing uncertainty, the evader's exact position is never available to the pursuer. Thus that this impossible for the pursuer to move onto the evader's location and the notion of capture must be adjusted to make the game meaningful. After the pursuer's move, if the evader is within a fixed radius (r) the pursuer wins the game. Otherwise, the evader may make his move in the same way as the pursuer.

Definition 2 ((α, r) pursuers)**.** *A pursuer is known as (α, r) if it has a capture radius r and sensing uncertainty α, where $0 < \alpha \leq \frac{\pi}{4}$*

To win the Lion-and-Man game, the evader (the man) must maintain a separation from the pursuer (the lion) which is greater than the capture radius (r), regardless of the pursuer strategy. We will show it is possible: For any given $\alpha > 0$, there exist environments in which the evader can forever escape a deterministic pursuer.

The evader's strategy proceeds in three phases, each illustrated in Figure 11.1. During the first phase, the evader will move away from the pursuer and repeatedly use Algorithm 1 to increase the separation between the players. In the second phase, the evader will execute a local maneuver, which ensures the evader is offset from the line between the center of the arena and the pursuer by an angle greater than $\frac{\alpha}{3}$. In the third phase, the evader will exploit the separation between itself and the pursuer to make a dash toward the center of the arena. When it is "close enough" to the center,

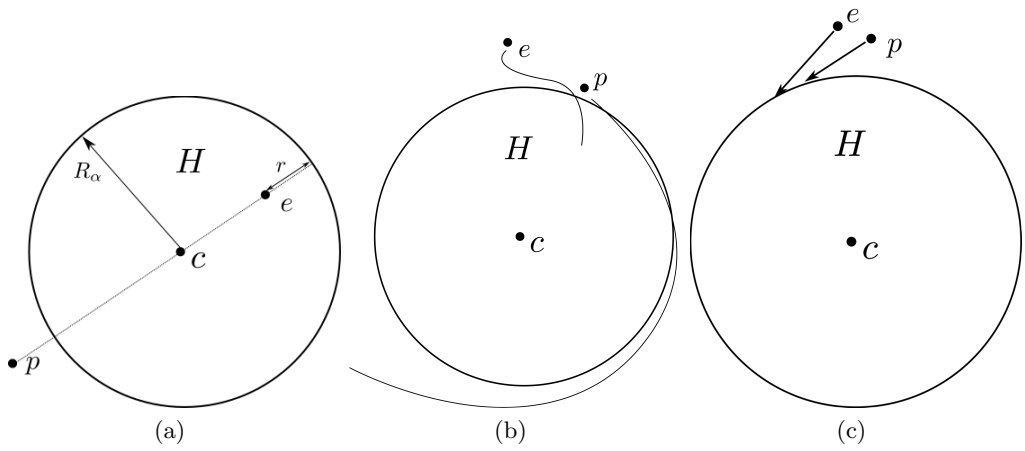

Figure 11.1: 11.1a: The lion-and-man starting configuration (Note the boundary of the playing area is not shown. At the start of the game, the evader chooses his location diametrically opposite the pursuer's location inside a home region H. 11.1b: The three-phase strategy starts when the pursuer enters (or starts within) the *home region* H, a circle of radius R_α, or moves to within distance $2r$ of the evader. The boundary of the arena is assumed to be much larger than R_α, but is upper-bounded in Theorem 11.1. 11.1c After sufficiently increasing the distance between players (Phase 1), and inducing an angular offset (Phase 2) the evader dashes back to the home region, re-entering without being captured (Phase 3).

the evader will start over from Phase 1. In the next part we will show the evader can repeat these three steps indefinitely while avoiding capture, regardless of the pursuer's strategy.

11.1.1 Evader's Winning Strategy

The technical details of the three phases are given in proofs (Corollary 1 and Lemmas 11.1 and 11.2). In Theorem 11.1, we show how the evader can repeat these three phases forever.

The starting configuration is depicted in Figure 11.1a. As shown, let c be the center of the arena. The evader will identify a *home region* H inside the arena where H is a circle centered at c. The radius of H, R_α is a function of α and r and specified in Theorem 11.1. Let the pursuer start at location p, at distance $|p|$ from c. The evader will choose to start inside the boundary of H at distance $R_\alpha - 2r$ diametrically opposite

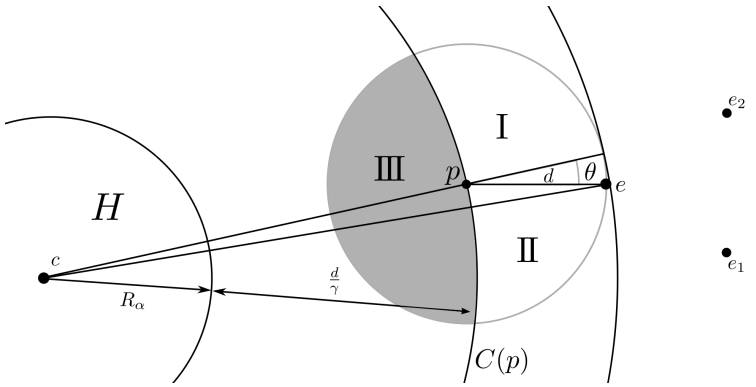

Figure 11.2: At the end of Phase 1 the pursuer p and evader e are separated by a distance d given in Corollary 1. At the start of Phase 2, the evader examines the angle θ. If $\theta > \frac{\alpha}{3}$ the evader can move on to Phase 3. Otherwise, he chooses his next move based on the next pursuer location, in region I, II, or III, as stated in Lemma 11.1.

the pursuer. Before the first Phase, the evader will simply wait until the pursuer enters H. Then, the evader will move directly away from the pursuer's current location until he reaches the boundary of H. At this time, Phase 1 begins.

The beginning of Phase 1 is illustrated in Figure 11.1a. In Phase 1, the evader will repeatedly apply the distance-increasing strategy from Section 10.1 (Algorithm 10.1). Each application of the strategy is called a round, and Phase 1 ends when enough rounds have been completed to increase the separation between the players to a desired distance $d > \frac{1}{\sin\frac{\alpha}{3}}$. The key to the analysis of Phase 1 is to show that the players do not travel an unbounded distance from the center of the arena. Since Theorem 10.1 provides a lower bound on the separation between the players as a function of the number of turns spent, we can bound the number of turns required in Phase 1 as follows.

Corollary 1 (Effect of Phase 1)**.** *Let the distance between the pursuer and evader at the start of Phase 1 be $d(0) \geq r$. After T turns, the separation is greater than $d(T) \geq \gamma T$, where $\gamma = \frac{1}{\cos\frac{\alpha}{2}} - 1$, is given in Theorem 10.1. For any given desired separation d, $T \leq \frac{d}{\gamma} = d\left(\frac{\cos\frac{\alpha}{2}}{1-\cos\frac{\alpha}{2}}\right)$ turns are required.*

After Phase 1, the players are in the configuration shown in Figure 11.2. Let the pursuer's distance from c at the end of Phase 1 be $|p|$, and let $C(p)$ be the circle of radius $|p|$ centered on c. Similarly, let $|e|$ be the distance of the evader from c. Because the players traveled at most distance $\frac{d}{\gamma}$ from the region H, we know Phase 1 ensures

$|p| \leq R_\alpha + \frac{d}{\gamma}$. Since the distance between the players is d, we know Phase 1 also ensures $|e| \leq R_\alpha + d(1 + \frac{1}{\gamma})$. The evader will check the angle θ, which is the orientation of the line $\overline{pe}$ with respect to the line $\overline{cp}$ (i.e., the angle $\pi - \widehat{epc}$), as labelled in Figure 11.2. If $\theta > \frac{\alpha}{3}$, the evader will move on to Phase 3. Otherwise, the evader must make a local move (Phase 2) to create the desired value of θ as described next.

First, the evader will wait until the pursuer makes a move outside the circle $C(p)$ or $\theta \geq \frac{\alpha}{3}$. While the pursuer remains inside $C(p)$, the evader does not need to take any action, and does not adjust the pursuer's bearing measurements from their true value. When the pursuer exits the circle $C(p)$, *and* θ is still less than $\frac{\alpha}{3}$, the evader will look ahead at the result of the pursuer's strategy, exactly as described in Section 10.1, for d turns (just enough time for the pursuer to reach the evader's initial location, e).

Let e_1 and e_2 be two points, offset by $\pm\alpha$ from the line $\overline{pe}$ at distance d from e. As before, the evader constructs the bearing measurement sequence to be the orientation between the current simulated pursuer location $\hat{p}(i)$ and the point distance i along the line segment $\overline{ee_2}$, starting at the point e when $i = 0$. The bearings are offset by negative α.

Let $\hat{p}$ be the final pursuer location after the simulated move. First, if $\hat{p}$ is inside the circle $C(p)$ (in region III in Figure 11.2), the evader does not need to take any action, and will continue to wait in Phase 2. Otherwise, we partition the possible locations of $\hat{p}$ into two sets, I and II, divided by the line $\overline{ce}$, as shown in Figure 11.3a and 11.3b, respectively. If $\hat{p} \in I$, the evader will choose to move to e_1, otherwise he moves to e_2. In such a case, Phase 2 ends when the evader reaches e_1 or e_2 after d turns. We use the following lemma to show the configuration of the players after Phase 2.

Lemma 11.1 (Phase 2: Gaining Angular Offset)**.** *Let p and e be the pursuer and evader positions after Phase 1 as shown in Figure 11.3. Consider the point $\hat{p}$, at most distance d from p, and falling into region I or II (outside the radius $|p|$). For any such $\hat{p}$ there exists a corresponding point $\hat{e}$, at most distance d from e such that all of the following hold.*

1. *The maximum distance between $\hat{p}$ and the center is $d(1 + \frac{1}{\gamma}) + R_\alpha$*
2. *The maximum distance between $\hat{e}$ and the center is $d(2 + \frac{1}{\gamma}) + R_\alpha$*
3. *The distance between $\hat{p}$ and $\hat{e}$ is at least d.*

4. *Angular Offset: The angle θ, which is measured between the line $\overline{\hat{p}\hat{e}}$ and the line $\overline{c\hat{p}}$ is at least $\frac{\alpha}{3}$.*

Proof. As illustrated in Figure 11.3, let c be the center of the playing environment. Let the pursuer be at position p and distance $|p|$ from c, and the evader be distance $|e| \geq |p| + d$. From Corollary 1, we know the players travelled at most distance $\frac{d}{\gamma}$ after exiting H and the evader is distance d away.

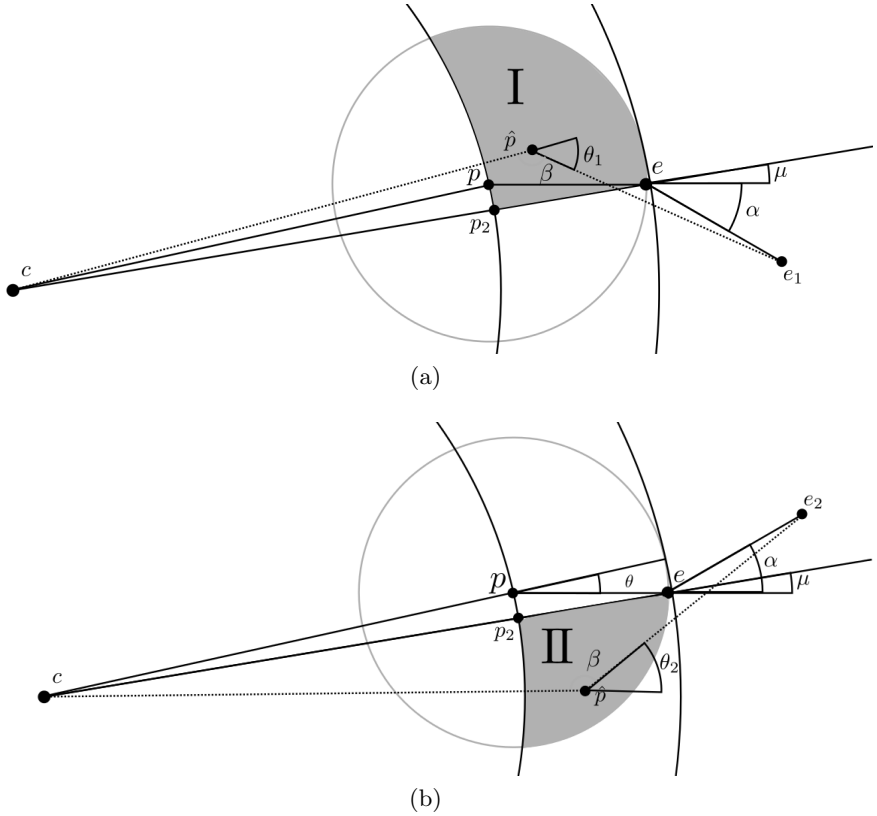

Figure 11.3: 11.3a and 11.3b By Lemma 11.1, the evader can choose to move to location e_1 or e_2, based on the pursuer's chosen location in region I or II, producing θ_1 or θ_2 greater than $\frac{\alpha}{3}$, respectively. If the pursuer moves to region III, the evader will remain at position e.

For any pursuer location, $\hat{p}$, and evader location $\hat{e}$, we notice the first two conditions stated in the theorem hold, since the evader and pursuer move at most distance d. Also note for any $\hat{p}$ above (resp. below) the line $\overline{ce}$, the point e_1 (resp. e_2) is at least distance d away, since $|ee_1| = d$ and $|ee_2| = d$. It remains to show that the evader has achieved

an angular offset as stated.

Consider Case I: $\hat{p} \in$I, and the evader has moved to e_1, as illustrated in Figure 11.3a. Let β be the angle $\widehat{e_1 \hat{p} c}$, implying $\theta_1 = \pi - \beta$. Of all $\hat{p} \in$I, β is maximized (θ_1 minimized) when $\hat{p} = p_2$. To see this, draw the line $\overline{ce_1}$, find its midpoint, and recall from Lemma 10.1 that β increases by moving $\hat{p}$ toward the midpoint. We now show $\theta_1 \geq \frac{\alpha}{3}$.

First, find the perpendicular projection of e_1 onto the line $\overline{ce}$. The distance of the projection from the point p_2 is $d + d\cos(\alpha + \mu)$. The length of the projection is $d\sin(\alpha + \mu)$. Since $\tan\theta_1 = \frac{d\sin(\alpha+\mu)}{d+d\cos(\alpha+\mu)} = \tan\left(\frac{\alpha+\mu}{2}\right)$, $\theta_1 > \frac{\alpha}{2}$.

Consider Case II: $\hat{p} \in$II, and the evader has moved to e_2, as illustrated in Figure 11.3b. By a similar argument in Case I, we see β is maximized when $\hat{p} = p_2$. We again find the projection of e_2 onto the line $\overline{ce}$, which has length $d\cos(\alpha - \mu)$, and intersects $\overline{ce}$ at distance $d + d\sin(\alpha - \mu)$ from p_2. Now, we note $\mu < \theta < \frac{\alpha}{3}$ by assumption. Therefore $\tan\theta_2 > \frac{d\sin\left(\frac{2\alpha}{3}\right)}{d+d\cos\left(\frac{2\alpha}{3}\right)}$ which implies $\theta_2 > \frac{\alpha}{3}$. Thus, all four conditions are proved.

□

To recap the result of Phase 1 and 2, we know the pursuer is inside a circle with radius $|p| \leq R_\alpha + d(1 + \frac{1}{\gamma})$, and the evader is inside the circle with radius $|e| \leq |p| + d$. We also know the evader is offset from the line $\overline{cp}$ by an angle at least $\frac{\alpha}{3}$ and is distance at least d from the pursuer. The evader will now move on to the last phase. Now the evader will move at an angle from the line $\overline{pe}$, given by $\frac{\pi}{2} + \phi$, where $\phi = \theta - \sin^{-1}\frac{r}{d}$. The angle ϕ is chosen so that for any r, there exists a separation d which makes it possible for the evader to move closer to the center of the arena without being captured. This move is called Phase 3, and is illustrated in Figures 11.4a and 11.4b.

Lemma 11.2 (Effect of Phase 3)**.** *Let c be the center of the playing circle, and a pursuer with capture radius r be distance $|p|$ from c. Let the evader be distance d away from the pursuer, and offset from the line between the pursuer and center of the circle by an angle θ. The evader can reach a point distance $r^\star$ from the center of the circle without being captured where $r^\star$ satisfies*

$$r^\star \leq |p|\cos(\phi) + \sqrt{d^2 - r^2} \tag{11.1}$$

$$\text{with } \phi = \theta - \sin^{-1}\left(\frac{r}{d}\right) > 0. \tag{11.2}$$

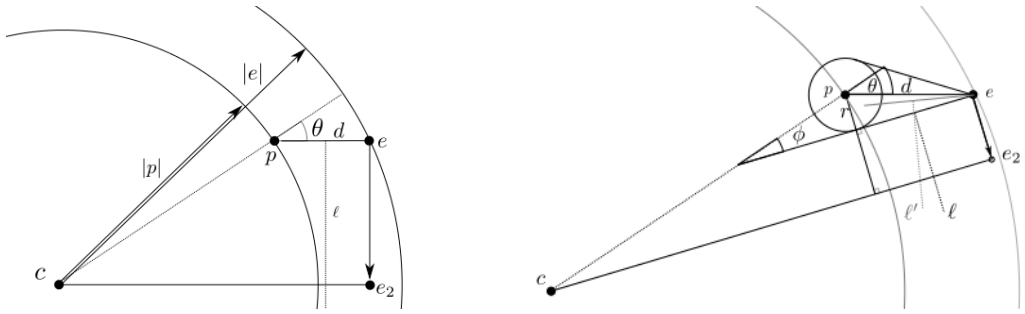

Figure 11.4: During Phase 2, the evader will move at an angle $\phi+\frac{\pi}{2}$, where ϕ is measured with respect to the line from the center of the circle to the point p. After Phase 2, the evader is at position e_2. Lemma 11.1 shows $\theta \geq \frac{\alpha}{3}$ and bounds $|p|$ and Lemma 11.2 bounds the distance from the center to e'. Note $\phi = \theta - \sin^{-1}\frac{r}{d}$ and d is chosen such to ensure $\phi > 0$.

Proof. For simplicity, let us consider the case of $r = 0$ as illustrated in Figure 11.4a. The locus of all points equidistant from p and e is given by the perpendicular bisector of the line $\overline{pe}$, which we label ℓ. By travelling parallel to ℓ the evader can reach the point e_2 before the pursuer can. Since the line $\overline{pe}$ and $\overline{ce_2}$ are parallel, we see the angle $\widehat{pce_2}$ is exactly θ. The distance $|pe_2|$ is given by $|p|\cos\theta + |pe| = |p|\cos\theta + d$, as desired.

In the case of $r > 0$, the evader modifies his strategy as follows. We observe escaping capture by a pursuer with $r > 0$ is the same as escaping any pursuer p' with $r = 0$, when the initial position of p' is at most distance r from the point p. We will find an escape path for the evader such that no p' can achieve capture.

To proceed we draw a line tangent to the circle of radius r and passing through e. Let the tangent point on the circle be p_t. The evader will travel parallel to the perpendicular bisector of the line segment $\overline{ep_t}$, labelled ℓ until he reaches the location closest to c, labelled e_2 in Figure 11.4b.

To see the evader can reach e_2 without being captured, consider any pursuer with no capture radius ($r = 0$) at location p', at most distance r from the point p. Let ℓ' be the perpendicular bisector of the line $\overline{ep'}$. For any $p' \neq p_t$, the line ℓ' rotates away from e_2, leaving e_2 safely on the evader's side. For any p' closer to e, the line ℓ' moves closer to e_2, but for e_2 to lie on ℓ', p' must be coincident with e. Since the evader enters Phase 2 with separation $d > 0$, this is not possible.

To find the inner radius, note $\overline{ce_2}$ is parallel with the line passing through e and tangent to the capture circle, implying $\widehat{pce_2}$ is exactly $\theta - \sin^{-1}\left(\frac{r}{d}\right)$. The distance $|pe_2|$ is given as stated in the lemma.

□

We now show that an (α, r) pursuer cannot capture the evader in large environments.

Theorem 11.1. *For any (α, r) pursuer, there exists a playing arena of radius R in which the pursuer can never capture the evader.*

Proof. We make use of the following constants in the proof.

First, let $\phi = \frac{\alpha}{3} - \sin^{-1}\frac{r}{d}$ from Lemma 11.2 where d is the final separation between the pursuer and evader (as yet a free parameter).

Let γ be the constant $\left(\sqrt{\frac{2}{1+\cos\alpha}} - 1\right)$ from Theorem 10.1.

We will show that an evader beginning inside a circle H of radius R_α can, after all three phases described, return to the circle H without being captured.

The evader begins in Phase 1, and moves away from the pursuer until the desired separation d is reached. After Phase 2, as stated in Lemma 11.1, the pursuer's distance from the center is at most

$$|p| = R_\alpha + d(1 + \frac{1}{\gamma}). \tag{11.3}$$

Finally, let

$$R_\alpha = \frac{d(1+\frac{1}{\gamma})\cos\phi + \sqrt{d^2 - r^2}}{1 - \cos\phi}. \tag{11.4}$$

Then,

$$\begin{aligned} |p| &= R_\alpha + d(1 + \frac{1}{\gamma}) \\ &= \frac{d(1+\frac{1}{\gamma})\cos\phi + \sqrt{d^2 - r^2}}{1 - \cos\phi} + d(1 + \frac{1}{\gamma}) \end{aligned} \tag{11.5}$$

We now apply Lemma 11.2 to find the inner radius reachable by the evader. Let the inner radius be $r^\star$.

$$\begin{aligned} r^\star = \\ \left[\frac{d(1+\frac{1}{\gamma})\cos\phi + \sqrt{d^2 - r^2}}{1 - \cos\phi} + d(1 + \frac{1}{\gamma})\right]\cos\phi + \sqrt{d^2 - r^2} \end{aligned} \tag{11.6}$$

After distributing $\cos\phi$ and the denominator we have,

$$
\begin{aligned}
r^\star = & \\
& \frac{d(1+\frac{1}{\gamma})\cos^2\phi + \sqrt{d^2-r^2}\cos\phi}{1-\cos\phi} \\
& + \frac{d(1+\frac{1}{\gamma})\cos\phi(1-\cos\phi) + \sqrt{d^2-r^2}(1-\cos\phi)}{1-\cos\phi} && (11.7)\\
= & \frac{d(1+\frac{1}{\gamma})\cos\phi(\cos\phi+1-\cos\phi)}{1-\cos\phi} \\
& + \frac{\sqrt{d^2-r^2}(\cos\phi+1-\cos\phi)}{1-\cos\phi} && (11.8)\\
= & \frac{d(1+\frac{1}{\gamma})\cos\phi + \sqrt{d^2-r^2}}{1-\cos\phi} && (11.9)
\end{aligned}
$$

First, note that Eq (11.9) is equal to the radius of H, given in Eq (11.4). Thus, the pursuer is back within the home and is outside the capture radius of the pursuer, thus the game is reset.

Second, since $\phi = \frac{\alpha}{3} - \sin^{-1}\frac{r}{d}$, for any $d > \frac{r}{\sin\frac{\alpha}{3}}$ the value R_α is finite.

Thus, at the end of Phase 3, assuming R_α, ϕ, and d are chosen as stated, the evader is again inside the home region, H and is outside the capture radius of the pursuer.

The maximum radius of the evader during the three phases is the maximum pursuer radius plus the separation, d, as given in Lemma 11.1. Thus,

$$
\begin{aligned}
|e| &< |p| + d && (11.10)\\
&< \frac{d(1+\frac{1}{\gamma})\cos\phi + \sqrt{d^2-r^2}}{1-\cos\phi} + d(1+\frac{1}{\gamma}) + d && (11.11)\\
&< \frac{d(1+\frac{1}{\gamma})\cos\phi + \sqrt{d^2-r^2}}{1-\cos\phi} + d(2+\frac{1}{\gamma}) && (11.12)
\end{aligned}
$$

□

The previous theorem shows that (α, r) pursuers cannot win in large environments. To derive a cleaner bound, we can make two further simplifying assumptions.

For simplicity, let $r = 1$ and fix the evader's choice of d to be $\frac{1}{\sin\frac{\alpha}{6}}$. Under these assumptions we arrive at the following theorem.

Theorem 11.2 (Evader-win environments)**.** *A pursuer with capture unit capture radius, unit velocity, and sensing uncertainty α cannot capture an evader with equal speed if the radius of the playing environment, R, satisfies,*

$$R > \frac{\csc\frac{\alpha}{6}(1-2\sec\frac{\alpha}{2})}{(\cos\frac{\alpha}{6}-1)(\sec\frac{\alpha}{2}-1)} \tag{11.13}$$

Proof. The proof proceeds by substituting $d = \frac{1}{\sin\frac{\alpha}{6}}$ into Eq (11.12). Thus, $\phi = \frac{\alpha}{6}$ the equation can be simplified as shown. □

The results in this section show that the evader can win in some environments. In the next section, we present a strategy for a pursuer to ensure capture of the evader in smaller environments, or with smaller sensing uncertainty.

11.1.2 Pursuer Strategy for Small Uncertainty

The previous section showed that an evader in large environments (as a function of sensor uncertainty) can escape the pursuer. We now show the converse: That for a given sensor noise there exists a winning pursuer strategy for small environments.

In the traditional Lion-and-Man game, the pursuer would move to stay on the line segment between the evader and the center. At each step, the pursuer will increase his radius and the evader will be forced outward or be captured. Thus, the notion of progress is the distance of the pursuer from the center. By introducing sensing uncertainty, the evader's position is no longer precisely known, but is estimated. Using the lion's strategy in this setting is therefore not possible. But, in this section, we will show that a strategy very similar to the original lion's strategy will actually result in capture, so long as the environment is not too large. We show that by keeping the evader "outside" the pursuer's position, the evader is forced against the boundary of the circle and eventually is within the capture radius of the pursuer.

As before, the pursuer's goal is to move within distance r of the evader. We propose a strategy which works for small step sizes relative to the capture radius. Specifically, Lemma 11.3 requires that $s \leq \frac{r}{\sqrt{2}}$, where s is the step size. In Theorem 11.3, it is shown that if the environment has a radius smaller than $\frac{r}{\tan\alpha}$, the proposed strategy will enable a pursuer to capture the evader. As before, we normalize all distances so that the step size is unitary.

To establish the pursuer's strategy and generalize the lion's move, we define a region of the arena which is considered *covered* as follows. The goal of the pursuer is to ensure that the evader is always in the covered region.

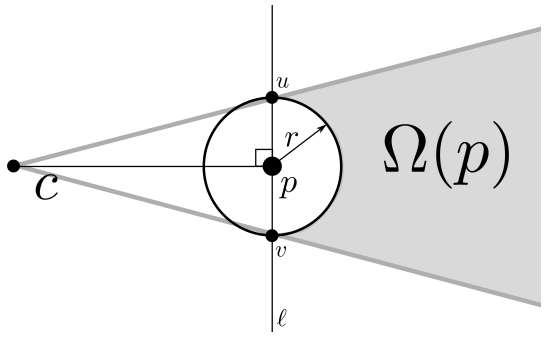

Figure 11.5: The shaded region is $\Omega(p)$, the area covered by the pursuer at position p as defined in Definition 3.

Definition 3 (Covered Region of the pursuer: $\Omega(p)$)**.** *The covered region is illustrated in Figure 11.5. Let p be the pursuer position, $C(p, r)$ be the capture region around the pursuer, and ℓ be the line perpendicular to $\overline{cp}$ and passing through p. If p is the center, ℓ can be any line passing through c. Let $u(p)$ and $v(p)$ be the so-called* anchor points *where ℓ intersects the boundary of $C(p, r)$. Let S be the cone defined by the two lines which start at the center of the circle and pass through $u(p)$ and $v(p)$. The covered region from the pursuer location, $\Omega(p)$, is the set of all points x which satisfy:*

1. *The covered points are further from the center than the pursuer ($|p| < |x|$)*
2. *The points are outside the capture radius around the pursuer ($|px| > r$)*
3. *The points are in the cone S, i.e., the absolute value of $\widehat{xcp}$ is at most $\tan^{-1} \frac{r}{|p|}$.*

As $r \to 0$, we have the invariant from the original lion and man game, which requires that the pursuer stay on the line between the center and the evader position. If the pursuer is at the center of the circle, the anchor points $u(p)$ and $v(p)$ are undefined and we define $\Omega(p)$ as the half plane containing the evader.

The pursuer's strategy we propose is as follows. First, it will move to the center of the circle. After the evader moves and the bearing measurement is received, the pursuer will move so that it increases its distance from the center of the circle, while

simultaneously keeping the evader in the covered region. Formally, we define the two requirements as Progress and Coverage as follows.

Definition 4 (Requirements of Pursuer's Move)**.** *After each pursuer move from p to its new location p', the following two conditions are satisfied assuming the evader is not captured:*

1. **Progress:** *The distance of the new pursuer position from the center satisfies* $|p'|^2 \geq |p|^2 + 1$.

2. **Coverage:** *The new pursuer position covers the evader:* $e \in \Omega(p')$.

In the remainder of the section we show that for any pursuer position p, there exists a move satisfying these two requirements. Then, we show than in combination they lead to capture. The notion of coverage will allow us to simplify the pursuer's strategy. We show the pursuer needs only the current bearing measurement and the notion of coverage to keep track of the evader's location and make the appropriate move.

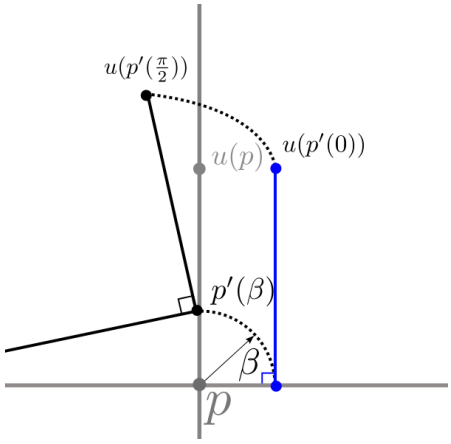

Figure 11.6: Placing the pursuer on the lower dashed curve (defined by β and one step from p), will place the point $u(p')$ on the upper dashed curve. Two configurations are shown: $\beta = 0$ (blue) and $\beta = \frac{\pi}{2}$ (black).

When the pursuer at position p moves to its next location, p', we will parameterize its next location by the angle β, where β is the angle between $\overline{cp}$ and $\overline{pp'}$. Thus, $\beta = 0$ implies a step directly away from the center of the circle as illustrated in Figure 11.6.

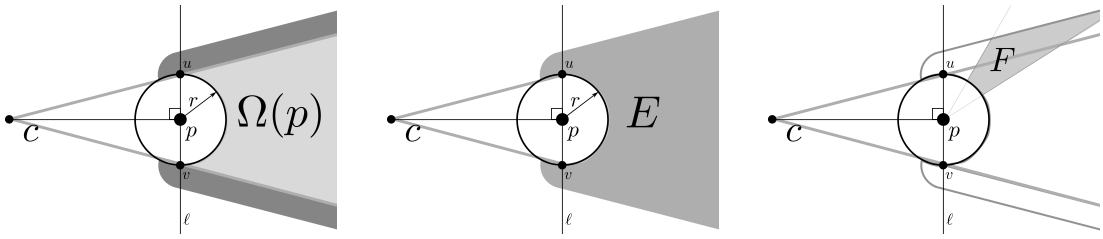

Figure 11.7: Illustration of the "Feasible Region", defined in Definition 5. Before the evader's turn, it is known to be inside the covered region, $\Omega(p)$. After the evader's move the region is dilated by one step, forming E. At the start of the pursuer's turn, a bearing measurement, b is obtained. Since the bearing measurement may be adjusted by up to α by the evader, the evader may be within $\pm\alpha$ of the bearing measurement. Thus, the feasible region for the evader is the intersection of E and a cone of angular width 2α.

Suppose the pursuer begins its turn at point p, and consider the area that the evader could reach from inside the pursuer's starting coverage region, $\Omega(p)$. To keep track of the possible evader locations after it moves and the pursuer takes a bearing measurement, we define the region which may contain the evader as follows.

Definition 5 (Feasible evader region before the pursuer's move: F)**.** *Let E and E' be the set of possible evader locations before and after its move. E' is E dilated by one step. Then, the pursuer takes a bearing measurement. The feasible set (F) is the set of possible evader locations which agree with the prior, possible motion, and the bearing measurement. As illustrated in Figure 11.7, F is the intersection of a cone of angular width 2α around the bearing measurement, and E'.*

To maintain coverage, the pursuer must ensure that it moves to a point p' such that all points in F are in $\Omega(p')$. We now show that coverage can be re-established after every evader move even if the evader's precise position is not known. We prove the objective can be achieved so long as the pursuer is not more than distance $\frac{r}{\tan\alpha}$ from the center.

Lemma 11.3 (Maintaining Coverage with Sensing Uncertainty)**.** *Let the pursuer with capture radius $r \geq \sqrt{2}$ be at position p. Let the evader's position, e, be known to fall within the region covered by the pursuer, $e \in \Omega(p)$. Let the feasible evader region, F, be the expansion of $\Omega(p)$ by one step intersected with the received bearing measurement*

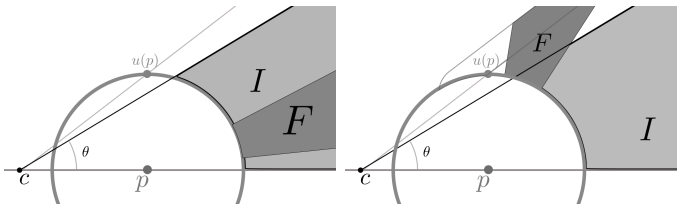

(a) Case I (b) Case II

Figure 11.8: Separation of the cases in Lemma 11.3. The region I is a subset of $\Omega(p)$, such that all points in I are covered and have angle θ of less than $\tan^{-1}\left(\frac{r}{|p|+1}\right)$. If $F \subseteq I$ then the pursuer can make a single step outward to cover it. If, however, some point in F has a larger angle, then the pursuer must move with $\beta > 0$ to cover it, but no larger than $\frac{\pi}{2}$.

as described in Definition 5. Then for any bearing measurement and resulting F, there exists a pursuer location $p^\star$ within one step of p such that $F \subseteq \Omega(p^\star)$. Furthermore, $p^\star$ satisfies progress.

Proof. First, let β be the angle between the lines $\overline{pp'}$ and $\overline{cp}$.

We will break the proof into cases, based on the configuration of the feasible region within E. Let a be the point in F which has the maximum angular deviation from $\overline{cp}$. That is, $a = \arg\max_{e \in F} \widehat{ecp}$. Let b be the point in F such that, $b = \arg\min_{e \in F} \widehat{ecp}$. Finally, without loss of generality, if the absolute value of $\widehat{acp}$ is greater than that of $\widehat{bcp}$, then swap the labels on the points. We will consider the case where $\widehat{acp} > 0$. The other case is symmetric.

Note, the region F does not include any points inside the capture radius, or closer to the center than the pursuer. By Definition 3, and since all points e in F have an angle $\widehat{bcp} \leq \widehat{ecp} \leq \widehat{acp}$, showing that both a and b are covered is equivalent to showing that all points in F are covered.

Consider the possible locations of a. We will separate out two cases as shown in Figure 11.8.

Case I: $\widehat{acp} \leq \tan^{-1}\left(\frac{r}{|p|+1}\right)$.

This case is illustrated in Figure 11.9. In this case, the pursuer will move with $\beta = 0$,

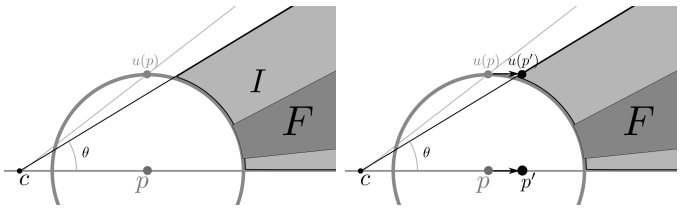

Figure 11.9: Case I: When the feasible region F is a subset of I (the set of covered points with "small" angle relative to $\overline{cp}$), the pursuer steps outward by one step to location p'. Now, $\Omega(p') = I$, and therefore all points in F are covered.

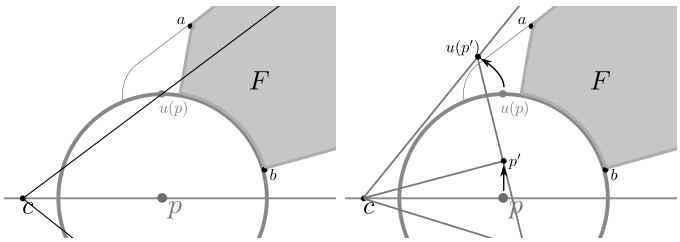

Figure 11.10: Case IIa: When the feasible region F is above the line $\overline{cp}$. The pursuer moves vertically one step. A pursuer at p' covers all possible evader locations above the line $\overline{cp}$. It is proven that the line $\overline{cv(p)}$ passes below b, meaning all points in F are in $\Omega(p')$.

i.e., one step outward along the line $\overline{cp}$ as shown in Figure 11.9. Then, by Definition 3,

$$\widehat{u(p')cp} = \tan^{-1}\left(\frac{r}{|p'|}\right) \tag{11.14}$$

$$= \tan^{-1}\left(\frac{r}{|p|+1}\right). \tag{11.15}$$

By assumption this angle is at least $\widehat{acp}$. Therefore, the point a is covered. The point b also falls within $\Omega(p')$ since its angle was also less in absolute value than $\tan^{-1}\left(\frac{r}{|p|+1}\right)$.

Case IIa: $\widehat{acp} > \tan^{-1}\left(\frac{r}{|p|+1}\right)$ and b above $\overline{cp}$.

In this case, the feasible region F falls entirely above the line $\overline{cp}$, as illustrated in Figure 11.10. Let the pursuer move with $\beta = \frac{\pi}{2}$ to the point p'. We will first show that b is covered. The point b is above (or on) the line $\overline{cp}$. Since $|p| \geq 1$ and p' is just above p by one step, the angle $\widehat{p'cp}$ is at most $\frac{\pi}{4}$. The lower anchor point, $v(p')$ is distance r from p' along the line perpendicular to $\overline{cp'}$. Since $s = 1 \leq \frac{r}{\sqrt{2}}$, the anchor point is far enough from p' to lie on or below the line $\overline{cp}$. Thus, b is in $\Omega(p')$.

We will now show the pursuer at point p' also covers the point a. Let E be all

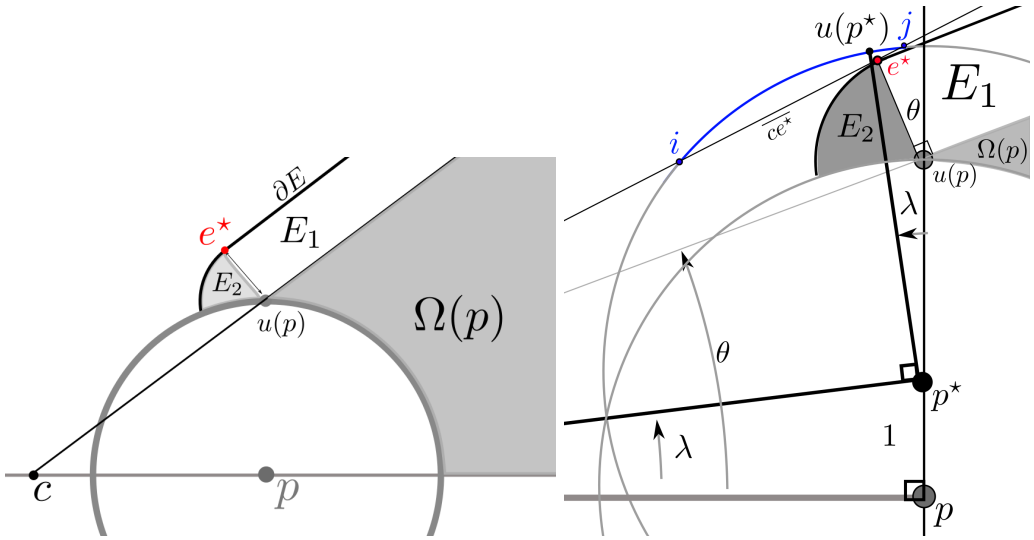

Figure 11.11: Illustration of Case IIa. 11.11a: The definition of the point $e^\star$, and the regions E_1 and E_2. Note $E_1 \bigcup E_2 \bigcup \Omega(p)$ represents all possible evader locations after its move. 11.11b: With a move of $\beta = \frac{\pi}{2}$, the upper boundary of $\Omega(p')$, defined by the line $\overline{cu(p')}$ would pass above $e^\star$. In the proof, it is shown that $u(p')$ is on the arc between a and b, the points where the line $\overline{ce^\star}$ intersects the capture radius of the pursuer after the move to p'.

points x reachable from within $\Omega(p)$, satisfying $\widehat{xcp} > \tan^{-1}\left(\frac{r}{|p|+1}\right)$. As illustrated in Figure 11.11b, the upper boundary of E is a straight line parallel to $\overline{cu(p)}$ and a curve around the point $u(p)$. Let $e^\star$ be the point on the linear part of the boundary of E, labelled ∂E. which is closest to the center, shown in Figure 11.11a. We will subdivide $E \setminus \Omega(p)$ along the line $\overline{u(p)e^\star}$ into E_1 which is all points left of the line, and E_2 which is to the right.

Since $\beta = \frac{\pi}{2}$, p' is distance $r-1$ from $u(p)$. Note, the distance to any point x in E_2 satisfies,

$$|xp'| \leq |p'u(p)| + |u(p)x| \leq r - 1 + 1 = r. \tag{11.16}$$

Thus, all points in E_2 are captured by the pursuer move with $\beta = \frac{\pi}{2}$.

We now show that all points in E_1 are covered to complete the proof of this case. In what follows, refer to Figure 11.11b. The point in E_1 with the highest angle from

the line $\overline{cp}$ is clearly $e^\star$. Thus, if $e^\star$ can be covered, then any point in E_1 can be as well (including a). To cover $e^\star$, the upper anchor point, $u(p^\star)$, must lie above the line $\overline{ce^\star}$ (see Definition 3).

The point $e^\star$ is less than distance r from the pursuer, and therefore the line $\overline{ce^\star}$ passes through the capture circle around $p^\star$. Let i and j be the points where the line intersects the capture circle.

If $u(p^\star)$ is above the line $\overline{ce^\star}$, then it lies between the points i and j on the capture circle around $p^\star$. We will prove this is the case.

Let λ be the angle that the line $\overline{p^\star u(p^\star)}$ makes with respect to $\overline{pu(p)}$. The angle λ is therefore equal to the angle subtended by p and $p^\star$ with respect to the center. Thus,

$$\lambda = \widehat{p^\star cp} = \sin^{-1}\frac{1}{\sqrt{|p|^2+1}}. \tag{11.17}$$

Let θ be the angle that the line $\overline{u(p)e^\star}$ makes with respect to $\overline{pu(p)}$. The angle θ is therefore equal to the angle subtended by the points p and $u(p)$ with respect to the center. Thus,

$$\theta = \widehat{u(p)cp} = \sin^{-1}\frac{r}{\sqrt{|p|^2+r^2}}. \tag{11.18}$$

Clearly, $0 < \lambda < \theta$, and therefore $u(p^\star)$ is to the right of i, and to the left of the line $\overline{pu(p)}$. But $e^\star$ is distance $\sin\theta$ from the line $\overline{pu(p)}$, and $u(p^\star)$ is distance $r\sin\lambda$ from the same line. By inspection,

$$\sin\theta = \frac{r}{\sqrt{|p|^2+r^2}} \tag{11.19}$$

and

$$r\sin\lambda = \frac{r}{\sqrt{|p|^2+1}}. \tag{11.20}$$

Since $r\sin\lambda > \sin\theta$, $u(p^\star)$ lies to the left of $e^\star$, and is therefore between i and j. Thus, a is covered, completing the proof for this case.

Case IIb: $\widehat{acp} > \tan^{-1}\left(\frac{r}{|p|+1}\right)$ and b below $\overline{cp}$.

In this case, the line $\overline{cp}$ passes through the region F. As before, subdivide the set evader locations into E_1 and E_2. Note that, because b is below $\overline{cp}$, a cannot be left of the line $\overline{pu(p)}$ because the angle between a and b must be less than $2\alpha = \frac{\pi}{2}$. Therefore, the

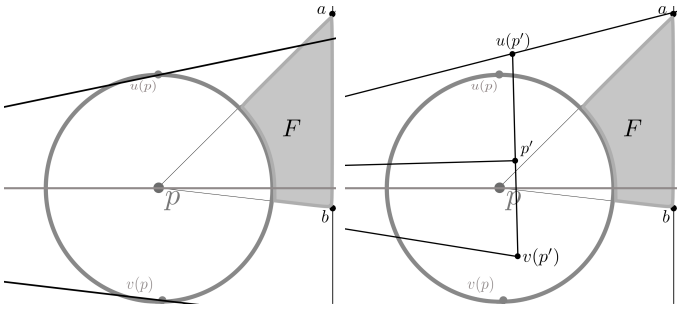

Figure 11.12: Case IIb: When F straddles the line $\overline{cp}$. The point p' covers the point which lies outside of $\Omega(p)$ (shaded region) by moving to p' which places the upper anchor point, $u(p')$ on the line $\overline{ca}$. A pursuer making this move also covers all other points in F because the angle between a and b is less than the angle between $u(p')$ and $v(p')$.

point a is somewhere in E_1. In the previous case, it was shown that the pursuer moving with $\beta = \frac{\pi}{2}$ will cover all points in E_1. Note that the angle $\widehat{u(p')cp}$ varies smoothly as a function of β. Therefore, if any point in E_1 lies in the interior of $\Omega(p')$ after the pursuer moved at angle β, then there exists a smaller angle β' which will cover the point $a \in E_1$ so that the boundary of the covered region passes through a.

Let the pursuer move to the point p' such that a is on the upper boundary of $\Omega(p')$. From this point, $\Omega(p')$ covers a cone of angular width greater than 2α. This is because the pursuer cannot increase his distance from the center to more than $\frac{r}{\tan\alpha}$, and by Definition 3 the angular width of Ω is $2\tan^{-1}\left(\frac{r}{|p|}\right) \geq 2\alpha$.

The angular difference between a and b is less than 2α with respect to the center. To see this, let there be a coordinate frame centered on p with the x axis aligned with $\overline{cp}$. Let x_a and y_a be the coordinates of a in this frame (respectively b).

$$\widehat{apb} = 2\alpha \tag{11.21}$$

$$= \tan^{-1}\left(\frac{y_a}{x_a}\right) + \tan^{-1}\left(\frac{y_b}{x_b}\right). \tag{11.22}$$

But the center of the circle is distance $|p|$ from the origin of this coordinate frame. Thus,

$$\widehat{acb} = \tan^{-1}\left(\frac{y_a}{|p| + x_a}\right) + \tan^{-1}\left(\frac{y_b}{|p| + x_b}\right) \tag{11.23}$$

which is clearly less than the value of $\widehat{apb}$ above.

Therefore, the angular width of F is less than that of Ω, and since they share a boundary at a, $F \subseteq \Omega(p')$. □

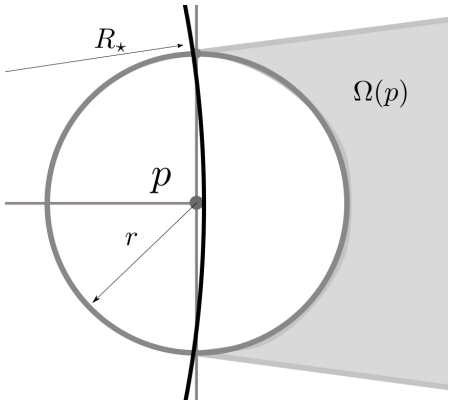

Figure 11.13: The pursuer can reach a radial distance of $\frac{r}{\tan\alpha}$ from the center while keeping the evader in the covered region. If the arena is no larger than this, the covered region falls entirely outside the arena, implying the pursuer must move into the capture region.

The previous lemma shows that coverage and progress can be maintained for every turn, so long as the pursuer does not move outside a circle of radius $\frac{r}{\tan\alpha}$. Now, we show that if the radius of the arena is less than this, the combined notion of coverage and progress lead to the evader being within the capture radius of the pursuer.

Theorem 11.3. *A pursuer can move to within distance r of an evader in a circular arena despite sensing uncertainty of magnitude α so long as the arena has a radius at most $\frac{r}{\tan\alpha}$.*

Proof. The pursuer will first move to the center of the arena. Then, by Lemma 11.3, the pursuer can increase his distance from the center out to a radius $\frac{r}{\tan\alpha}$, while maintaining coverage of the evader. Note that $\Omega(p)$ is entirely outside the circle of radius $|p|$, since the line $\overline{u(p)v(p)}$ is perpendicular to the line $\overline{cp}$, and $\Omega(p)$ does not include any points in the capture radius. If the arena has radius no more than $\frac{r}{\tan\alpha}$, then the pursuer will reach the boundary while keeping the evader inside the covered region. Thus, the covered region is entirely outside the arena, implying the evader has nowhere to move but into the capture radius, since, by Lemma 11.3 it is always between the upper and lower boundary of $\Omega(p)$. See Figure 11.13 for an illustration.

□

11.2 Discussion

We have studied classical pursuit-evasion games in which the pursuer can obtain only uncertain bearing measurements. We showed that the evader can exploit bearing uncertainty to win the open-plane pursuit game. In the more complex lion-and-man game, we showed that the tradeoff between sensing uncertainty and environment size determines the outcome of the game. We gave bounds on the size of the environment for both pursuer-win and evader-win scenarios, but a gap remains between the two.

We have studied the problems of locating targets which are both stationary and moving. In all cases we conducted theoretical analysis of our proposed solutions, showing the strengths and limitations analytically and experimentally when appropriate. In the next chapter, we further discuss our contributions and identify some key open problems that remain.

Chapter 12

Conclusions and Future Work

This thesis has been devoted to the study of using bearing sensors to locate (and sometimes capture) targets of interest. The bearing measurement model is widely used in literature, making the problem fundamental to robotic tracking applications. The work was motivated by a real-world application and the primary results were field tested in the intended application domain on a working robotic system.

The key to the results was the idea of competitiveness, or a comparison of the proposed algorithms to the (possibly unknown) optimal algorithm. Analyzing the results in this way allowed firm guarantees about the performance of our proposed algorithms regardless of starting conditions or changes to the system. In the next section we review the details of our contributions and identify some open problems or extensions.

12.1 Contributions and Open Problems

In Chapters 5 through 7 we have examined the problem of using a mobile robot to locate a radio transmitter using a directional antenna. Algorithms were developed and analyzed to show an upper bound on the time required to locate a stationary target as a function of the system parameters (sensing noise, measurement time, chassis velocity) and tracking objective (initial uncertainty versus final requested uncertainty). For this reason, the resulting closed form analysis is amenable to engineering trade-offs in the system itself, as well as providing a method for comparisons with other bearing-only active localization algorithms.

An interesting direction for future work is to focus on tightening the logarithmic approximation of our online algorithm from Section 7.1 in Chapter 7. We expect that a constant factor approximation is possible. Another avenue for future work is reducing the number of communication steps in the online algorithm.

Of particular interest is an extension to localizing multiple targets using multiple robots. A corollary of Chapter 6 is that as the number of robots dedicated to finding a target increases, the time required to do so scales by $\mathcal{O}\left(\frac{T}{\sqrt{N}}\right)$ for N robots, where T is the time for a single robot. An interesting direction for future work would be to incorporate this tradeoff into a many-robot, many-target assignment problem. This would allow minimum-time localization of a group of dispersed targets.

A primary contribution of Chapter 7 was a method for converting an arbitrary offline strategy into a field-deployable online algorithm. An offline-to-online conversion structured according to Theorem 7.1 was shown to be a logarithmic approximation of the optimal algorithm. It is important to note that the requirements for Theorem 7.1 are not very restrictive. It is required that the subroutine place the robots so that two measurements exist which are not collinear with any point in the region known to contain the target. Furthermore, the measurement locations should not be arbitrarily far from the boundary of the region. Thus, other routines could be used to accommodate e.g., kinematic constraints of the robots, communications constraints, or some other system-specific parameter.

Another extension is to obtain results in three dimensional environments. For example, given a target in the plane, but allowing sensors to move in three dimensions is a reasonable model for using aerial vehicles for surveillance. In this case, the localization uncertainty is a function of both the angle between the sensor locations with respect to the target (see e.g., Eq (6.2)), but also of the altitude of the vehicles. This follows since the knowledge that the target lies in the plane can be exploited to simplify the estimation task [90].

Finally, a clear next step for this work is locating mobile targets. If the target loiters in a small region, we expect that the motion of the target will have negligible affect on the cost to localize. However, if the motion is large, new methods are needed.

Chapters 8 and 9 dealt with the proper initialization of targets from the moment

they are first detected, paving the way for a multi-target localization of aggregated targets. While the algorithm developed worked well in combination with the single-target localization strategy from Chapter 5, no strong theoretical guarantees were provided with respect to the optimal algorithm. In Chapter 9, was presented a method for localizing many stationary targets regardless of their configuration, and with much stronger guarantees about optimality. A possible extension to the work in Chapter 9 is to use multiple robots. Since the problem is effectively a TSPN instance with circular discs, extending to k robots could follow a similar track as that defined in [91] or [92].

Chapters 10 and 11 dealt with localization and capture of an adversarial target. It was shown that in large environments and with high sensing noise, a target becomes impossible to capture if it is adversarial. However, if the environment is smaller or the sensing noise is reduced, the target can be captured.

The pursuer strategy presented in Chapter 11, required that the step size was smaller than the capture radius. In Theorem 11.3, it was shown that this requirement is only necessary to allow the first few steps of the pursuer strategy (when it begins at the center of the circle). It is very likely that a similar strategy which operates differently on the first few steps would not have this requirement.

Similarly, the pursuer strategy worked for bearing uncertainty of up to $\frac{\pi}{4}$. The upper bound on the noise stems from the fact that the pursuer is required to move so that his radius increases at every step. In Theorem 11.3, we see that if the noise is greater than $\frac{\pi}{4}$, Case IIa and IIb are not separable. It is possible that if the pursuer could stay at the same radius after its move, or even decrease its radius for a limited time, then the pursuer could still capture the evader with greater sensing uncertainty. If so, the key is to show that the pursuer still makes progress after a finite amount of time. A similar analysis was performed in [75].

Another possible way to tip the open-plane game (Chapter 10) back in favor of the pursuer is to increase the pursuer's speed. This is exactly what Klein et al. propose [71] for a similar problem. Another method would be to use multiple pursuers. A second pursuer may help to resolve the ambiguity which allowed the evader to increase the separation. Both of these are possible extensions.

An extension of the Lion and Man game from Chapter 11 to higher dimensions seems straightforward by simply allowing each player to make its move in the plane defined

by the center and both player positions.

In the games we considered, there is only one pursuer and the players have the same maximum speed. It is likely that the evader can be captured in larger environments by increasing the number of pursuers or the maximum speed of the (single) pursuer. A simple first step in this direction would be using the pursuers to form a chain, thus increasing the effective capture radius of the single, controlling pursuer, similar to Bopardikar in [93]. Thus, N pursuers should be able to win the lion-and-man game in environments of $\mathcal{O}(\frac{N}{\tan\alpha})$ in two dimensional games. However, it would be even more interesting to show that multiple pursuers can use their combined sensing to capture the evader in even larger environments. In this scenario, some pursuers may switch to a passive, sensing role to provide information. Obtaining bounds for these versions are interesting avenues for future research.

Another avenue is to allow randomization in pursuer strategies. The evader strategy in the open plane can be modified to work against randomized strategies since this game is infinite. In the lion-and-man game however, when the pursuer can measure the true location, the number of steps until capture is finite. It is plausible that by discretizing the disk, we can obtain a finite set containing all pursuit strategies. No matter which strategy the evader plays, at least one element of this set would capture the evader and this strategy can be "guessed" using randomization. Hence the evader can be captured even without any measurements. The capture time resulting from this argument would be exponential in the duration of the game. In [94], it was shown that the capture time is indeed exponential when the game takes place on arbitrary graphs. Whether this bound can be improved when bearing measurements are available is left for future research.

Finally, the gap between evader-win and pursuer-win environments can be further explored. If it could be shown that a particular pursuer strategy scales at the same rate as an evader strategy, then the pursuer strategy would be proven asymptotically tight.

12.2 Future Research Directions

This thesis presents fundamental bounds on several target localization problems. These bounds will hopefully be useful to future system designers and researchers as autonomous robots are used for more day-to-day tasks. The results were primarily motivated by the problem of tracking invasive fish, but they should generalize to other bearing-only tracking problems. However, each application will have its own restrictions and complications. Moving forward, we expect the following issues will arise in research, presenting exciting extensions to this work.

12.2.1 Kinematic Models

In this thesis we have considered robots as point objects which can move freely in the two dimensional plane. However, in practice, robots are often not capable of moving in this way. While the *lower* bounds, e.g., the time bounds on the optimal algorithm, remain valid, incorporating kinematic models would allow a tighter bound to be obtained. New upper bounds on localization time would be required. We remedied this by providing field results which show that the robots can execute the strategies and localize the targets as predicted. However, in other, more difficult settings, or with other types of robots, this may not be possible. Thus, proving new upper bounds for other kinematic models is an interesting direction for future work. For example, the Dubins path, defined by straight-line segments and circular curves [95], could be a good model for the boats if a more realistic upper-bound was required.

The pursuit-evasion games could also incorporate more realistic control laws. For example, given the wide proliferation of quadcopters, the pursuit strategy in Chapter 11, could be adapted to allow a quadcopter to guard the airspace around a vital target from incursion by other quadcopters. In this case, the pursuer's motion model needs to be updated to include kinematic constraints. However, by allowing the evader arbitrary, but fixed-velocity motion, it is possible to prove capture or intercept against any type of vehicle. Some initial progress on the pursuer's strategy for differential-drive pursuers was provided by [96].

12.2.2 Long-Term, Collaborative Autonomy

The problems considered in this thesis focused almost exclusively on a single task with a definite ending condition. These tasks are likely to become subtasks of a much larger mission statement. In the future, a robotic system will likely be expected to remain *in situ*, providing constant updates and being "on call" for more data-gathering tasks. Such a network of robotic sensors will likely serve as the data-gathering layer for future scientists or agriculturalists, much as large telescopes, particle collides, or seismic monitoring stations have been collaboratively built to serve as the data-gathering tools for astronomers, physicists, and geologists. Thus, while it is critical to study these task-specific solutions, several larger issues come into play when deploying such a system.

First, the system will degrade over time. Over long time scales, the sensors of the robot are likely to wear or break, producing false positive or negative signals. Thus, the localization routines must begin to take into account the possibility of false targets in the environment. Measurements which seem valid may in fact be originating from radio interference or component failure. This is known as the "measurement origin uncertainty" problem [97]. An algorithm which can route the robot to possibly discern between these failure modes and true targets would be an exciting future direction.

Second, the tradeoff in energy and cost to localize will become extremely important. Though battery life is increasing at a rapid pace, the long time deployments that are required for a reconfigurable robotic sensor network will require that the robots can coordinate their energy use. While it may be quick for one robot to localize a nearby target, the energy saved by allowing multiple robots to help could be substantial. Of key importance to address this problem is both knowing the energy profile for the robots (e.g., [98]) and knowing how to gain energy from the environment (e.g., solar power in [99, 100]).

Third, the survivability of the system becomes paramount. The complex interplay of energy use, wear to the system, and tracking objectives will become more important to model. The optimal *time* required to localize a target is studied in this thesis. But future work should focus on optimizing algorithms which can produce safe, reliable trajectories that allow the robot to e.g., stay in communication with other robots or remain in a safer area. This becomes particularly important when operating around people. Algorithms which can prove the *safety* of the system but still achieve the objectives in near-optimal

time are required.

12.2.3 Self and Collaborative Localization

A major simplifying assumption made in these works was that each robot knows its own position in the environment. This is reasonable, in practice, given the availability of accurate GPS in our intended operating environment. However, in environments for which GPS is not available (or after a GPS equipment failure), such an assumption is no longer valid. In this case, each robot must spend time to localize both itself and possibly to help localize other stranded robots.

The first problem this introduces in collaboration is that each robot is no longer certain how much information can be gathered by the other robots. For example, the symmetry arguments made in Chapter 6 break if one of the robots spends all of its time measuring from the incorrect position.

Second, if the robots are not confident of their position in the environment, it may not be possible to re-establish communication. In this case, the robots may have to make the decision to locate missing members or continue with the localization task. A rendezvous with unknown starting location is a very difficult two-sided search problem, but initial steps were studied in [101].

Third, there may be only limited areas of the environment in which GPS is available. A measurement strategy which seeks to minimize both the target uncertainty and the robots' uncertainty will likely prioritize measurements (or at least waypoints) inside these areas.

12.3 Concluding Remarks

Automation has proved useful for hundreds of years for improving production in industrial settings. Today we see robots advancing beyond the factory and entering the real world. The kinds of problems now being automated are less structured and less controlled. Robots now work on farms and in lakes or oceans monitoring our water. They slowly search the planets for signs of ancient life. They hunt coral reefs for invasive starfish [102]. The tools we have built in these systems have enabled solutions to tough industrial, agricultural, and scientific problems. This thesis investigated one

such application and the general problems we encountered during our development of a robotic solution.

But we as researchers have just begun. Though many challenges remain in the development of reliable systems and useful algorithms, the mobile, unconstrained, and likely prolific robotic systems of the future will, optimistically, be one of the greatest tools of humanity's search for knowledge. With time, we will find that networks of robots will help future generations improve not only their understanding of the planet, but their ability to responsibly manage it. In closing, we hope that more industries and scientists will make use of robotics, and that future robotic engineers and researchers will seek out applications in which their work can be used to better the world around them.

References

[1] "Two-robot field experiment," 2013. [Online]. Available: https://www.youtube.com/watch?v=jZWTUxqTskY

[2] C. Brown, "Autonomous vehicle technology in mining," *Engineering and Mining Journal*, vol. 213, no. 1, p. 30, 2012.

[3] R. D'Andrea, "Guest editorial: A revolution in the warehouse: a retrospective on kiva systems and the grand challenges ahead," *IEEE Transactions on Automation Science and Engineering*, vol. 9, no. 4, pp. 638 – 639, 2012.

[4] J. Carsten, A. Rankin, D. Ferguson, and A. Stentz, "Global path planning on board the mars exploration rovers," in *Aerospace Conference, 2007 IEEE*. IEEE, 2007, pp. 1–11.

[5] M. J. Weber and M. L. Brown, "Effects of Common Carp on Aquatic Ecosystems 80 Years after Carp as a Dominant: Ecological Insights for Fisheries Management," *Reviews in Fisheries Science*, vol. 17, no. 4, pp. 524–537, Oct. 2009.

[6] J. Vander Hook, P. Tokekar, E. Branson, P. G. Bajer, P. W. Sorensen, and V. Isler, "Local-search strategy for active localization of multiple invasive fish," in *Experimental Robotics*, B. Siciliano and O. Khatib, Eds., vol. 88. Springer Tracs in Advanced Robotics, 2013, pp. 859–873.

[7] H. Bayram, J. Vander Hook, and V. Isler, "Gathering bearing data for target localization," 2016, in Review.

[8] J. Vander Hook and V. Isler, "Pursuit and evasion with uncertain bearing measurements," in *Canadian Conference on Computational Geometry*, 2014, pp. 332–340.

[9] J. Vander Hook, P. Tokekar, and V. Isler, "Algorithms for cooperative active localization of static targets with mobile bearing sensors under communication constraints," *Robotics, IEEE Transactions on*, vol. 31, no. 4, pp. 864–876, Aug 2015.

[10] J. VanderHook, P. Tokekar, and V. Isler, "Cautious greedy strategy for bearing-based active localization: Experiments and theoretical analysis," in *Robotics and Automation (ICRA), 2012 IEEE International Conference on*, 2012, pp. 1787–1792.

[11] J. Vander Hook, P. Tokekar, and V. Isler, "Cautious greedy strategy for bearing-only active localization: Analysis and field experiments," *Journal of Field Robotics*, vol. 31, no. 2, pp. 296–318, April 2014.

[12] "Clearpath robotics," "http://clearpathrobotics.com", accessed November, 2012.

[13] "Advanced telemetry systems," "http://atstrack.com", accessed November, 2012.

[14] "Signal hound," "http://signalhound.com", accessed September, 2015.

[15] P. Tokekar, J. Vander Hook, and V. Isler, "Active target localization for bearing based robotic telemetry," in *Intelligent Robots and Systems (IROS), 2011 IEEE/RSJ International Conference on*. IEEE, 2011, pp. 488–493.

[16] P. Tokekar, E. Branson, J. Vander Hook, and V. Isler, "Tracking aquatic invaders: Autonomous robots for monitoring invasive fish," *IEEE Robotics and Automation Magazine*, vol. 20, no. 3, pp. 33–41, September 2013.

[17] "Robot operating system," "http://ros.org", accessed November, 2012.

[18] J. N. Franklin, *Matrix Theory*, ser. Dover books on mathematics. Mineola, New York: Dover Publications, 1968.

[19] Y. Bar-Shalom, X.-R. Li, and T. Kirubarajan, *Estimation with Applications to Tracking and Navigation*. New York, USA: John Wiley & Sons, Inc., 2001.

[20] S. Thrun, W. Burgard, D. Fox *et al.*, *Probabilistic Robotics*. MIT press Cambridge, MA, 2005, vol. 1.

[21] H. Van Trees, *Detection, Estimation, and Modulation Theory: Nonlinear Modulation Theory*, ser. Wiley Classics Library. Wiley, 1971.

[22] B. Grocholsky, "Information-theoretic control of multiple sensor platforms," Ph.D. dissertation, University of Sydney. School of Aerospace, Mechanical and Mechatronic Engineering, 2006.

[23] M. Morelande, C. Kreucher, and K. Kastella, "A Bayesian Approach to Multiple Target Detection and Tracking," *Signal Processing, IEEE Transactions on*, vol. 55, no. 5, pp. 1589–1604, 2007.

[24] X. R. Li and V. P. Jilkov, "Survey of Maneuvering Target Tracking: II. Ballistic Target Models," *Proceedings of SPIE*, vol. 4473, no. August, pp. 559–581, 2001.

[25] ——, "Survey of Maneuvering Target Tracking: III. Measurement Models," *Proceedings of SPIE*, vol. 4473, no. August, pp. 423–446, 2001.

[26] ——, "Survey of Maneuvering Target Tracking: IV: Decision-Based Methods," *Proceedings of SPIE*, vol. 4728, no. April, pp. 511–534, 2002.

[27] ——, "Survey of Maneuvering Target Tracking: I: Dynamic Models," *IEEE Transactions on Aerospace and Electronic Systems*, vol. 39, no. 4, pp. 1333–1364, Oct. 2003.

[28] X.-R. Li, "A Survey of Maneuvering Target Tracking: Approximation Techniques for Nonlinear Filtering," *Proceedings of SPIE*, vol. 5428, no. April, pp. 537–550, 2004.

[29] X. R. Li and V. P. Jilkov, "Survey of Maneuvering Target Tracking: V: Multiple-Model Methods," *IEEE Transactions on Aerospace and Electronic Systems*, vol. 41, no. 4, pp. 1255–1321, Oct. 2005.

[30] ——, "Survey of Maneuvering Target Tracking-Part VIb: Approximate Nonlinear Density Filtering in Mixed Time," *Most*, vol. 7698, no. April, pp. 76 981E–76 981E–12, 2010.

[31] ——, "Survey of Maneuvering Target Tracking-Part VIa: Density-Based Exact Nonlinear Filtering," *Data Processing*, vol. 7698, no. April, pp. 76 981D–76 981D–12, 2010.

[32] D. Reid, "An algorithm for tracking multiple targets," *IEEE Transactions on Automatic Control*, vol. ac-24, no. 6, 1979.

[33] D. Mušicki, "Bearings Only Single-Sensor Target Tracking using Gaussian Mixtures," *Automatica*, vol. 45, no. 9, pp. 2088–2092, Sep. 2009.

[34] J. Derenick, J. Fink, and V. Kumar, "Localization Using Ambiguous Bearings from Radio Signal Strength," *2011 IEEE/RSJ International Conference on Intelligent Robots and Systems*, pp. 3248–3253, Sep. 2011.

[35] C. Forney, E. Manii, M. Farris, M. Moline, and C. Lowe, "Tracking of a Tagged Leopard Shark with an AUV: Sensor Calibration and State Estimation," in *International Conference on Robotics and Automation*, 2012, pp. 5315–5321.

[36] K. Zhou and S. Roumeliotis, "Multirobot active target tracking with combinations of relative observations," *Robotics, IEEE Transactions on*, vol. 27, no. 4, pp. 678–695, 2011.

[37] E. Frew and S. Rock, "Exploratory Motion Generation for Monocular Vision-Based Target Localization," vol. 7, 2002, pp. 3633–3643.

[38] E. W. Frew, "Observer Trajectory Generation for Target-Motion Estimation Using Monocular Vision," Ph.D. dissertation, Stanford University, 2003.

[39] J. Passerieux and D. Van Cappel, "Optimal Observer Maneuver for Bearings-Only Tracking," *IEEE Transactions on Aerospace and Electronic Systems*, vol. 34, no. 3, pp. 777–788, Jul. 1998.

[40] Y. Oshman and P. Davidson, "Optimization of Observer Trajectories for Bearings-Only Target Localization," *Aerospace and Electronic Systems, IEEE Transactions on*, vol. 35, no. 3, pp. 892–902, Jul. 1999.

[41] G. Hoffmann and C. Tomlin, "Mobile Sensor Network Control Using Mutual Information Methods and Particle Filters," *IEEE Transactions on Control*, pp. 1–16, 2010.

[42] E. Frew, "Providing quality of service of information through mobility," in *Proceedings of the American Control Conference*, 2009, pp. 2160–2165.

[43] R. Sutton and A. Barto, *Reinforcement Learning: An Introduction*, ser. Adaptive Computation and Machine Learning Series. MIT Press, 1998.

[44] S. C. Ong, S. W. Png, D. Hsu, and W. S. Lee, "Planning under uncertainty for robotic tasks with mixed observability," *The International Journal of Robotics Research*, vol. 29, no. 8, pp. 1053–1068, 2010.

[45] S. D. Bopardikar, "Pursuit Strategies for Autonomous Vehicles," Ph.D. dissertation, University of California, Santa Barbara, 2010.

[46] A. Borri, S. D. Bopardikar, J. P. Hespanha, and M. D. D. Benedetto, "Hide-and-Seek with Directional Sensing," in *Proceedings of the 18th IFAC World Congress, Milan, Italy*, 2011, pp. 9343–9348.

[47] L. Merino, F. Caballero, and A. Ollero, "Active sensing for range-only mapping using multiple hypothesis," in *Intelligent Robots and Systems (IROS), 2010 IEEE/RSJ International Conference on.* IEEE, 2010, pp. 37–42.

[48] F. Morbidi and G. L. Mariottini, "Active target tracking and cooperative localization for teams of aerial vehicles," *Control Systems Technology, IEEE Transactions on*, vol. PP, no. 99, pp. 1–1, 2012.

[49] P. Scerri, R. Glinton, S. Owens, D. Scerri, and K. Sycara, "Geolocation of rf emitters by many uavs," in *AIAA Infotech@Aerospace 2007 Conference and Exhibit*, 2007.

[50] S. Hammel, P. Liu, E. Hilliard, and K. Gong, "Optimal observer motion for localization with bearing measurements," *Computers & Mathematics with Applications*, vol. 18, no. 1, pp. 171–180, 1989.

[51] A. Logothetis, A. Isaksson, and R. J. Evans, "An information theoretic approach to observer path design for bearings-only tracking," in *Decision and Control, 1997., Proceedings of the 36th IEEE Conference on*, vol. 4. IEEE, 1997, pp. 3132–3137.

[52] A. N. Bishop, B. Fidan, B. D. Anderson, K. Doançay, and P. N. Pathirana, "Optimality Analysis of Sensor-Target Localization Geometries," *Automatica*, vol. 46, no. 3, pp. 479–492, Mar. 2010.

[53] A. Bishop and P. Pathirana, "Optimal Trajectories for Homing Navigation with Bearing Measurements," in *Proceedings of the 2008 International Federation of Automatic Control Congress*, 2008.

[54] S. Martinez and F. Bullo, "Optimal Sensor Placement and Motion Coordination for Target Tracking," *Automatica*, vol. 42, no. 4, pp. 661–668, Apr. 2006.

[55] G. Hollinger and S. Singh, "Multi-robot coordination with periodic connectivity," in *Robotics and Automation (ICRA), 2010 IEEE International Conference on*. IEEE, 2010, pp. 4457–4462.

[56] A. Makarenko and H. Durrant-Whyte, "Decentralized data fusion and control in active sensor networks," in *Proceedings of the Seventh International Conference on Information Fusion*, 2004.

[57] E. D. Nerurkar and S. Roumeliotis, "Asynchronous multi-centralized cooperative localization," in *Intelligent Robots and Systems (IROS), 2010 IEEE/RSJ International Conference on*, Oct 2010, pp. 4352–4359.

[58] E. D. Nerurkar, S. Roumeliotis, and A. Martinelli, "Distributed maximum a posteriori estimation for multi-robot cooperative localization," in *Robotics and Automation, 2009. ICRA '09. IEEE International Conference on*, May 2009, pp. 1402–1409.

[59] K. Y. K. Leung, S. Member, T. D. Barfoot, and H. H. T. Liu, "Decentralized Localization of Sparsely-Communicating Robot Networks : A Centralized-Equivalent Approach," vol. 26, no. 1, pp. 62–77, 2010.

[60] J. R. Spletzer and C. J. Taylor, "Dynamic sensor planning and control for optimally tracking targets," *The International Journal of Robotics Research*, vol. 22, no. 1, pp. 7–20, 2003.

[61] D. Song, S. Member, C.-y. Kim, and J. Yi, "On the Time to Search for an Intermittent Signal Source Under a Limited Sensing Range," *Robotics, IEEE Transactions on*, vol. 27, no. 2, pp. 313–323, 2011.

[62] D. Song, C.-Y. Kim, and J. Yi, "Simultaneous localization of multiple unknown and transient radio sources using a mobile robot," *IEEE Transactions on Robotics*, vol. 28, no. 3, pp. 668 –680, june 2012.

[63] E. Galceran and M. Carreras, "A survey on coverage path planning for robotics," *Robotics and Autonomous Systems*, vol. 61, no. 12, pp. 1258 – 1276, 2013.

[64] A. Kelly, "Precision dilution in triangulation based mobile robot position estimation," in *Proceedings of the International Conference on Intelligent Autonomous Systems*, Amsterdam, 2003.

[65] O. Tekdas, N. Karnad, and V. Isler, "Efficient strategies for collecting data from wireless sensor network nodes using mobile robots," in *14th International Symposium on Robotics Research (ISRR)*, 2009.

[66] J. Fink and V. Kumar, "Online methods for radio signal mapping with mobile robots," in *Proc. IEEE International Conference on Robotics andAutomation*, 2010, pp. 1940–1945.

[67] J. Twigg, J. Fink, L. Paul, and B. Sadler, "RSS Gradient-Assisted Frontier Exploration and Radio Source Localization," in *Proc. IEEE International Conference on Robotics and Automation*, 2012.

[68] G. Hollinger and J. Djugash, "Target Tracking Without Line of Sight Using Range from Radio," *Autonomous Robots*, no. July 2011, pp. 1–14, 2011.

[69] T. H. Chung, G. A. Hollinger, and V. Isler, "Search and pursuit-evasion in mobile robotics: A survey," *Autonomous robots*, vol. 31, no. 4, pp. 299–316, 2011.

[70] G. Rote, "Pursuit-Evasion with Imprecise Target Location," in *Proceedings of the Fourteenth Annual ACM-SIAM Symposium on Discrete Algorithms (SODA)*. Society for Industrial and Applied Mathematics, 2003, pp. 747–753.

[71] K. Klein and S. Suri, "Trackability with Imprecise Localization," *arXiv preprint arXiv:1312.6573*, 2013.

[72] J. E. Littlewood, *Littlewood's Miscellany*. Cambridge University Press, 1986.

[73] L. Alonso, A. S. Goldstein, and E. M. Reingold, "Lion and man: Upper and lower bounds," *ORSA Journal on Computing*, vol. 4, no. 4, pp. 447–452, 1992.

[74] J. Sgall, "Solution of david gale's lion and man problem," *Theoretical Computer Science*, vol. 259, no. 12, pp. 663 – 670, 2001.

[75] N. Karnad and V. Isler, "Bearing-only pursuit," in *Robotics and Automation, 2008. ICRA 2008. IEEE International Conference on*, May 2008, pp. 2665–2670.

[76] S. Blackman, "Multiple hypothesis tracking for multiple target tracking," *IEEE AE Systems Magazine*, vol. 19, no. 1, January 2004.

[77] I. Cox and S. Hingorani, "An efficient implementation of reid's multiple hypothesis tracking algorithm and its evaluation for the purpose of visual tracking," *IEEE Transactions on Pattern Analysis and Machine Intelligence*, vol. 18, no. 2, February 1996.

[78] F. Pukelsheim, *Optimal Design of Experiments*, ser. Classics in Applied Mathematics. Society for Industrial and Applied Mathematics, 2006.

[79] D. Alspach and H. Sorenson, "Nonlinear bayesian estimation using gaussian sum approximations," *IEEE Transactions on Automatic Control*, vol. 17, no. 4, August 1972.

[80] Y. Bar-Shalom and E. Tse, "Tracking in a cluttered environment with probabilistic data association," *Automatica*, vol. 11, pp. 451—460, 1975.

[81] G. H. Golub and C. F. V. Loan, *Matrix Computations (3rd ed.)*. Johns Hopkins University Press, 1996.

[82] A. Bishop and B. Fidan, "Optimality Analysis of Sensor-Target Geometries in Passive Localization:Part 1-Bearing-Only Localization," *ISSNIP 2007*, vol. 1, pp. 7–12, 2007.

[83] P. G. Bajer, C. J. Chizinski, and P. W. Sorensen, "Using the Judas Technique to Locate and Remove Wintertime Aggregations of Invasive Common Carp," *Fisheries Management and Ecology*, Oct. 2011.

[84] P. G. Bajer and P. W. Sorensen, "Recruitment and Abundance of an Invasive Fish, the Common Carp, is Driven by its Propensity to Invade and Reproduce in Basins that Experience Winter-Time Hypoxia in Interconnected Lakes," *Biological Invasions*, vol. 12, no. 5, pp. 1101–1112, Aug. 2009.

[85] P. Johnsen and A. Hasler, "Winter Aggregations of Carp (Cyprinus carpio) as Revealed by Ultrasonic Tracking," *Transactions of the American Fisheries Society*, vol. 106, no. 6, pp. 556–559, 1977.

[86] C. Penne and C. Pierce, "Seasonal Distribution, Aggregation, and Habitat Selection of Common Carp in Clear Lake, Iowa," *Transactions of the American Fisheries Society*, vol. 137, no. 4, pp. 1050–1062, Jul. 2008.

[87] O. Tekdas and V. Isler, "Sensor placement for triangulation-based localization," *Automation Science and Engineering, IEEE Transactions on*, vol. 7, no. 3, pp. 681–685, July 2010.

[88] O. Tekdas, D. Bhadauria, and V. Isler, "Efficient data collection from wireless nodes under the two-ring communication model," *The International Journal of Robotics Research*, 2012.

[89] H. Bayram, J. Vander Hook, and V. Isler, "Gathering bearing data for target localization," Department of Computer Science, University of Minnesota, Tech. Rep. 15-014, 2015.

[90] P. Tokekar, V. Isler, and A. Franchi, "Multi-target visual tracking with aerial robots," in *Proceedings of IEEE/RSJ International Conference on Intelligent Robots and Systems*, 2014.

[91] D. Bhadauria and V. Isler, "Data gathering tours for mobile robots," in *IEEE International Conference on Intelligent Robots and Systems (IROS)*, 2009.

[92] P. Tokekar, J. V. Hook, D. Mulla, and V. Isler, "Sensor planning for a symbiotic uav and ugv system for precision agriculture," in *Proc. International Conference on Intelligent Robots and Systems (IROS)*, 2013.

[93] S. D. Bopardikar, F. Bullo, and J. P. Hespanha, "A Pursuit Game with Range-Only Measurements," in *2008 47th IEEE Conference on Decision and Control*, 2008, pp. 4233–4238.

[94] V. Isler and N. Karnad, "The role of information in the cop-robber game," *Theoretical Computer Science*, vol. 399, no. 3, pp. 179–190, 2008.

[95] L. E. Dubins, "On curves of minimal length with a constraint on average curvature, and with prescribed initial and terminal positions and tangents," *American Journal of Mathematics*, vol. 79, no. 3, pp. pp. 497–516, 1957. [Online]. Available: http://www.jstor.org/stable/2372560

[96] U. Ruiz and V. Isler, "Capturing an omnidirectional evader in convex environments using a differential drive robot," *CoRR*, vol. abs/1508.06333, 2015. [Online]. Available: http://arxiv.org/abs/1508.06333

[97] Y. Bar-Shalom, P. K. Willett, and X. Tian, "Tracking and data fusion," *A Handbook of Algorithms. Yaakov Bar-Shalom*, 2011.

[98] P. Tokekar, N. Karnad, and V. Isler, "Energy-optimal trajectory planning for car-like robots," *Autonomous Robots*, 2014, to appear.

[99] P. A. Plonski, J. Vander Hook, and V. Isler, "Environment and solar map construction for solar-powered mobile systems," Department of Computer Science, University of Minnesota, Tech. Rep., 2014, in review for publication in IEEE Transactions on Robotics.

[100] P. A. Plonski and V. Isler, "A competitive online algorithm for exploring a solar map," in *Proc. International Conference on Robotics and Automation*, 2014, to appear.

[101] D. Ozsoyeller, A. Beveridge, and V. Isler, "Symmetric rendezvous search on the line with an unknown initial distance," *IEEE Transactions on Robotics*, 2013, to appear.

[102] F. Dayoub, M. Dunbabin, and P. Corke, "Robotic detection and tracking of crown-of-thorns starfish," 2015.